**EDGEWOOD
RESEARCH,
DEVELOPMENT &
ENGINEERING
CENTER**

ERDEC-CR-019

AEROSOL SAMPLING MODELS SURVEY

DTIC

S ELECTE **D**
E JUN 17 1993

Dennis Metz
Paul Harvey

GENERAL MANAGEMENT ASSOCIATES
Abingdon, MD 21009

March 1993

Approved for public release; distribution is unlimited.

**U.S. ARMY
CHEMICAL
AND BIOLOGICAL
DEFENSE AGENCY**

Aberdeen Proving Ground, Maryland 21010-5423

Disclaimer

The findings in this report are not to be construed as an official Department of the Army position unless so designated by other authorizing documents.

REPORT DOCUMENTATION PAGE

Public reporting burden for this collection of information is estimated to average 1 hour per response, including the time for reviewing instructions, searching existing data sources, gathering and maintaining the data needed, and completing and reviewing the collection of information. Send comments regarding this burden estimate or any other aspect of this collection of information, including suggestions for reducing this burden, to Washington Headquarters Services, Directorate for Information Operations and Reports, 1215 Jefferson Davis Highway, Suite 1204, Arlington, VA 22202-4302, and to the Office of Management and Budget, Paperwork Reduction Project (0704-0188), Washington, DC 20503.

1. AGENCY USE ONLY (Leave blank)	2. REPORT DATE 1993 March	3. REPORT TYPE AND DATES COVERED Final, 90 Jun - 90 Dec

4. TITLE AND SUBTITLE

Aerosol Sampling Models Survey

5. FUNDING NUMBERS

C-DAAA15-87-D-0021
TA-99

6. AUTHOR(S)

Metz, Dennis, and Harvey, Paul

7. PERFORMING ORGANIZATION NAME(S) AND ADDRESS(ES)

General Management Associates
1308 Continental Drive, Suite K
Abingdon, MD 21009

8. PERFORMING ORGANIZATION REPORT NUMBER

ERDEC-CR-019

9. SPONSORING/MONITORING AGENCY NAME(S) AND ADDRESS(ES)

DIR, ERDEC,* ATTN: SCBRD-RTB,
APG, MD 21010-5423

10. SPONSORING/MONITORING AGENCY REPORT NUMBER

11. SUPPLEMENTARY NOTES

COTR: Robert Doherty, SCBRD-RTB, (410) 671-2326
*When this work was performed, ERDEC was known as the U.S. Army
Chemical Research, Development and (Continued on page 2)

12a. DISTRIBUTION/AVAILABILITY STATEMENT

Approved for public release; distribution is unlimited.

12b. DISTRIBUTION CODE

13. ABSTRACT (Maximum 200 words)

The Obscuration Sciences Branch of Physics Division, Research Directorate at the U.S. Army Chemical Research, Development and Engineering Center, has undertaken a research project. This effort is aimed at identifying a comprehensive algorithm, computer program, or theory that might already exist and could be used to design aerosol sampling and transport systems. Initially, a literature survey was performed by the Obscuration Sciences Branch which began with several hundred potential articles and has been distilled to four candidate reports.

This report evaluates the four candidate aerosol sampling models for self consistency and compares the numerical calculations resulting from four models. Finally a comparison of these model-derived results is made to the experimentally-derived results.

14. SUBJECT TERMS

Aerosol science	Polydispersed aerosols
Aerosol particles	Aerosol sampling train
Monodispersed aerosols	(Continued on page 2)

15. NUMBER OF PAGES

149

16. PRICE CODE

17. SECURITY CLASSIFICATION OF REPORT UNCLASSIFIED	18. SECURITY CLASSIFICATION OF THIS PAGE UNCLASSIFIED	19. SECURITY CLASSIFICATION OF ABSTRACT UNCLASSIFIED	20. LIMITATION OF ABSTRACT UL

11. SUPPLEMENTARY NOTES (Continued)

Engineering Center, and the Contracting Officer's Representative
was assigned to the Research Directorate.

14. SUBJECT TERMS (Continued)

Aerosol sampling models
Experimental verification
Aerosol penetrating efficiency
Aerosol sampling and transport systems

Accesion For	
NTIS CRA&I	X
DTIC TAB	☐
Unannounced	☐
Justification	
By	
Distribution /	
Availability Codes	
Dist	Avail and / or Special
A-1	

PREFACE

The work described in this report was authorized under Contract No. DAAA15-87-D-0021, Task 99. This work was started in June 1990 and completed in December 1990.

The use of trade names or manufacturers' names in this report does not constitute an official endorsement of any commercial products. This report may not be cited for purposes of advertisement.

Reproduction of this document in whole or in part is prohibited except with permission of the Director, U.S. Army Edgewood Research, Development and Engineering Center (ERDEC),* ATTN: SCBRD-RT, Aberdeen Proving Ground, MD 21010-5423. However, the Defense Technical Information Center and the National Technical Information Service are authorized to reproduce the document for U.S. Government purposes.

This report has been approved for release to the public.

Acknowledgments

The authors express their appreciation to Robert Doherty, ERDEC, for his support and guidance during the effort. In addition, appreciation is given to Dr. Andrew McFarland and his staff from the Department of Mechanical Engineering at Texas A&M University (College Station, TX) in performing the numerical model calculations and conducting the wind tunnel experiments; Dr. Vladimir Kogan, Battelle (Columbus, OH) in performing numerical model calculations; and Dr. Narayanan Rajendran, IITRI (Chicago, IL) in performing numerical model calculations.

---

*When this work was performed, ERDEC was known as the U.S. Army Chemical Research, Development and Engineering Center, and the Contracting Officer's Representative was assigned to the Research Directorate.

3

THIS PAGE INTENTIONALLY LEFT BLANK

CONTENTS

Page

6

LIST OF TABLES AND FIGURES

Table

Figure

9

THIS PAGE INTENTIONALLY LEFT BLANK

AEROSOL SAMPLING MODELS SURVEY

SECTION 1 - INTRODUCTION

1.1   BACKGROUND

Aerosol sampling and transport systems are extensively used for various applications that include measuring airborne particle size distributions and concentrations. Characterization of obscuration smokes is an example of such a use (Ref. 1).

In aerosol measurements, as in many other measurements, it is often not feasible to perform an _in situ_ measurement. There is a spatial distance between the site of measurement and the instrument in which the actual analysis is performed. In order to bridge this gap, a sample must be taken since in almost all cases it is impossible to analyze the total amount of aerosol (Ref. 2). The aerosol sample is then transported to the instrument.

Generally, aerosol sampling devices include an inlet sampling probe and a detector. Results of these measurements, as observed by the detector, do not usually reflect potential losses of particulate matter within the probe. Therefore, in many cases, accuracy of these measurements is not known due to the removal of particles from air streams in the inlet trains (Ref. 1).

The Obscuration Sciences Branch of Physics Division, Research Directorate at the U.S. Army Chemical Research, Development and Engineering Center, has undertaken a research project. This effort is aimed at identifying a comprehensive algorithm, computer program, or theory that might already exist and could be used to design aerosol sampling and transport systems. Initially, a literature survey was performed by the Obscuration Sciences Branch which began with several hundred potential articles and has been distilled to four candidate reports.

1.2   OBJECTIVE

The objective of this effort is two-fold: the first is to evaluate the four candidate aerosol sampling models for self consistency. The second is to compare the numerical calculations resulting from the four models and compare these model-derived results to the experimentally-derived results.

1.3 STUDY APPROACH

The technical approach used to accomplish the task objective hinged on the implementation of four key steps (phases).

In the first phase, information on each of the models was reviewed in order to gain an understanding of the theory, capabilities, limitations, and input parameters to the model. This first phase involves a write-up describing each of the models.

The second phase required development of an aerosol sampling train configuration upon which the numerical calculations would be performed and the experimental data would be generated. This phase required a write-up detailing the sampling train configuration.

The third phase required that numerical calculations be made for each of the four models based on the design parameters of a baseline simulated set of conditions.

The fourth phase required a comparison of the numerical calculations generated by the four models. In addition, a comparison will be made of these model-generated results to the experimentally-derived results. Findings, conclusions and recommendations will be compiled resulting from these comparisons.

SECTION 2 - AEROSOL SAMPLING MODEL DESCRIPTION

2.1 INTRODUCTION

As part of the literature search conducted by the Obscuration Sciences Branch to identify algorithms, computer programs, or theory which already exist and could be used to design aerosol sampling and transport systems, four candidate models/computer programs and/or theory/algorithms/equations were identified. The four candidates were the following:

- A numerical model and computer program developed by Texas A&M University, College Station, TX, to predict particle deposition in aerosol sampling lines due to turbulent diffusion and gravitational settling.

- An analytical model and computer program (SAMPF) developed by Battelle, Columbus, OH, to predict aerosol deposition in straight and bent circular pipes under turbulent flow conditions.

- A theoretical model and computer program developed by IITRI, Chicago, IL, to estimate sampling errors as a function of various inlet geometrics and parallel plates of various openings.

- A report authored by Drs. Fissan and Schwientek, University of Duisburg, GE, which gives the conditions for representative sampling in the case of a ducted aerosol flow, as well as equations that allow a first estimation of errors.

A description of the four candidate models is presented in the subsequent sections (i.e., Sections 2.2 to 2.5).

2.2 NUMERICAL MODEL DEVELOPED BY TEXAS A&M UNIVERSITY

A computer-based model to predict particle deposition in aerosol sampling lines due to turbulent diffusion and gravitational settling was developed by Mr. N.K. Anand and Dr. A. R. McFarland of Texas A&M University at College Station, TX (Ref. 3). Models developed by others for determining penetration through tube bends are included.

In modeling the individual components of the aerosol sampling train, consideration was first given to the inlet aspiration ratio A, where:

$$A = \frac{C_{in}}{C_o} \tag{1}$$

Here: C_o = aerosol concentration in the free stream and C_{in} = aerosol concentration at the entrance plane of the inlet. The model of Vincent et al. (Ref. 4) was used to compute the aspiration ratio, which gives:

$$A = 1 + \left[1 - \frac{1}{1 + 1.05 \cdot Stk \cdot (\cos\theta + 4 \cdot (R \cdot \sin\theta)^{0.5})} \right] (R \cdot \cos\theta - 1)$$

(2)

Where: $R = W/V$, W = airstream velocity, V = velocity at the entrance plane of the inlet, θ = angle between the wind velocity vector and the tube axis vector (which faces into the inlet), and Stk = Stokes number. The Stokes number is given by:

$$Stk = \frac{C \cdot d \cdot D_p^2 \cdot W}{9 \cdot \mu \cdot D_s}$$

(3)

The additional parameters in the Stokes number are: C = Cunningham's slip correction (Ref. 5), d = particle density, D_p = particle diameter, μ = air viscosity, and D_s = inlet diameter (which, in this system, is the same as the tube inside diameter).

Once the aerosol is inside the inlet there are losses in the developing boundary layer due to gravitational and inertial forces. Okazaki and Willeke (Ref. 6) presented a semiempirical model which predicts these inlet losses. They note that supportive experiments were mostly conducted with tube Reynolds numbers less than 2000. Their model is:

$$P = 1 - \exp\left[-4.7 \cdot K^{0.75} \right]$$

(4)

where:

$$K = \left[\frac{Z \cdot Stk}{Re^{0.5}} \right]^{0.5}$$

(5)

The parameter Z used in Equation 5 is the gravitational settling number and is given by:

$$Z = \frac{L \cdot V_g}{W \cdot D_s}$$

(6)

where: L = tube length over which sedimentation in the developing boundary layer is important and V_g = particle gravitational settling terminal velocity. In turn, V_g is calculated from:

14

$$V_g = \frac{C \cdot d \cdot D_p^2 \cdot g}{18 \cdot \mu} \tag{7}$$

where: g = local gravitational constant.

In using the model of Okazaki and Willeke, Texas A&M assumed that the phenomena were of consequence over the first 20 cm of the first horizontal straight section of tubing. For the remainder of this section and the other straight sections, Texas A&M used the model of Anand and McFarland (Ref. 3) which takes into account both gravitational settling and turbulent deposition and which is applicable to horizontal, inclined and vertical tubes. The model uses the expression for the penetration of aerosol particles through a straight tube:

$$P = \exp \left[-\frac{\pi \cdot D_s \cdot V_e \cdot L}{Q} \right] \tag{8}$$

where: V_e = effective depositional velocity of aerosol particles to the tube walls, L = length of tube and Q = volumetric flow rate. The depositional velocity is comprised of that due to turbulent diffusion, V_{td}, that due to gravitational settling, V_g, and that due to thermal diffusion, V_d. The velocity vectors for thermal and turbulent diffusional deposition are both normal to the tube wall whereas the gravitational deposition is antiparallel to the gravitational vector. In the present application, the depositional losses due to diffusion are of no consequence and will be neglected. For the model of Anand and McFarland (Ref. 3), the effective depositional velocity is calculated from:

$$V_e = \frac{1}{2\pi} \int_0^{2\pi} (V_d - V_{ge}\sin\alpha) \, d\alpha \tag{9}$$

where: $V_{ge} = V_g \sin\phi$, ϕ = angle of inclination of the pipe relative to the vertical direction, α = angle in the tube cross section between a radius vector and x-axis of the horizontal plan. The integral is subject to the constraint:

$$(V_d - V_{ge} \sin \alpha) > 0 \tag{10}$$

15

If the constraint is not satisfied, $V_e = 0$. This constraint is necessary since otherwise the physical situation would be equivalent to mass being transported from the environment through the top (relative to the gravitational vector) side of the tube wall.

The Texas A&M model originally utilized the results of Liu and Agarwal (Ref. 7) to predict the turbulent depositional velocity, V_{td}. Their semiempirical expression is:

$$V_{td} = V_+ \cdot W \cdot (f/2)^{0.5} \qquad (11)$$

Here, f is the friction factor of the airflow in the tube which, for a smooth wall pipe, can be represented by Blasius' equation:

$$f = \frac{0.316}{4 \cdot Re^{0.25}} \qquad (12)$$

The parameter V_+ is the dimensionless particle deposition velocity and is given by:

$$V_+ = 6.9 \times 10^{-4} \, \tau_+ \qquad \text{for } \tau_+ \leq 15$$

$$V_+ = 0.16/ \, \tau_+^{0.086} \qquad \text{for } \tau_+ > 15 \qquad (13)$$

Here, τ_+ is the dimensionless stopping distance and is given by:

$$\tau_+ = \tau \cdot V_*^2 \, / \, v \qquad (14)$$

where: τ = particle stopping distance, V_* = friction velocity and v = kinematic viscosity of air. In turn, these parameters may be expressed as:

$$\tau = V_g \, / \, g \qquad (15)$$

$$V_* = (f/2)^{0.5} \cdot V \qquad (16)$$

where: V = spatial mean air velocity in the tube.

Recently, Texas A&M has modified their model to utilize the predictive capabilities of the Beal (Ref. 8) formulation for turbulent and thermal diffusional losses in straight tubes. Beal's model is much more complicated than that of Liu and Agarwal and its basis will not be discussed herein; however, for particles in the inertial range, the two models give similar results. The computations which were carried in the present study employed the model of Beal.

Particle deposition in tube bends can be correlated with the Stokes number (Cheng and Wang (Ref. 9), Pui et al., (Ref. 10)). For this task, Texas A&M has used the model of Pui et al., which for 90° bends is:

$$P = 10^{-0.963 \, Stk} \tag{17}$$

For 45° bends, the numerical factor in the exponent of Equation (17) is 0.482.

To calculate overall aerosol penetration through the tubing system, $P_{o,i}$, for monodisperse aerosols of size $D_{p,i}$, Texas A&M used the expression (Ref. 11):

$$P_{o,i} = \pi_j \, P_{i,j} \tag{18}$$

where: $P_{i,j}$ = penetration of the ith particle size through the jth component (inlet aspiration, turbulent deposition, etc.). Data are reported for both the overall penetration and the penetration for the individual components.

For the calculational cases involving aerosol penetration through the individual tubing components, the order of the calculations makes no difference if the aerosol is monodisperse; however, if the aerosol is polydisperse, the calculations must be carried out for the actual sequence of components in the tubing system layout.

The calculations for polydisperse aerosols were performed by first subdividing a log-normal distribution into thirty particle size increments. The aerosol penetration through the jth component of the system is based on:

$$P_j = C_j \, / \, C_{j-1} \tag{19}$$

where: C_j = relative aerosol concentration at the exit plane of the jth component and C_{j-1} = relative aerosol concentration at the entrance of the jth component. It was assumed that the aerosol concentration in the free stream was unity. The parameter C_j was determined by adding the concentration values associated with each of k particle size increments.

$$C_j = \sum_k C_{j,k} \tag{20}$$

The change in aerosol concentration of the kth particle size increment was obtained from the appropriate component model (inlet aspiration, elbow, etc.).

17

2.3 NUMERICAL MODEL DEVELOPED BY IITRI

A theoretical model and computer program was developed by IITRI (Ref. 12) to estimate sampling errors as a function of various inlet geometries (e.g., circular tube of thick and thin wall and parallel plates), of various openings. Samplers whose face is not perpendicular to the ambient flow are simulated by a line sink/source in a uniform stream.

The computer program actually consists of two separate programs (Ref. 12). Program "FLOWFI" solves the fluid flow in and around the sampling head with circular/parallel plate geometry. Program "TRAJEC" computes the particle trajectories in the specified flow region. The IITRI model accounts for inertial and sedimentation effects on particle motion. Types of flow simulated include calm air, variable flow directions, and turbulent flow.

General equations of the IITRI model are the following:

$$\text{Sampling efficiency} = n = \frac{C}{C_o} = \frac{C_I}{C_o} \cdot \frac{C}{C_I} = E \cdot \frac{U_o}{U} \cdot \frac{\delta C}{C_I}$$

$$= E \cdot \frac{U_o}{U} \cdot \frac{C_I - \delta C}{C_I} \tag{21}$$

Where:
  C_o = number of particles/unit volume in free stream
  C = actual number of particles sensed by instrument
  C_I = concentration at inlet to probe
  δC = loss of particles in probe (= C_I - C)
  E = efficiency of capture of inlet
  U_o = free stream velocity
  U = suction velocity of the sample

To determine the "C" terms, equations of motion/particle trajectory equations are derived and solved, to include solutions for samples at various angles to oncoming flow. An iterative solution is used to determine when a particle in the free stream actually passes through the inlet. The equations are a function of Stokes number, sedimentation velocities, fluid velocities, and particle velocities, all relative to the orientation thickness of the inlet (i.e., the equations solved indicate whether a particle goes into the inlet, hits the inlet wall, or goes "around" the inlet).

Assumptions made for solving motion/particle equations are the following:

- Particles are uniformally distributed and move with same velocity as free stream when far from inlet.

- Particles are spherical and do not change in size due to agglomeration or other factors.

- Particles are "small" in comparison to probe size and move as individual particles with no hydrodynamic interactions among themselves or between probe walls.

2.4   NUMERICAL MODEL DEVELOPED BY BATTELLE

Battelle had developed earlier an analytical model which addressed aerosol deposition in straight and bent circular pipes under turbulent flow conditions (Ref. 13). In order to perform the model calculations required under this effort for the Obscuration Sciences Branch, Battelle modified it's existing computer models. The models were modified to specifically address aerosol deposition in a sampling probe which resulted in the SAMPLF computer program (Ref. 1). The calculation of particle behavior in SAMPLF is done using turbulent air flow models for straight pipes and round circular bends.

Turbulent deposition of particles in straight pipes is treated with the assumption that the deposition surface may not be ideally smooth, and even the particles deposited may result in an increased roughness. The calculation of aerosol deposition from turbulent flow to a rough surface is performed in SAMPLF using correlations developed by Wood (Ref. 14). According to this approach, deposition of particles due to molecular diffusion enhanced by turbulent eddies and due to inertial effect are both considered.

In bends, there exists a secondary flow that promotes a more energetic hydrodynamic regime and higher pressure drop as compared to a smooth straight pipe of the same length. This provides favorable conditions for the diffusional and inertial deposition of aerosol particles from the turbulent flow in a bent pipe.

The Battelle model uses an assumption that turbulent deposition velocities of suspended particles in a curved pipe and in a straight rough pipe of the same length are equal if the pressure drops across them, which are caused by the wall friction, are the same. In other words, SAMPLF calculates turbulent deposition in a round bend by calculating deposition in

19

a section of a pressure-equivalent straight pipe of identical length and of such a roughness that it provides a identical resistance coefficient.

In addition to turbulent deposition, SAMPLF considers gravitational settling of particles to the horizontal surfaces of the pipes. As a first approximation, the Stokes' formulation of settling velocity is used.

SAMPLF calculates the steady-state deposition and transport of aerosols through the sampling system. It calculates fluid thermo- and hydrodynamics properties for an arbitrary set of sample flow rates, temperature, and air humidity, and uses these properties for evaluating the transport parameters for airborne particulate matter.

Since aspiration, or inlet efficiency is currently not considered by the model, isokinetic sampling is assumed in the calculations. Also, this version of the program does not consider the potential for resuspension of deposited particles.

2.5   NUMERICAL MODEL DEVELOPED BY UNIVERSITY OF DUISBURG

The Fissan and Schwientek paper (referred to in this report as the University of Duisburg model) (Ref. 2) gives the conditions for representative sampling of aerosols for the case of sampling of an aerosol flowing through a duct using a thin walled probe facing upstream (0° inlet orientation). Equations are presented which allow a first estimation of errors caused by anisokinetic sampling. In addition, equations are presented which address the particle deposition effects in the transport of the aerosol to the site of the analysis. The transport deposition effects considered, in laminar and turbulent flow, are Brownian diffusion, gravitational settling, and inertial deposition. Although these effects are interdependent, they are treated separately in the paper.

The discussion of the paper will be presented in three parts. These three parts relate specifically to different regions of the aerosol sampling train. The three parts are the following:

- Calculation of the sampling efficiency
- Calculation of transport efficiency through a straight tube
- Calculation of transport efficiency through a 90° bend

A listing of the computer program by General Management Associates (GMA) which incorporates and extends the equations presented in the Fissan and Schwientek paper is attached at Appendix A.

20

2.5.1   CALCULATION OF THE SAMPLING EFFICIENCY

The sampling efficiency, e_s, is the ratio of the sampled aerosol concentration to the ambient aerosol concentration. This efficiency is a function of the Stokes number, Stk_w, and the ratio W/V, where W is the face velocity of the aerosol and V is the suction veloctiy created by the sampling probe. For sampling, the Stokes number is given by the following relation.

$$Stk_w = \frac{C \cdot d \cdot D_p^2 \cdot W}{9 \cdot \mu \cdot D_s} \qquad (22)$$

where W = Face velocity
         D_s = Inside diameter of probe
         μ = Dynamic viscosity of fluid
         d = Density of aerosol particle
         D_p = Diameter of aerosol particle
         C = Cunningham slip correction

The Cunningham slip correction is given by:

$$C = 1 + \frac{2}{P \cdot D_p} \left[6.32 + 2.01 \cdot \exp(-.1095 \cdot P \cdot D_p) \right] \qquad (23)$$

where P = Ambient pressure in cm Hg
         D_p = Diameter of aerosol particle in microns

The sampling efficiency is given by:

$$e_s = 1 + (W/V - 1) \left[\frac{2 \cdot (W/V) + 0.62}{(W/V) \cdot Stk_w^{-1} + 2 \cdot (W/V) + 0.62} \right] \qquad (24)$$

2.5.2   CALCULATION OF TRANSPORT EFFICIENCY THROUGH A STRAIGHT TUBE

In laminar flow, the aerosol particle losses occur by two mechanisms, Brownian diffusion and gravitational sedimentation. The losses through a section of straight tube by Brownian diffusion are independent of the orientation of that tube within a gravitational field. The following are the equations describing aerosol particle losses due to Brownian diffusion under laminar flow conditions.

21

$$n = 0.819 \cdot e^{-3.657X} + 0.097 \cdot e^{-22.3X} + 0.032 \cdot e^{-57X}$$

for $X > 0.02$ (25)

$$n = 1 - 2.56 \cdot X^{2/3} + 1.2 \cdot X + 0.177 \cdot X^{4/3}$$

for $X < 0.02$ (26)

where X = $\pi \cdot D \cdot L / Q$
               D = Brownian diffusion coefficient of aerosol particle
               L = Length of the tube
               Q = Volumetric flow rate within tube

      The Brownian diffusion coefficient of the aerosol particle is calculated from the following equation.

$$D = \frac{k \cdot T \cdot C}{3 \cdot \pi \cdot \mu \cdot D_p} \qquad (27)$$

where k = Boltzman's constant
               T = Absolute temperature within probe
               C = Cunningham slip correction
               μ = Dynamic viscosity of fluid
               D_p = Diameter of aerosol particle

      The aerosol particle losses in a *horizontal tube* due to gravitational sedimentation is representated by the following equation.

$$n = 1 - \frac{2}{\pi} \left[2 \cdot \phi \cdot (1 - \phi^{2/3})^{1/2} + \sin^{-1} \phi^{1/3} - \phi^{1/3} \cdot (1 - \phi^{2/3})^{1/2} \right]$$

$$(28)$$

where ϕ = $(3/8) \cdot (L/R) \cdot (V_s/V)$
               L = Length of the tube
               R = Radius of the tube
               V_s = Sedimentation velocity
               V = Linear velocity in the tube

The aerosol particle sedimentation velocity can be expressed as:

$$V_s = 0.003 \cdot d \cdot D_p^2 \qquad (29)$$

where d = Aerosol particle density in gm/cm^3
               D_p = Aerosol particle diameter in microns

      Under conditions of turbulent flow, the aerosol particle losses are due to Brownian diffusion and inertial deposition effects. The model describing the transport

efficiency is the same for both Brownian diffusion and inertial deposition, differing only in the calculation of u, the particle deposition velocity. This model is given by the following relation:

$$n = \exp\left[\frac{-2 \cdot \pi \cdot R \cdot L \cdot u}{Q}\right] \qquad (30)$$

where   R = Radius of the tube
         L = Length of the tube
         Q = Volumetric flow rate within tube

For losses due to Brownian diffusion, the particle deposition velocity is given by the following equation.

$$u = 0.042 \cdot V \cdot f^{1/2} \cdot Sc^{-2/3} \qquad (31)$$

where   f = Fanning friction factor
         Sc = Schmidt number
         V = Linear velocity in the tube

The Schmidt number is given by:

$$Sc = \frac{v}{D} \qquad (32)$$

where   v = Kinematic viscosity of the fluid
         D = Brownian diffusion coefficient of aerosol particle

The Fanning friction factor is given by:

$$f = \frac{0.316}{4 \cdot Re^{1/4}} \qquad (33)$$

where   Re = Reynold's number for tube

The Reynold's number for flow through a tube is given by the following relation:

$$Re = \frac{D_s \cdot V \cdot d}{\mu} \qquad (34)$$

where D_s = Diameter of the tube
         V = Linear velocity in the tube
         d = Density of the fluid
         μ = Dynamic viscosity of the fluid

23

For inertial deposition of aerosol particles, the particle deposition velocity is given by:

$$u = u_+ \cdot u^*$$ (35)

where $u^* = (f/2)^{1/2} \cdot V$

$u_+ = (6 \times 10^{-4}) \cdot \tau_+^2$

τ_+ = Dimensionless relaxation time

The dimensionless relaxation time is given by:

$$\tau_+ = \frac{\tau \cdot u^{*2}}{V}$$ (36)

where τ = Particle relaxation time

V = Kinematic viscosity

The particle relaxation time may be calculated from the following equation:

$$\tau = \frac{D_p^2 \cdot d \cdot C}{\mu}$$ (37)

where D_p = Diameter of aerosol particle

d = Density of aerosol particle

C = Cunningham slip correction

μ = Dynamic viscosity of fluid

2.5.3 CALCULATION OF TRANSPORT EFFICIENCY THROUGH A 90° BEND

For conditions of laminar flow, the transport efficiency of an aerosol particle through a 90° bend is given by:

$$n = 1 - Stk$$ (38)

where Stk = Stokes number

For turbulent flow, the transport efficiency of an aerosol particle through a 90° bend is given by:

$$n = 10^{-0.963 Stk}$$ (39)

where Stk = Stokes number

For the 90° bend model, the Stokes number is given as:

$$Stk = \frac{C \cdot d \cdot D_p^2 \cdot V}{9 \cdot \mu \cdot D_s}$$ (40)

where V = Linear velocity within tube
                 D_s = Inside diameter of tube
                 μ = Dynamic viscosity of fluid
                 d = Density of aerosol particle
                 D_p = Diameter of aerosol particle
                 C^p = Cunningham slip correction

THIS PAGE INTENTIONALLY LEFT BLANK

SECTION 3 - AEROSOL SAMPLING TRAIN CONFIGURATION FOR NUMERICAL CALCULATIONS AND EXPERIMENTAL VERIFICATION

3.1 PHYSICAL DESCRIPTION

The geometry of the aerosol sampling train which was configured for the model calculations and the experimental verification is presented in Figure 1. As shown in the figure, the sampling train is subdivided into six consecutive sections. They are the following: inlet, three 2-foot long straight sections - horizontal, vertical, and inclined - connected by a 90° elbow and a 45° elbow, respectively. Both elbows have 3-inch radii as measured from their centers of curvature to the elbow centerlines. The whole train is made of a nominal 3/4-inch schedule 40 PVC smooth wall electrical conduit which has an inside diameter of 1.05 inches. The conduit is assumed to have a surface roughness typical for drawn tubing (brass, lead, glass, and the like) (Ref. 15). Two inlet configurations (inlet oriented parallel to the air stream (0°) and perpendicular to the air stream (90°)) are being considered.

3.2 REGION OF AEROSOL SAMPLING TRAIN ADDRESSED BY FOUR MODELS

Each of the four candidate "models" discussed in Section 2 simulate/characterize different regions of the six section aerosol sampling train. Each model's characterization of the different regions of the sampling train is presented in Table 1. As Table 1 points out, the Texas A&M and Battelle models are the only two which simulate the 90° and 45° bends, and the horizontal, vertical and inclined sections. The Texas A&M model is the only one which simulates the six regions of the sampling train. Figure 2 presents graphically the regions of the sampling train which are characterized/simulated in each model.

3.3 PARAMETERS OF MODEL CALCULATIONS AND EXPERIMENTAL VERIFICATION

Model calculations and experimental data (to determine cumulative sampling efficiency (% mass)) were generated for sampling flow rates, 70 l/min and 130 l/min, and an ambient wind speed of 3 m/sec. Seven monodispersed aerosols having aerodynamic equivalent particle diameter (AED) of 3,5,7,10,15,20, and 25 micrometers are generated and sampled. AED is defined as the diameter of a water droplet of unit specific gravity which has the same time constant, t, as an arbitrary particle of density d and equivalent diameter D_p. In addition, two log-normal aerosol distributions were generated having 5 and 10 aerodynamic mass median diameter (micrometers) and each with a geometric standard deviation of 1.5 micrometers. Unit density was assumed for all airborne aerosol particles. A matrix containing the 36 simulation cases to be conducted is presented in Table 2.

27
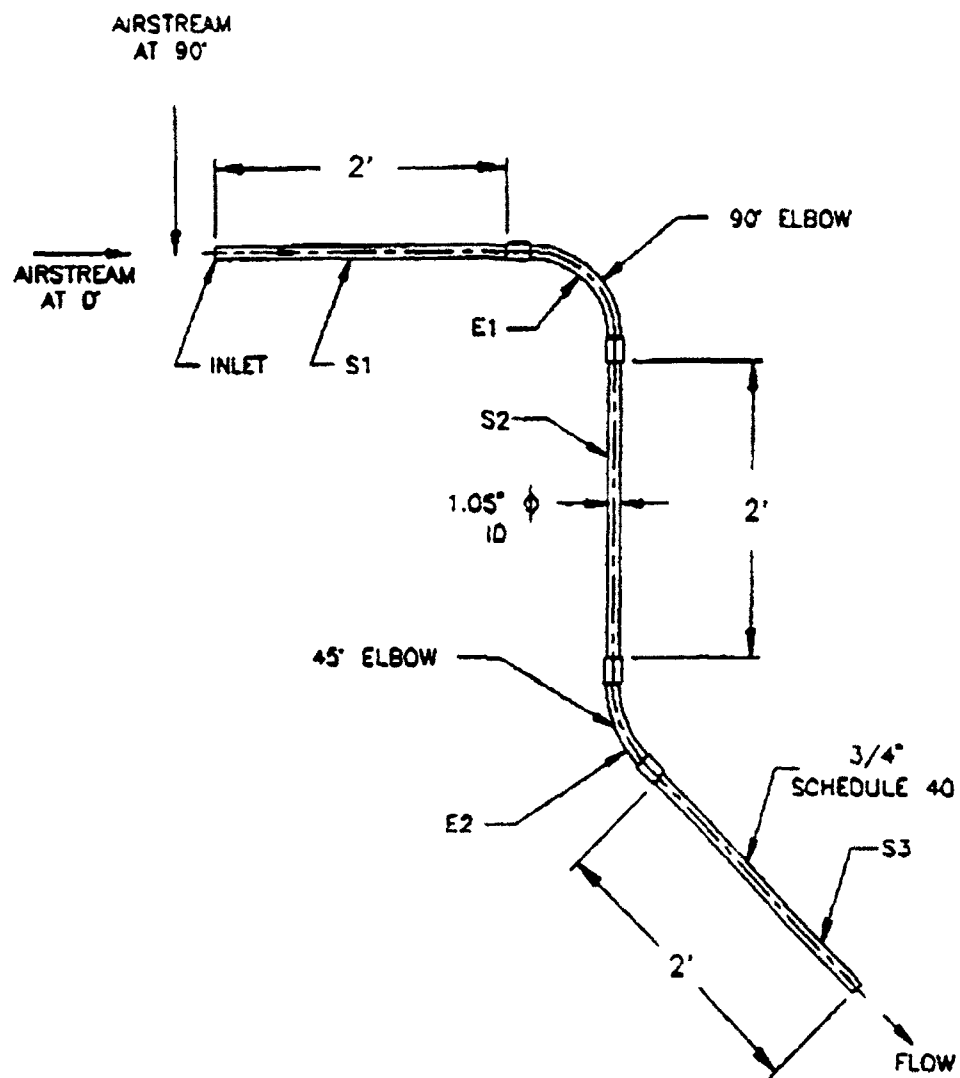
Figure 1. Schematic of Aerosol Sampling Train

REGIONS OF AEROSOL SAMPLING TRAIN SIMULATED/CHARACTERIZED

MODEL	INLET PROBE/ORIFICE	PROBE ORIENTATION TO FLOW	HORIZONTAL SECTION	90° BEND	VERTICAL SECTION	45° BEND	INCLINED SECTION
TEXAS A & M	YES: THIN WALL, CIRCULAR	0°, 90° and -90°	YES	YES	YES	YES	YES
BATTELLE	NO: ASSUMED IDEAL INLET (100% EFFICIENCY)	NONE	YES	YES	YES	YES	YES
IITRI	YES: THIN AND THICK WALL, CIRCULAR, RECTANGULAR, VARIABLE OPENINGS	0° to ± 90°	NO	NO	NO	NO	NO
UNIVERSITY OF DUISBURG	YES: DUCTED, THIN WALLED PROBE (CIRCULAR); DIAMETER OF INLET BASED ON RATIO OF FACE VELOCITY TO SUCTION VELOCITY (FUNCTIONALIZED DIAMETER)	0°	YES	YES	YES	NO	NO

Table 1. Four Candidates Models' Characterization/Simulation of Aerosol Sampling Train

Legend:

V_o = Windspeed
C_o = Aerosol Mass Concentration at Probe Inlet Location
V = Suction Velocity
C = Aerosol Mass Concentration Sampled by Instrument
α = Probe Orientation to Oncoming Air Flow
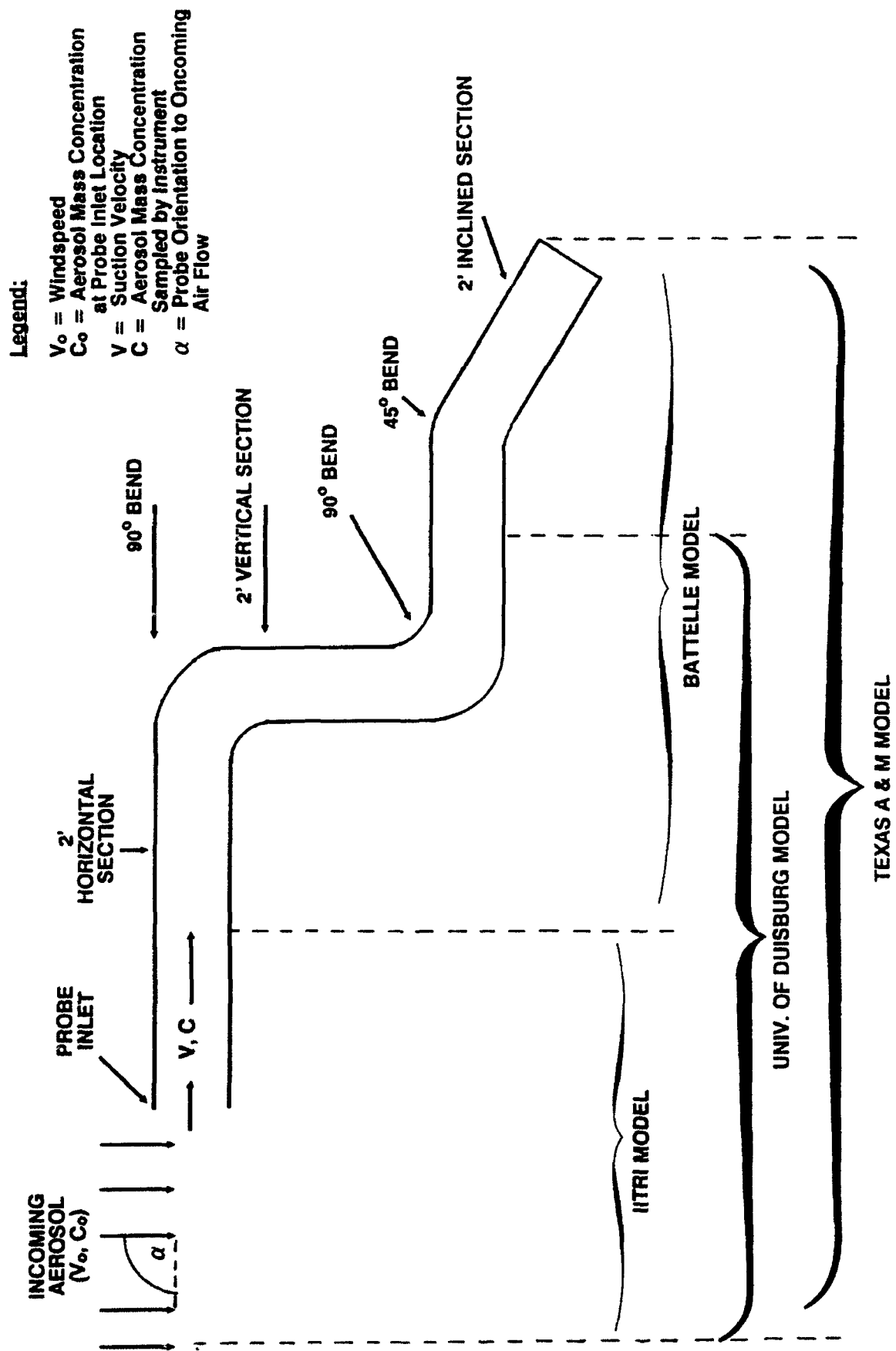
Figure 2. Regions of Sampling Train Characterized/Simulated by Each Candidate Model

TYPE OF PARTICLE DISTRIBUTION	PARTICLE SIZE (μ)	INLET PROBE ORIENTATION (α)	FLOW RATE (l/min)	WIND SPEED (m/sec)
1. MONODISPERSED	3	0°	70	3
2. MONODISPERSED	5	0°	70	3
3. MONODISPERSED	7	0°	70	3
4. MONODISPERSED	10	0°	70	3
5. MONODISPERSED	15	0°	70	3
6. MONODISPERSED	20	0°	70	3
7. MONODISPERSED	25	0°	70	3
8. MONODISPERSED	3	0°	130	3
9. MONODISPERSED	5	0°	130	3
10. MONODISPERSED	7	0°	130	3
11. MONODISPERSED	10	0°	130	3
12. MONODISPERSED	15	0°	130	3
13. MONODISPERSED	20	0°	130	3
14. MONODISPERSED	25	0°	130	3
15. MONODISPERSED	3	90°	70	3
16. MONODISPERSED	5	90°	70	3
17. MONODISPERSED	7	90°	70	3
18. MONODISPERSED	10	90°	70	3
19. MONODISPERSED	15	90°	70	3
20. MONODISPERSED	20	90°	70	3
21. MONODISPERSED	25	90°	70	3
22. MONODISPERSED	3	90°	130	3
23. MONODISPERSED	5	90°	130	3
24. MONODISPERSED	7	90°	130	3
25. MONODISPERSED	10	90°	130	3
26. MONODISPERSED	15	90°	130	3
27. MONODISPERSED	20	90°	130	3
28. MONODISPERSED	25	90°	130	3
29. POLYDISPERSED	MMAD=5 (σ =1.5)	0°	70	3
30. POLYDISPERSED	MMAD=15 (σ =1.5)	0°	70	3
31. POLYDISPERSED	MMAD=5 (σ =1.5)	0°	130	3
32. POLYDISPERSED	MMAD=15 (σ =1.5)	0°	130	3
33. POLYDISPERSED	MMAD=5 (σ =1.5)	90°	70	3
34. POLYDISPERSED	MMAD=15 (σ =1.5)	90°	70	3
35. POLYDISPERSED	MMAD=5 (σ =1.5)	90°	130	3
36. POLYDISPERSED	MMAD=15 (σ =1.5)	90°	130	3

Table 2. Matrix of Simulation Cases to be Generated for Aerosol Sampling Train Configuration

THIS PAGE INTENTIONALLY LEFT BLANK

SECTION 4 - RESULTS OF MODEL NUMERICAL CALCULATIONS

4.1   RESULTS FROM TEXAS A&M MODEL

As mentioned earlier, numerical calculations using the
Texas A&M model were made for two log-normally distributed
aerosols and seven monodispersed aerosols for two flow rates and
two probe inlet orientations. The cumulative sampling efficiency
results (% mass) for these 36 simulation cases are summarized in
Table 3 and graphically presented in Figures 3 and 4. The
complete set of numerical calculations produced by the Texas A&M
model are provided at Appendix B.

4.1.1   Results of Monodispersed Simulation Cases

The cumulative sampling efficiency results for a
monodispersed aerosol distribution indicate the following:

- As the particle size increases, the sampling efficiency
  decreases.

- An increase in the inlet probe orientation ($0°$ to $90°$)
  will result in a decreased sampling efficiency.

- As the flow rate increases from 70 1/min to 130 1/min,
  the sampling efficiency decreases.

- The larger the particle size the greater the decrease
  in sampling efficiency.

- Increase in the inlet probe orientation produces a more
  dramatic decrease in the sampling efficiency than does
  an increase in the flow rate.

- Particle depositional losses in the elbows are
  generally larger than those in the other components of
  the sampling train.

4.1.2   Results of Polydispersed Simulation Cases

The cumulative sampling efficiency results for a
polydispersed aerosol distribution indicate the following:

- As the mass median aerodynamic diameter (MMAD)
  increases, the sampling efficiency decreases.

- As the flow rate increases, the sampling efficiency
  decreases.

33

TYPE OF PARTICLE DISTRIBUTION	PARTICLE SIZE (μ)	INLET PROBE ORIENTATION (α)	FLOW RATE (l/min)	WIND SPEED (m/sec)	CUMULATIVE SAMPLING EFFICIENCY (% mass)
1. MONODISPERSED	3	0°	70	3	97.4
2. MONODISPERSED	5	0°	70	3	93.6
3. MONODISPERSED	7	0°	70	3	88.4
4. MONODISPERSED	10	0°	70	3	78.6
5. MONODISPERSED	15	0°	70	3	59.0
6. MONODISPERSED	20	0°	70	3	39.2
7. MONODISPERSED	25	0°	70	3	22.8
8. MONODISPERSED	3	0°	130	3	96.3
9. MONODISPERSED	5	0°	130	3	90.4
10. MONODISPERSED	7	0°	130	3	82.5
11. MONODISPERSED	10	0°	130	3	67.8
12. MONODISPERSED	15	0°	130	3	41.0
13. MONODISPERSED	20	0°	130	3	16.6
14. MONODISPERSED	25	0°	130	3	5.6
15. MONODISPERSED	3	90°	70	3	94.3
16. MONODISPERSED	5	90°	70	3	85.6
17. MONODISPERSED	7	90°	70	3	74.7
18. MONODISPERSED	10	90°	70	3	57.0
19. MONODISPERSED	15	90°	70	3	31.5
20. MONODISPERSED	20	90°	70	3	15.2
21. MONODISPERSED	25	90°	70	3	6.4
22. MONODISPERSED	3	90°	130	3	94.3
23. MONODISPERSED	5	90°	130	3	85.5
24. MONODISPERSED	7	90°	130	3	74.0
25. MONODISPERSED	10	90°	130	3	55.1
26. MONODISPERSED	15	90°	130	3	27.1
27. MONODISPERSED	20	90°	130	3	8.7
28. MONODISPERSED	25	90°	130	3	2.4
29. POLYDISPERSED	MMAD=5 (σ =1.5)	0°	70	3	91.9
30. POLYDISPERSED	MMAD=15 (σ =1.5)	0°	70	3	55.5
31. POLYDISPERSED	MMAD=5 (σ =1.5)	0°	130	3	87.8
32. POLYDISPERSED	MMAD=15 (σ =1.5)	0°	130	3	40.1
33. POLYDISPERSED	MMAD=5 (σ =1.5)	90°	70	3	82.6
34. POLYDISPERSED	MMAD=15 (σ =1.5)	90°	70	3	33.4
35. POLYDISPERSED	MMAD=5 (σ =1.5)	90°	130	3	82.2
36. POLYDISPERSED	MMAD=15 (σ =1.5)	90°	130	3	29.8

Table 3. Cumulative Sampling Efficiency Results by Texas A & M Model

Figure 3. Penetration Efficiency

Texas A&M Model Monodispersed Results

□   70 L/min 0°   +   1.30 L/min 0°   ◊   70 L/min 90°   △   1.30 L/min 90°
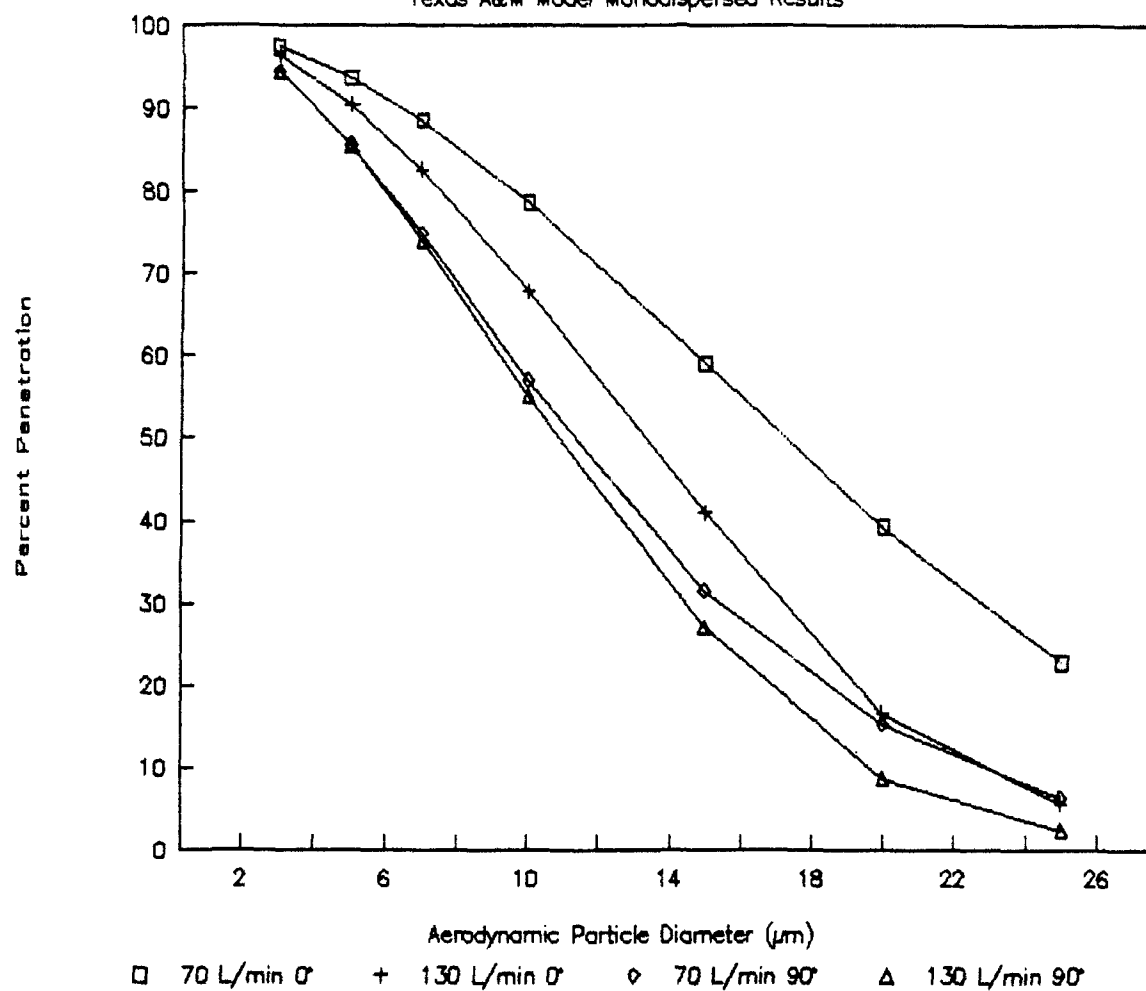
Figure 4. Penetration Efficiency

Texas A&M Model Polydispersed Results

Legend: □ 70 L/min 0°   + 130 L/min 0°   ◊ 70 L/min 90°   △ 130 L/min 90°

X-axis: Mass Median Aerodynamic Diameter (μm)

Y-axis: Percent Penetration
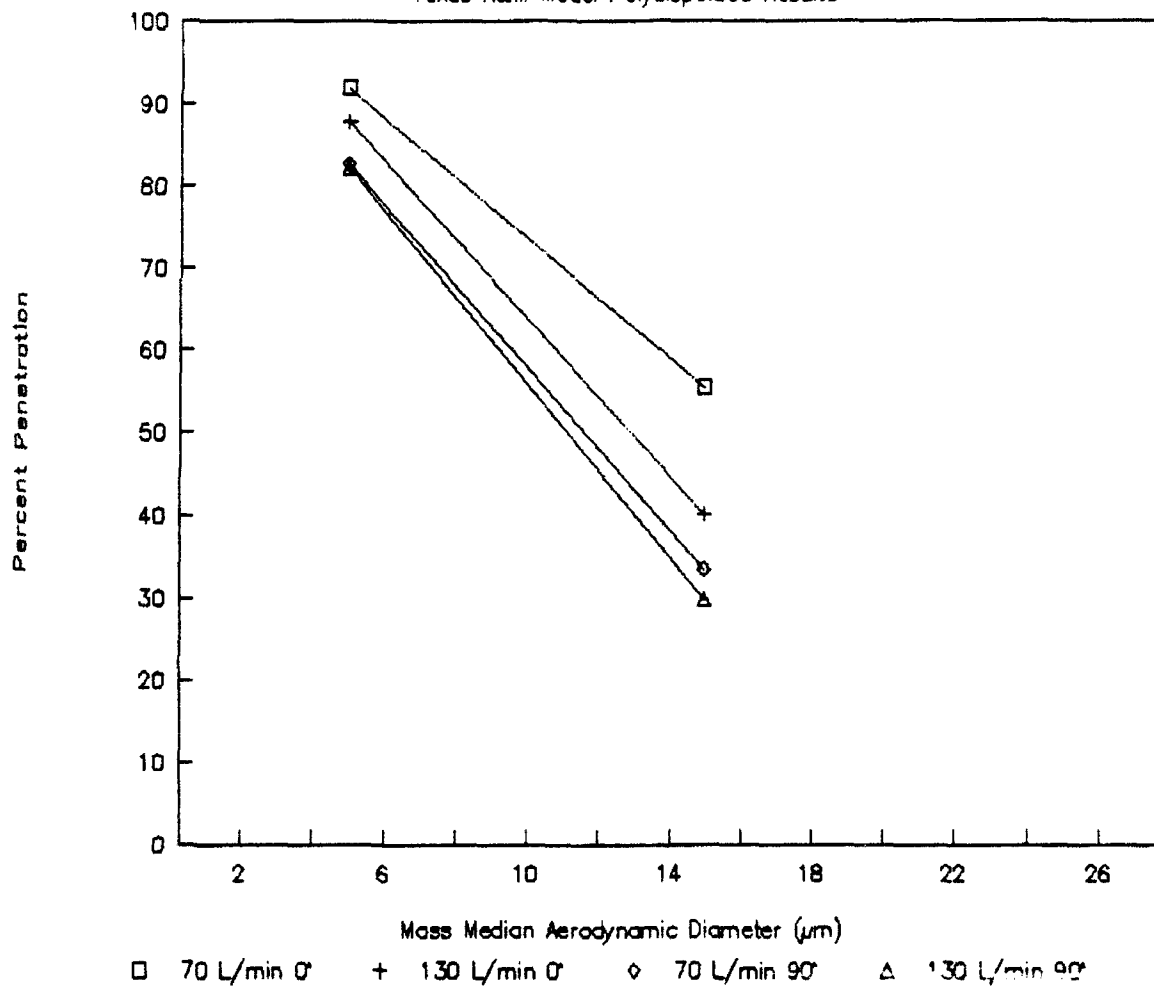
● As the inlet probe orientation increases, the sampling efficiency decreases.

● Increase in the inlet probe orientation produces a more dramatic decrease in the sampling efficie~ ~y than does an increase in the flow rate.

● The 5μm MMAD polydispersed particle distribution produces smaller sampling efficiencies than does the 5μm monodispersed particle distribution. However, the differences in efficiency (typically a few percent) are considered insignificant.

● The 15μm MMAD polydispersed particle distribution produces smaller sampling efficiencies than does the 15 μm monodispersed particle distribution for only the 0° inlet probe orientation and 70 l/min flow rate. Again, these differences are considered insignificant. For other combinations of inlet probe orientation and flow rate, the 15 μm MMAD polydispersed particle distribution produces greater sampling efficiencies than does the 15 μm monodispersed particle distribution. As with the other comparisons, the efficiency differences are considered insignificant.

4.2 RESULTS FROM IITRI MODEL

As discussed earlier, the IITRI model calculates sampling efficiencies based on characterization of the inlet probe only. None of the other regions of the aerosol sampling train are addressed. The complete set of numerical calculations produced by the IITRI model is provided at Appendix C.

Sampling efficiencies as a function of monodispersed particle size were calculated for 28 simulation cases and are presented in Table 4 and graphically presented in Figure 5. These results indicate the following:

● As the particle size increases, the sampling efficiency decreases for the conditions of an inlet probe orientation of 0° and 90° and a flow rate of 130 l/min, and also the cases for an inlet probe orientation of 90° and a flow rate of 70 l/min. The cases for a 0° inlet probe orientation and 70 l/min flow rate resulted in an increase in the sampling efficiency as the particle size increases.

● The following conditions in descending order resulted in the greatest decrease in sampling efficiency as the particle size increases.

TYPE OF PARTICLE DISTRIBUTION	PARTICLE SIZE (μ)	INLET PROBE ORIENTATION (α)	FLOW RATE (l/min)	WIND SPEED (m/sec)	SAMPLING EFFICIENCY OF INLET PROBE (% mass)
1. MONODISPERSED	3	0°	70	3	100.7
2. MONODISPERSED	5	0°	70	3	100.7
3. MONODISPERSED	7	0°	70	3	100.7
4. MONODISPERSED	10	0°	70	3	100.7
5. MONODISPERSED	15	0°	70	3	108.4
6. MONODISPERSED	20	0°	70	3	114.7
7. MONODISPERSED	25	0°	70	3	121.2
8. MONODISPERSED	3	0°	130	3	94.1
9. MONODISPERSED	5	0°	130	3	94.1
10. MONODISPERSED	7	0°	130	3	94.1
11. MONODISPERSED	10	0°	130	3	93.0
12. MONODISPERSED	15	0°	130	3	91.9
13. MONODISPERSED	20	0°	130	3	91.9
14. MONODISPERSED	25	0°	130	3	90.9
15. MONODISPERSED	3	90°	70	3	89.3
16. MONODISPERSED	5	90°	70	3	89.3
17. MONODISPERSED	7	90°	70	3	88.3
18. MONODISPERSED	10	90°	70	3	87.2
19. MONODISPERSED	15	90°	70	3	79.9
20. MONODISPERSED	20	90°	70	3	75.9
21. MONODISPERSED	25	90°	70	3	71.3
22. MONODISPERSED	3	90°	130	3	85.4
23. MONODISPERSED	5	90°	130	3	85.3
24. MONODISPERSED	7	90°	130	3	84.7
25. MONODISPERSED	10	90°	130	3	84.8
26. MONODISPERSED	15	90°	130	3	81.2
27. MONODISPERSED	20	90°	130	3	76.1
28. MONODISPERSED	25	90°	130	3	70.2

Table 4. Cumulative Sampling Efficiency Results Generated by IITRI Model

Figure 5. Penetration Efficiency

IITRI Model Monodispersed Results

Legend: □ 70 L/min 0° + 130 L/min 0° ◇ 70 L/min 90° △ 130 L/min 90°
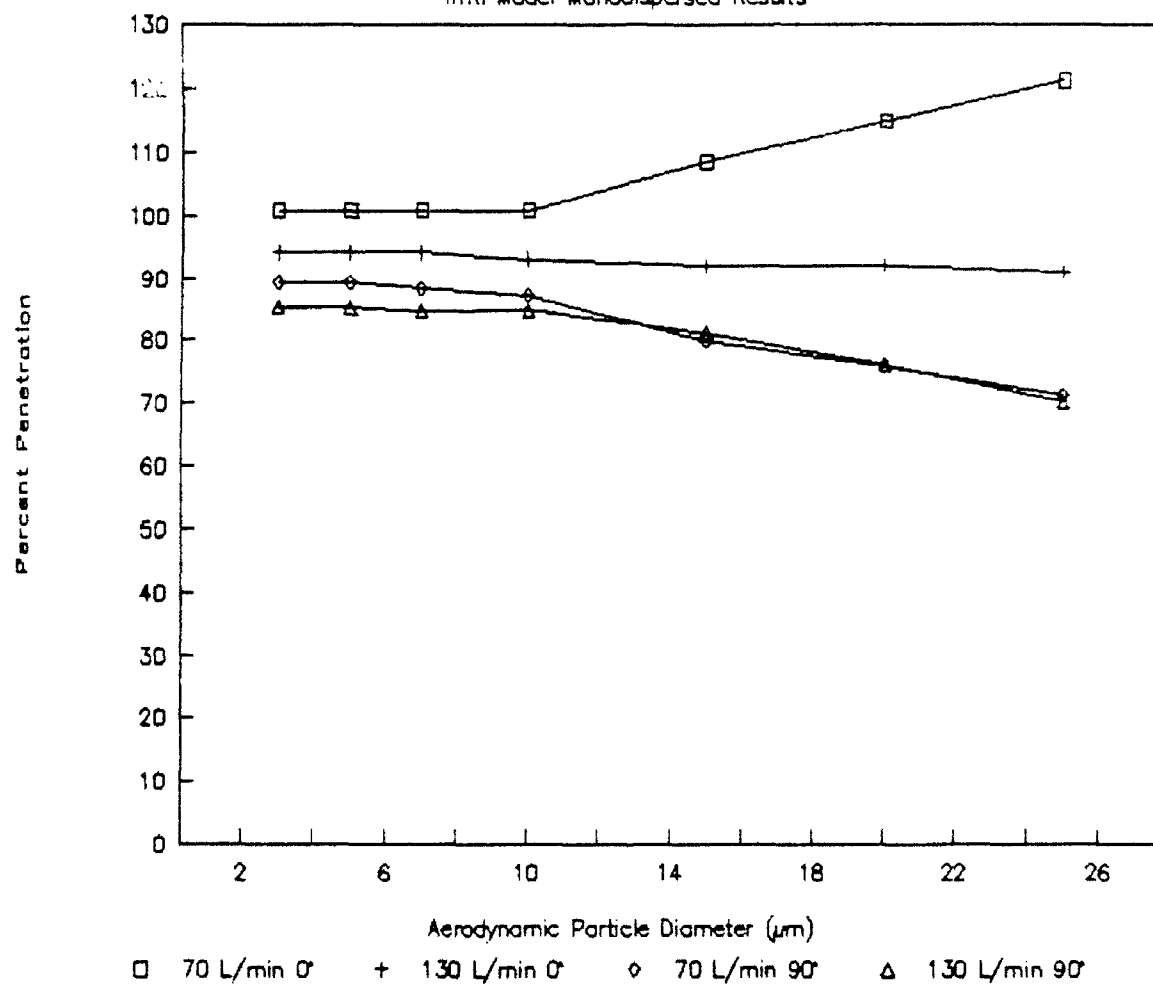
- 90° inlet probe orientation and 130 1/min flow rate

- 90° inlet probe orientation and 70 1/min flow rate

- 0° inlet probe orientation and 130 1/min flow rate

4.3 RESULTS FROM UNIVERSITY OF DUISBURG MODEL

4.3.1 Background

As mentioned earlier, the Fissan and Schwientek model simulates only one inlet probe orientation (0°) and does not account for a 45° bend or inclined section of the sampling train. Furthermore, it does not predict cumulative sampling efficiency resulting from a log-normal particle distribution. GMA, as part of its effort to develop a computer program for the German model, extended the model's capability to include a 45° bend, an inclined region of the train, and log-normal distribution.

This section of the report is to focus primarily on the cumulative sampling efficiencies generated by the model. Therefore, the results generated by the model and presented in this section will not include a 45° bend, inclined region, or log-normal distribution. However, Section 6 will include a comparison of the model results to the experimental data gathered by Texas A&M. The comparison will include the model results for the 45° bend, inclined section, and log-normal distribution. THe complete set of numerical calculations prcduced by the GMA computer program is provided at Appendix ᴗ.

4.3.2 Results of Monodispersed Simulation Cases

The cumulative sampling efficiency results presented in Table 5 and Figure 6 for a monodispersed aerosol distribution indicate the following:

- As the particle size increases the sampling efficiency decreases.

- As the flow rate increases from 70 1/min to 130 1/min, the sampling efficiency decreases.

- The larger the particle size, the greater the decrease in cumulative sampling efficiency.

Cumulative sampling efficiency resluts generated by the GMA computer program for a polydispersed aerosol distribution has been presented in Figure 7 for illustrative purposes only.

TYPE OF PARTICLE DISTRIBUTION	PARTICLE SIZE (μ)	INLET PROBE ORIENTATION (α)	FLOW RATE (l/min)	WIND SPEED (m/sec)	CUMULATIVE SAMPLING EFFICIENCY* (% mass)
1. MONODISPERSED	3	0°	70	3	98.4
2. MONODISPERSED	5	0°	70	3	95.7
3. MONODISPERSED	7	0°	70	3	91.7
4. MONODISPERSED	10	0°	70	3	83.3
5. MONODISPERSED	15	0°	70	3	64.6
6. MONODISPERSED	20	0°	70	3	43.8
7. MONODISPERSED	25	0°	70	3	25.6
8. MONODISPERSED	3	0°	130	3	95.9
9. MONODISPERSED	5	0°	130	3	89.1
10. MONODISPERSED	7	0°	130	3	79.8
11. MONODISPERSED	10	0°	130	3	63.0
12. MONODISPERSED	15	0°	130	3	34.6
13. MONODISPERSED	20	0°	130	3	14.2
14. MONODISPERSED	25	0°	130	3	3.9
15. POLYDISPERSED	MMAD=5 (σ =1.5)	0°	70	3	94.1
16. POLYDISPERSED	MMAD=15 (σ =1.5)	0°	70	3	59.9
17. POLYDISPERSED	MMAD=5 (σ =1.5)	0°	130	3	86.0
18.. POLYDISPERSED	MMAD=15 (σ =1.5)	0°	130	3	35.8

* Cumulative Efficiency Results reflect modifications made to the model by General Management Associates to allow calculations for 45° elbow and inclined section of the sampling train.

Table 5. Cumulative Sampling Efficiency Results Generated by University of Duisburg Model

Figure 6. Penetration Efficiency

Duisburg Model Monodispersed Results

□   70 L/min 0°   +   130 L/min 0°
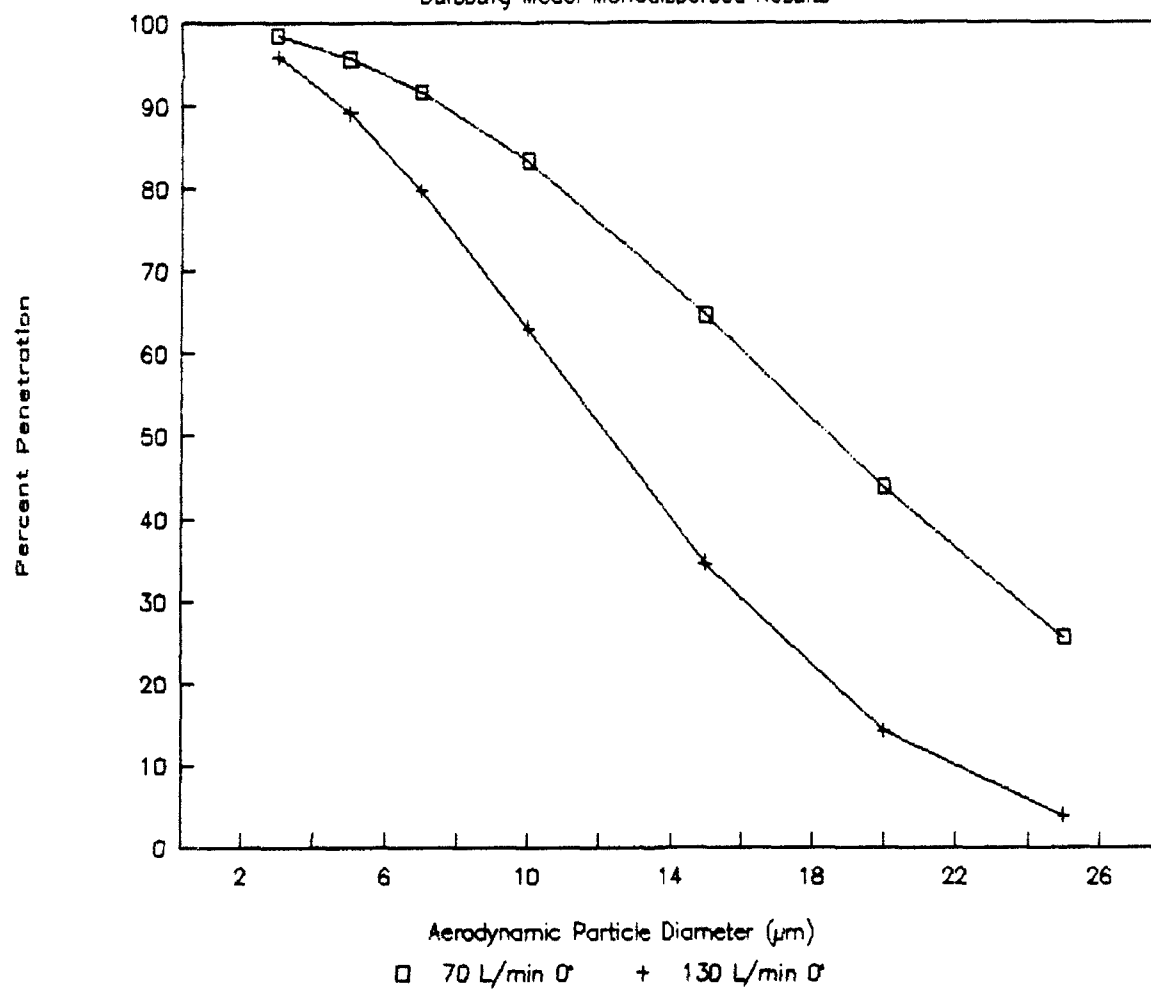
Figure 7. Penetration Efficiency

Duisburg Model Polydispersed Results

Mass Median Aerodynamic Diameter (μm)

□　70 L/min 0°　　+　130 L/min 0°
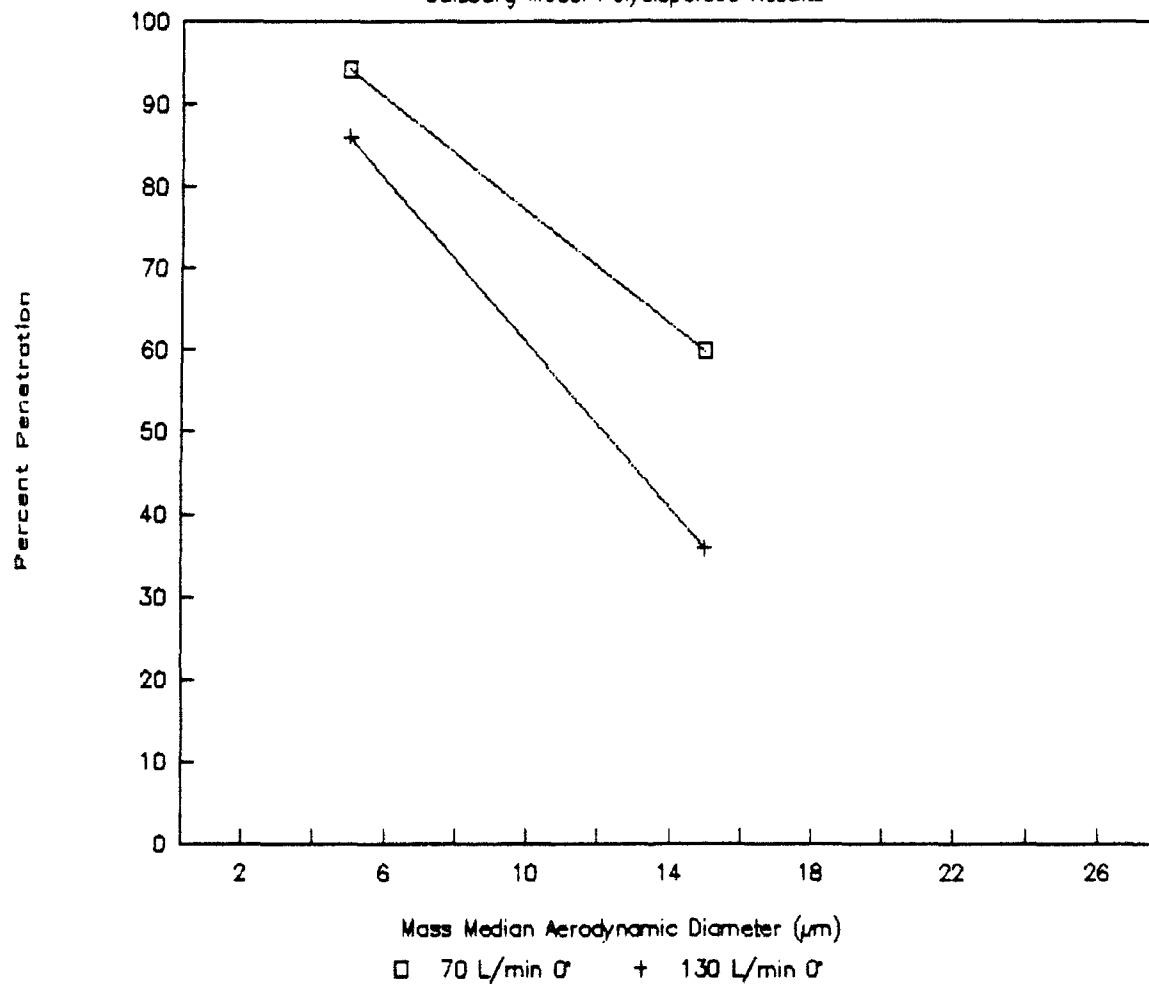
4.4   RESULTS FROM BATTELLE MODEL

For background purposes, the Battelle model does not account for an inlet probe orientation. However, the model does account for the three straight sections of the train and the 90° bend and 45° bend. Therefore, the model calculates cumulative sampling efficiencies for 18 simulation cases which are summarized in Table 6 and graphically presented in Figures 8 and 9. The complete set of numerical calculations produced by the Battelle model are provided at Appendix E.

4.4.1   Results of Monodispersed Simulation Cases

The cumulative sampling efficiency results for a monodispersed aerosol distribution indicate the following:

- As the particle size increases, the sampling efficiency decreases.

- An increase in the flow rate results in a decrease in the sampling efficiency. However, the differences are small (less than 2 percent).

- The larger the particle size, the greater the decrease in sampling efficiency.

- Particle depositional losses in the elbows are generally larger than those in the other components of the sampling train.

4.4.2   Results of Polydispersed Simulation Cases

The cumulative sampling efficiency results for a polydispersed aerosol distribution indicate the following:

- As the MMAD particle size increases, the sampling efficiency decreases.

- As the flow rate increases, the sampling efficiency decreases. However, the decrease is not considered significant for the range of particles evaluated.

- Particle depositional losses in the elbows are generally larger than those in the other compartments of the sampling train.

- The 5μm MMAD polydispersed particle distribution produces smaller sampling efficiencies than does the 5μm monodispersed particle distribution. However, the differences in efficiency (typically less than one percent) are considered insignificant.

44

TYPE OF PARTICLE DISTRIBUTION	PARTICLE SIZE (μ)	INLET PROBE ORIENTATION (α)	FLOW RATE (l/min)	WIND SPEED (m/sec)	CUMULATIVE SAMPLING EFFICIENCY* (% mass)
1. MONODISPERSED	3	N/A	7C	3	99.0
2. MONODISPERSED	5	N/A	70	3	97.8
3. MONODISPERSED	7	N/A	70	3	96.0
4. MONODISPERSED	10	N/A	70	3	92.4
5. MONODISPERSED	15	N/A	70	3	83.9
6. MONODISPERSED	20	N/A	70	3	73.1
7. MONODISPERSED	25	N/A	70	3	60.7
8. MONODISPERSED	3	N/A	130	3	98.8
9. MONODISPERSED	5	N/A	130	3	98.0
10. MONODISPERSED	7	N/A	130	3	96.7
11. MONODISPERSED	10	N/A	130	3	93.9
12. MONODISPERSED	15	N/A	130	3	83.7
13. MONODISPERSED	20	N/A	130	3	71.7
14. MONODISPERSED	25	N/A	130	3	60.2
15. POLYDISPERSED	MMAD=5 (σ =1.5)	N/A	70	3	97.1
16. POLYDISPERSED	MMAD=15 (σ =1.5)	N/A	70	3	79.8
17. POLYDISPERSED	MMAD=5 (σ =1.5)	N/A	130	3	97.4
18.. POLYDISPERSED	MMAD=15 (σ =1.5)	N/A	130	3	80.7

* Efficiency from different probe orientations is not considered in the Battelle model.

Table 6. Cumulative Sampling Efficiency Results Generated by Battelle Model

Figure 8. Penetration Efficiency

Battelle Model Monodispersed Results

Aerodynamic Particle Diameter (μm)

□   70 L/min   +   130 L/min
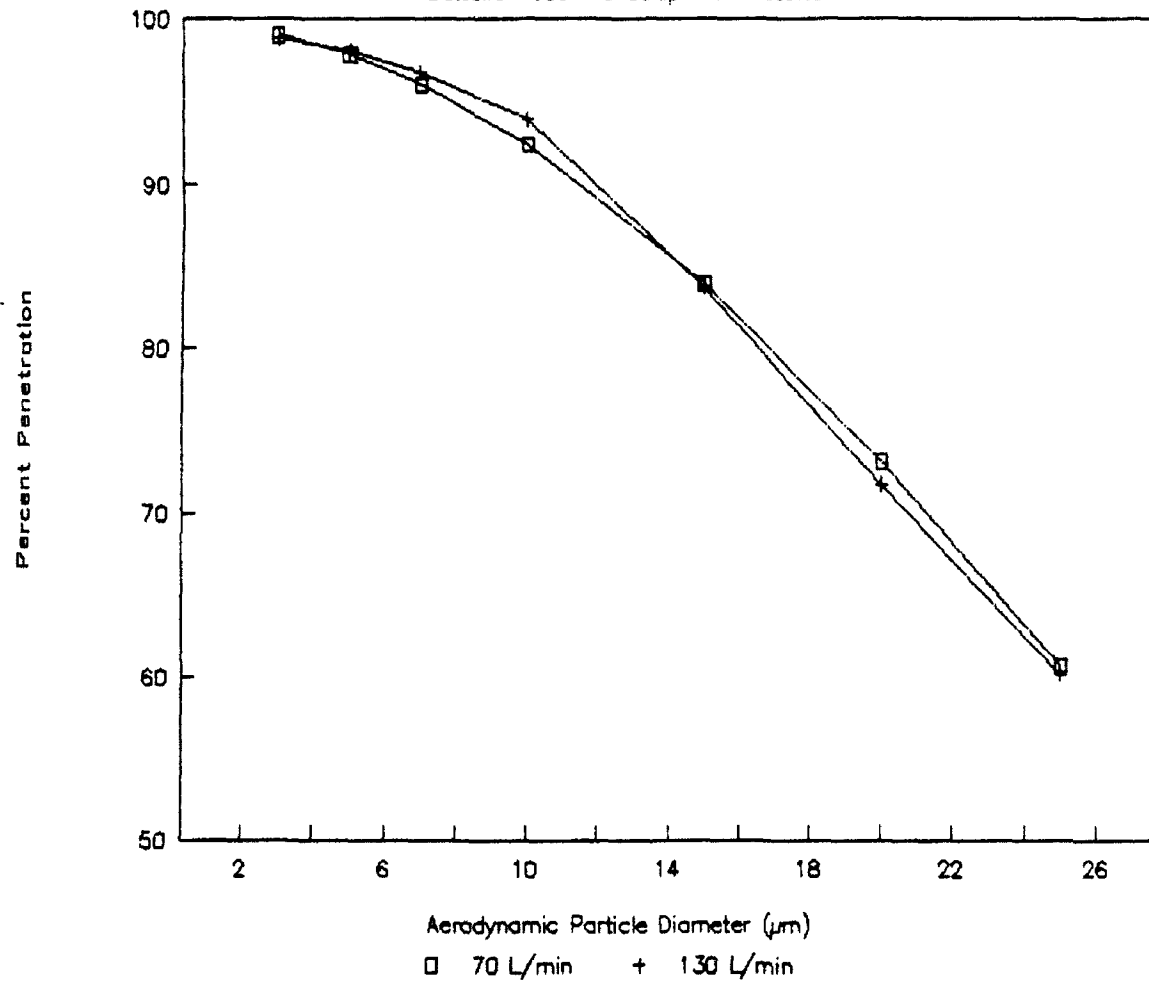
Figure 9. Penetration Efficiency
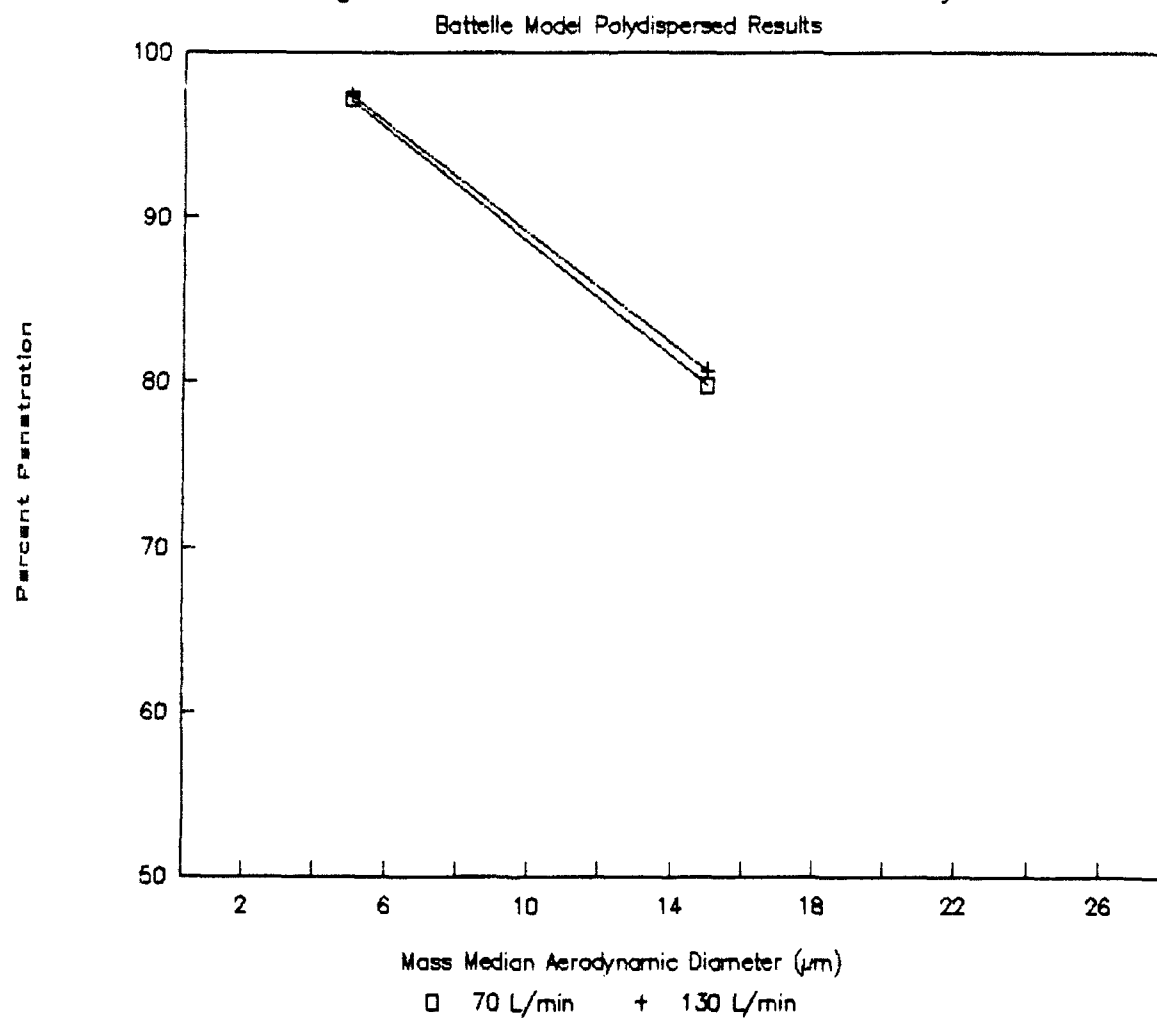
Battelle Model Polydispersed Results

Mass Median Aerodynamic Diameter (μm)

□   70 L/min   +   130 L/min

- The 15μm MMAD polydispersed particle distribution produces smaller sampling efficiencies than does the 15μm monodispersed particle distribution. These differences (3 to 4 percent) are larger than those seen with the 5μm particle size comparisons.

4.5   COMPARISON OF NUMERICAL CALCULATIONS

In order to perform a comparison of the numerical results among the four models, it is necessary to establish a common basis upon which the results can be compared. The four models individually do not provide numerical calculations for the six sections of the sampling train. Therefore, the common basis for comparison will be the numerical results for specific regions of the sampling train characterized/simulated by each model.

4.5.1   Numerical Model Calculations for Inlet Region of Aerosol Sampling Train

4.5.1.1   Monodispersed Particle Distribution - Inlet Region

Table 7 presents the three model's numerical results for the inlet region of the sampling train. Figures 10 and 11 provide a graphical presentation of the numerical results. It is important to note that only the Texas A&M model and the IITRI model consider air stream orientations other than parallel to the inlet. The University of Duisburg model only considers a 0° inlet orientation.

The inlet sampling efficiency results for a monodispersed particle distribution indicate the following:

- Both the Texas A&M and IITRI models predict a decrease in the efficiency as the inlet probe orientation increases from 0° to 90°.

- All three models predict a decrease in the inlet efficiency as the flow rate increases.

- The Texas A&M model predicts a decrease in the inlet efficiency as the particle size increases for all four combinations of inlet orientation and flow rate. The IITRI and German models, on the other hand, predict an increase in the efficiency as the particle size increases for the cases of 0° inlet orientation and 70 l/min flow rate. However, for the other combinations of inlet orientation and flow rate, these two models predict a decrease in the efficiency as the particle size increases.

48

	PARTICLE SIZE (μ)	INLET PROBE ORIENTATION (α)	FLOW RATE (l/min)	SAMPLING EFFICIENCY (% mass) FOR INLET REGION		
				TEXAS A & M	IITRI	UNIVERSITY OF DUISBURG
1.	3	0°	70	99.4	100.7	100.6
2.	5	0°	70	98.9	100.7	101.8
3.	7	0°	70	98.4	100.7	103.3
4.	10	0°	70	97.7	100.7	106.2
5.	15	0°	70	96.4	108.4	111.9
6.	20	0°	70	94.7	114.7	117.4
7.	25	0°	70	92.4	121.2	122.2
8.	3	0°	130	99.3	94.1	99.6
9.	5	0°	130	98.3	94.1	98.9
10.	7	0°	130	97.1	94.1	98.0
11.	10	0°	130	94.9	93.0	96.3
12.	15	0°	130	90.6	91.9	93.2
13.	20	0°	130	85.7	91.9	90.2
14.	25	0°	130	80.5	90.9	87.7
15.	3	90°	70	96.2	89.3	N/A
16.	5	90°	70	90.5	89.3	N/A
17.	7	90°	70	83.2	88.3	N/A
18.	10	90°	70	70.9	87.2	N/A
19.	15	90°	70	51.5	79.9	N/A
20.	20	90°	70	36.6	75.9	N/A
21.	25	90°	70	26.1	71.3	N/A
22.	3	90°	130	97.2	85.4	N/A
23.	5	90°	130	92.9	85.3	N/A
24.	7	90°	130	87.2	84.7	N/A
25.	10	90°	130	77.2	84.8	N/A
26.	15	90°	130	59.9	81.2	N/A
27.	20	90°	130	45.1	76.1	N/A
28.	25	90°	130	33.8	70.2	N/A

**Table 7. Numerical Model Calculations (Monodispersed Particle Sizes)
for Inlet Region of Aerosol Sampling Train**

Figure 10. Inlet Penetration Efficiency

Monodispersed Results – 0° Inlet

Legend:
- □ 70 L/min Texas A&M
- + 130 L/min Texas A&M
- ◇ 70 L/min IITRI
- △ 130 L/min IITRI
- X 70 L/min Duisburg
- ▽ 130 L/min Duisburg

Figure 11. Inlet Penetration Efficiency

Monodispersed Results – 90° Inlet

Legend:
- □ 70 L/min Texas A&M
- + 130 L/min Texas A&M
- ◊ 70 L/min IITRI
- △ 130 L/min IITRI

X-axis: Aerodynamic Particle Diameter (μm)

Y-axis: Percent Penetration

4.5.1.2   Polydispersed Particle Distribution - Inlet Region

Table 8 presents two model's numerical efficiency results for the inlet region of the sampling train. Figures 12 and 13 provide a graphical presentation of the numerical results. It is important to note that only the Texas A&M model considers air stream orientations other than parallel to the inlet. The IITRI model does not consider polydispersed particle distribution. The University of Duisburg model as extended by GMA considers polydispersed particle distribution but only for a 0° inlet orientation. The inlet sampling efficiency results for polydispersed particle distribution indicate the following:

- For the Texas A&M model, as the particle MMAD increases, the sampling efficiency decreases. The University of Duisburg model, on the other hand, predicts an increase or a decrease in the sampling efficiency depending on the flow rate.

- Both models predict a decrease in the sampling efficiency as the flow rate increases when the inlet orientation is parallel to the air stream. The Texas A&M results indicate an increase in the sampling efficiency as the flow rate increases when the inlet orientation is normal to the air stream.

4.5.2   Numerical Efficiency Calculations for Horizontal Region of Aerosol Sampling Train

4.5.2.1   Monodispersed Particle Distribution - Horizontal Region

Table 9 presents the three model's numerical results for the horizontal region of the sampling train. Figure 14 provides a graphical presentation of the numerical results. It is important to note that for these calculations, the horizontal region is not affected by the inlet's orientation to the air stream. Therefore, only the flow rate and particle size have been varied.

The horizontal region's sampling efficiency results for a monodispersed particle distribution indicate the following:

- All three models predict a decrease in the efficiency as the particle size increases.

- Both the Texas A&M and the Battelle models predict an increase in sampling efficiency as the flow rate increases. In addition the Texas A&M results indicate a decrease in the efficiency at the 20 and 25μm particle sizes as the flow rate increases. The German results, on the other hand, indicate a decrease in the efficiency as the flow rates increase.

52

MASS MEDIUM AERODYNAMIC DIAMETER (MMAD)(μ)	INLET PROBE ORIENTATION (α)	FLOW RATE (l/min)	SAMPLING EFFICIENCY (% mass) FOR INLET REGION			
			TEXAS A & M	IITRI	BATTELLE	UNIVERSITY OF DUISBURG
1. 5	0°	70	98.8	N/A	N/A	102.3
2. 15	0°	70	95.6	N/A	N/A	112.9
3. 5	0°	130	98.0	N/A	N/A	98.6
4. 15	0°	130	89.1	N/A	N/A	92.7
5. 5	90°	70	88.4	N/A	N/A	N/A
6. 15	90°	70	51.0	N/A	N/A	N/A
7. 5	90°	130	91.2	N/A	N/A	N/A
8. 15	90°	130	58.4	N/A	N/A	N/A

Table 8. Model Efficiency Calculations (Polydispersed Particle Sizes) for Inlet Region of Aerosol Sampling Train

Figure 12. Inlet Penetration Efficiency

Polydispersed Results — 0° Inlet
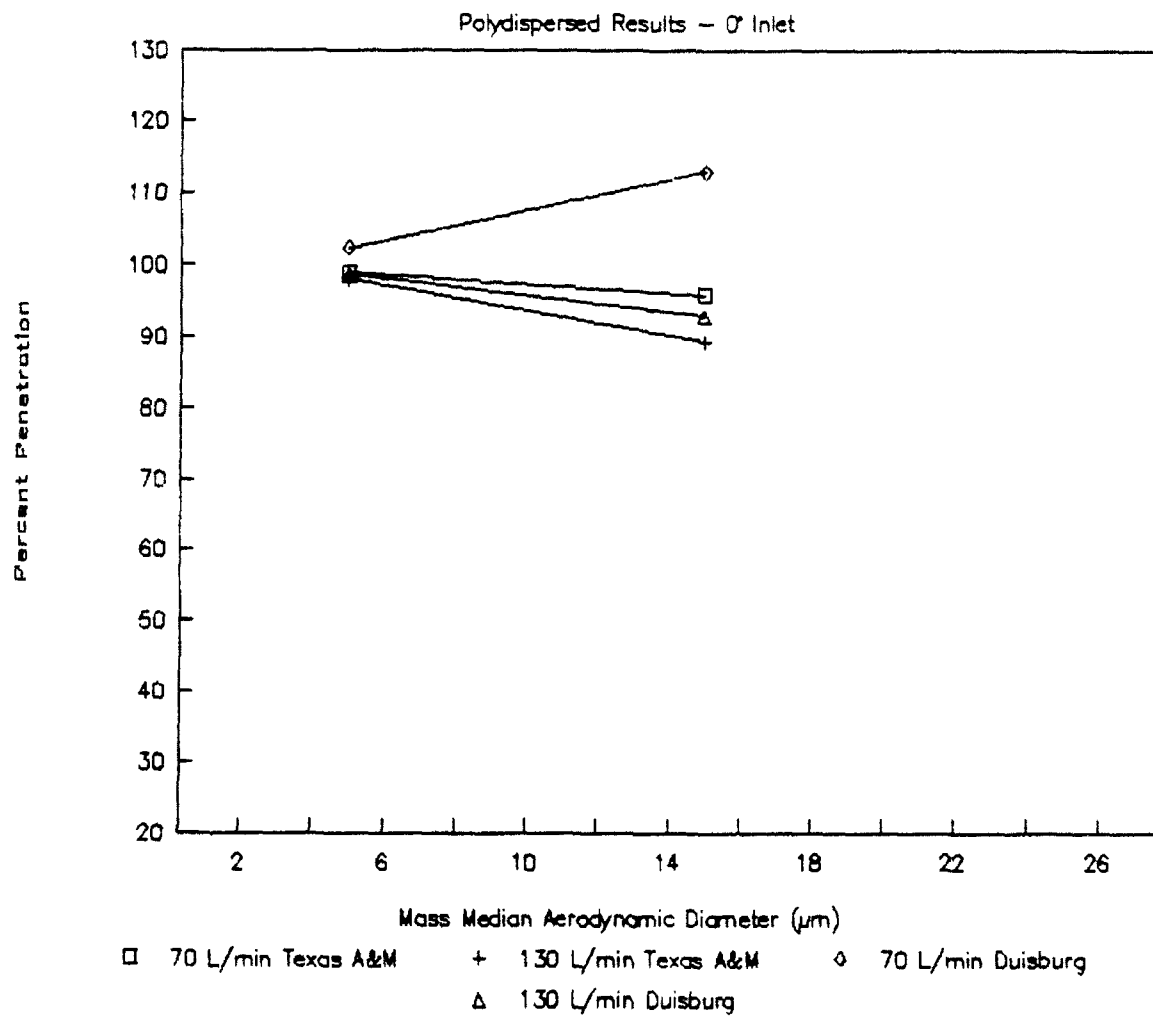
Figure 13. Inlet Penetration Efficiency

Polydispersed Results – 90° Inlet

55
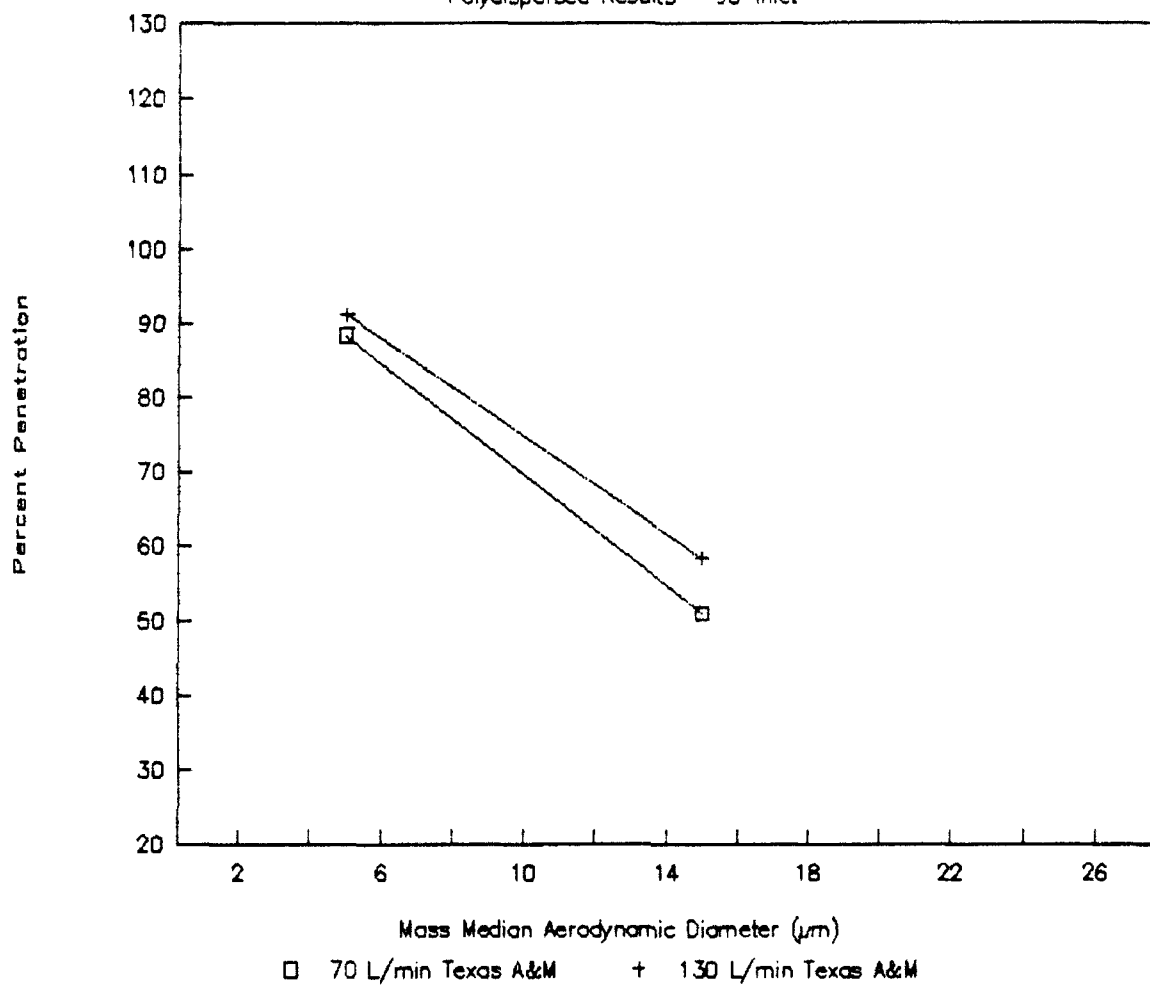
	PARTICLE SIZE (μ)	FLOW RATE (l/min)	SAMPLING EFFICIENCY (% mass) FOR HORIZONTAL REGION			
			TEXAS A & M	IITRI	BATTELLE	UNIVERSITY OF DUISBURG
1.	3	70	99.7	N/A	99.6	100.0
2.	5	70	99.3	N/A	98.9	99.99
3.	7	70	98.6	N/A	97.9	99.98
4.	10	70	97.2	N/A	95.8	99.9
5.	15	70	93.8	N/A	90.7	99.6
6.	20	70	89.1	N/A	84.1	98.8
7.	25	70	83.2	N/A	76.3	97.2
8.	3	130	99.9	N/A	99.8	99.99
9.	5	130	99.6	N/A	99.4	99.96
10.	7	130	99.2	N/A	98.9	99.9
11.	10	130	98.3	N/A	97.7	99.4
12.	15	130	95.6	N/A	94.9	97.1
13.	20	130	88.0	N/A	91.1	91.0
14.	25	130	80.2	N/A	86.4	79.6

Table 9. Model Efficiency Calculations (Monodispersed Particle Sizes) for Horizontal Region of Aerosol Sampling Train

Figure 14. Penetration Efficiency

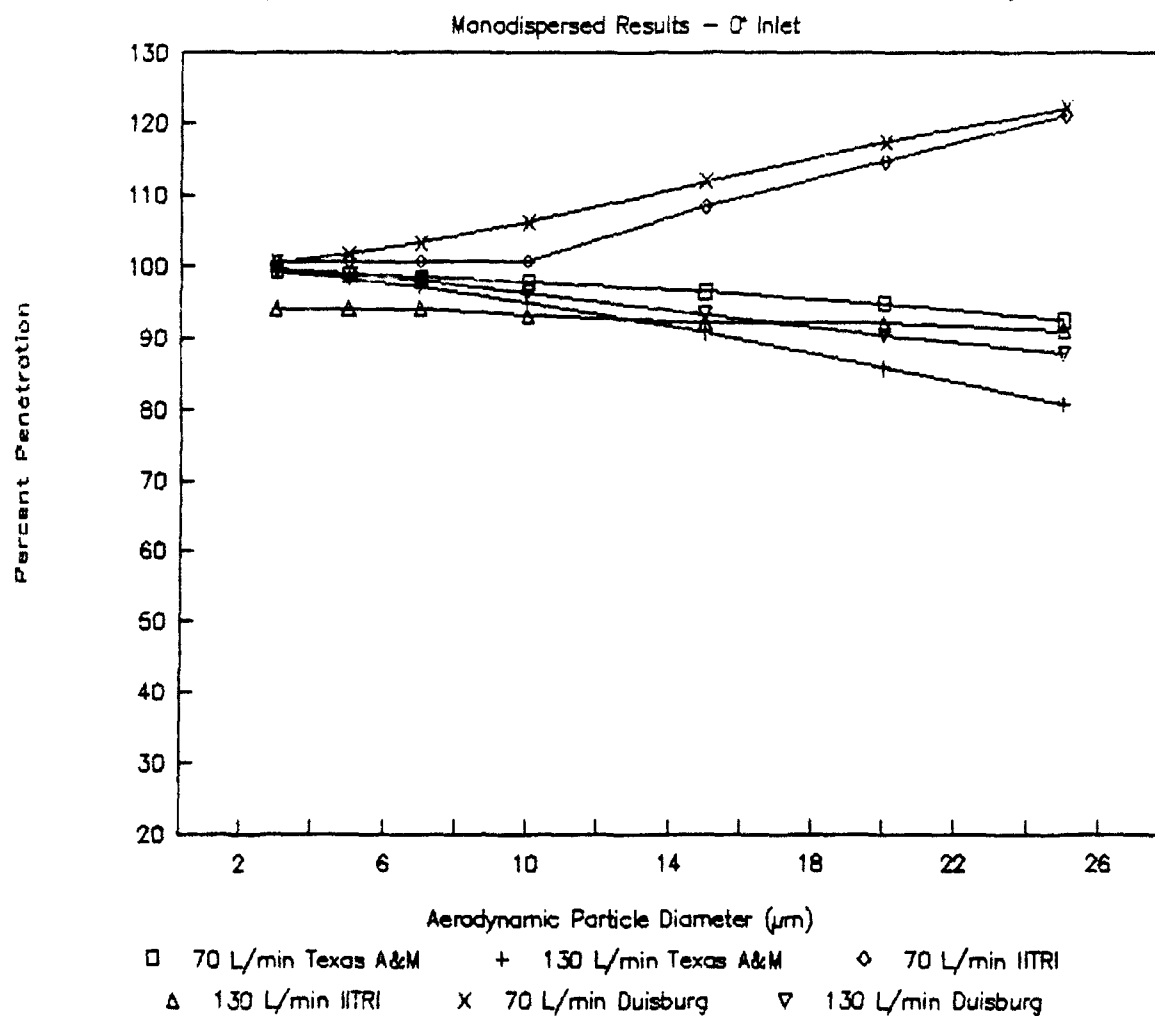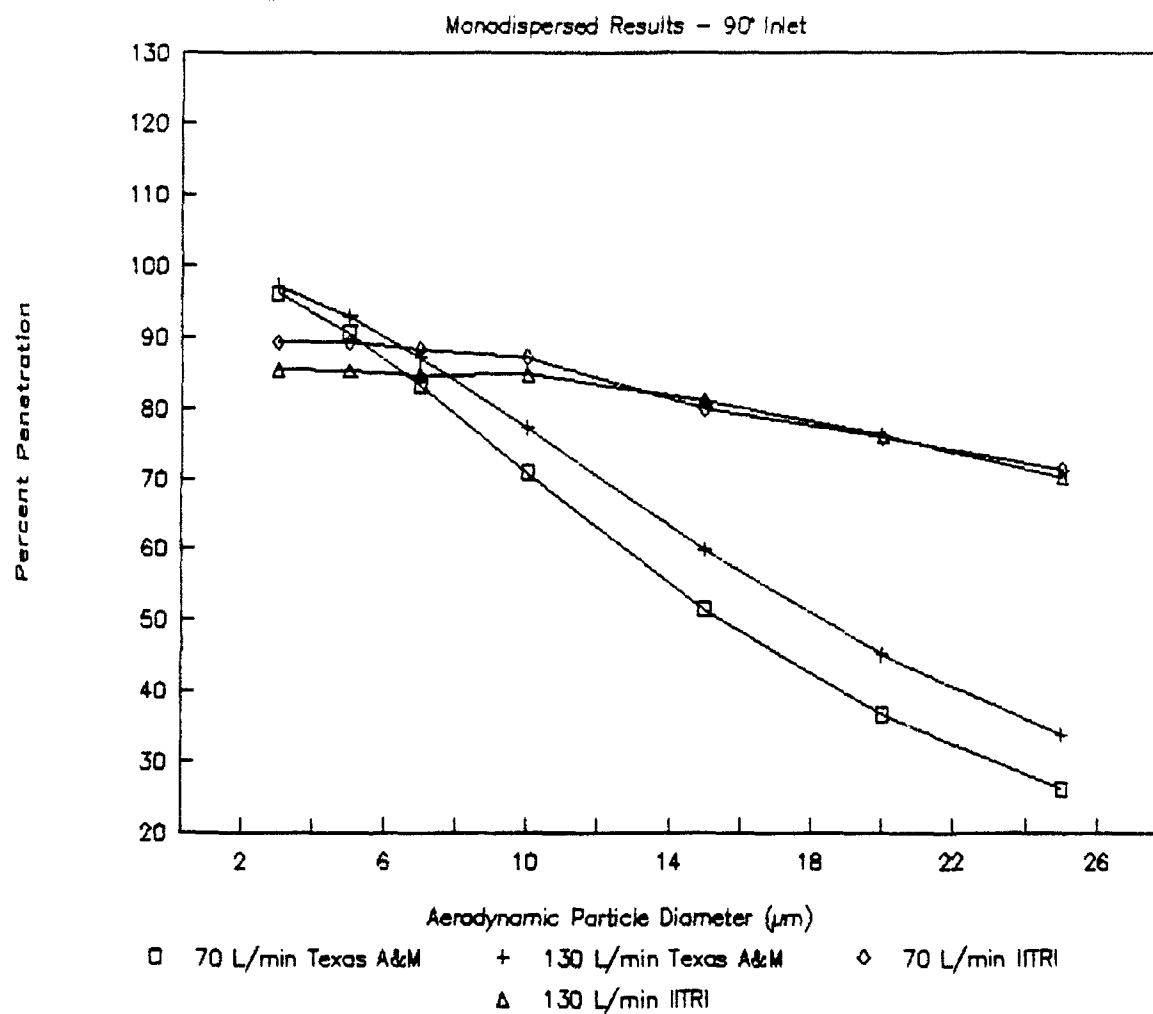Monodispersed Results — Horizontal Sec.

Aerodynamic Particle Diameter (μm)

□ 70 L/min Texas A&M   + 130 L/min Texas A&M   ◊ 70 L/min Battelle

△ 130 L/min Battelle   X 70 L/min Duisburg   ▽ 130 L/min Duisburg
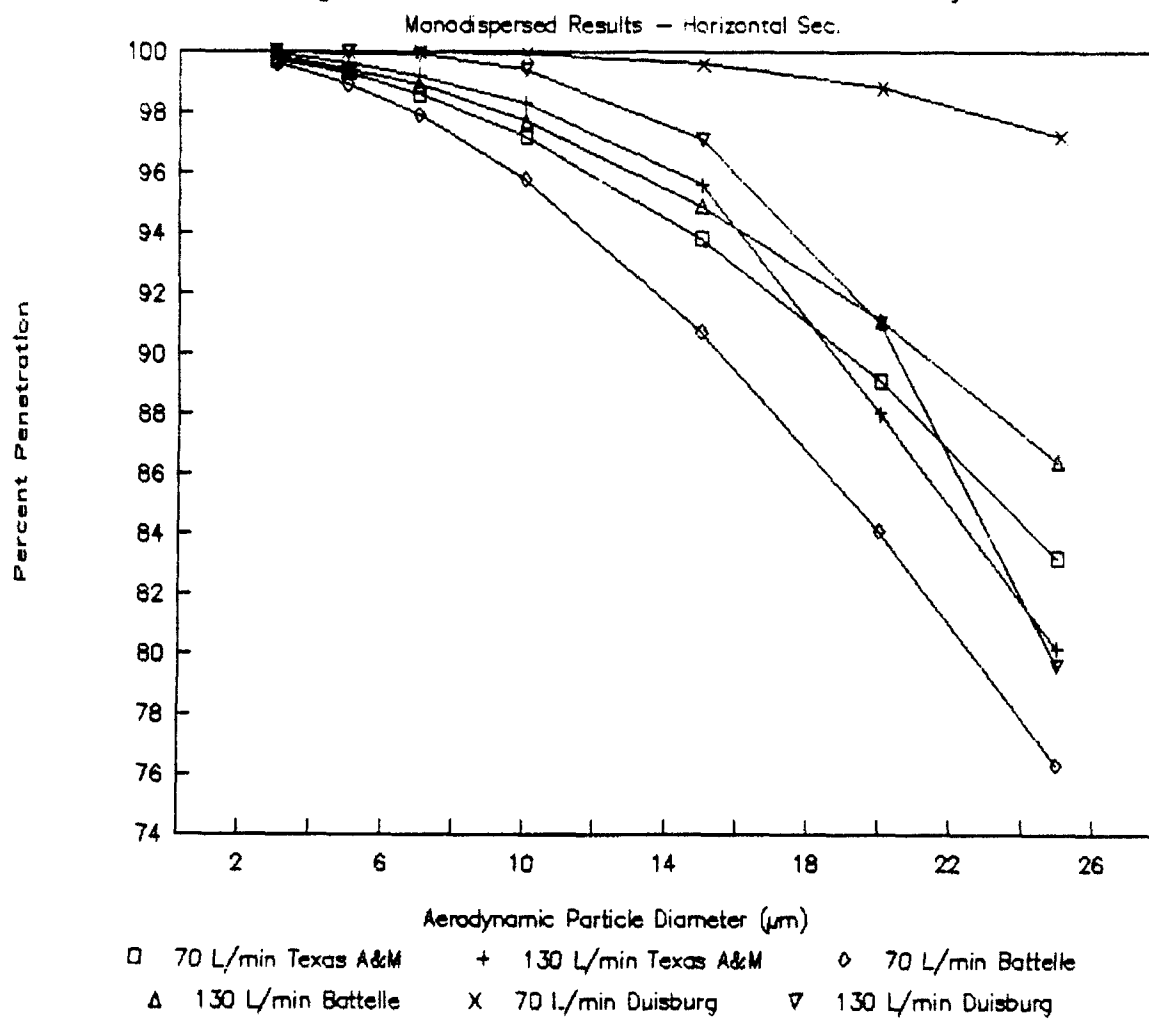
4.5.2.2 Polydispersed Particle Distribution - Horizontal Region

Table 10 presents the three model's numerical results for the horizontal region of the sampling train. Figures 15 and 16 provide a graphical presentation of the numerical results. It is important to note that only the Texas A&M model considers air stream orientations other than parallel to the inlet. The German model only considers a $0°$ inlet orientation. The Battelle model does not consider inlet orientations.

The horizontal sampling efficiency results for a polydispersed particle distribution indicate the following:

- All three models predict a decrease in the sampling efficiency as the particle MMAD increases.

- The Texas A&M and Battelle models predict an increase in the sampling efficiency as the flow rate increases for a $0°$ inlet orientation. The German model predicts a decrease in the sampling efficiency as the flow rate increases. The Texas A&M model also predicts an increase in the sampling efficiency as the flow rate increases for a $90°$ inlet orientation.

- All three models predict a decrease in the sampling efficiency as the flow rate increases.

4.5.3 Numerical Efficiency Calculations for $90°$ Elbow Region of Aerosol Sampling Train

4.5.3.1 Monodispersed Particle Distribution - $90°$ Elbow Region

Table 11 presents the three model's numerical results for the $90°$ elbow region of the sampling train. Figure 17 provides a graphical presentation of the numerical results. It is important to note that for these calculations the $90°$ elbow region is not affected by the inlet's orientation to the air stream.

The $90°$ elbow region's sampling efficiency results indicate the following:

- All three models predict a decrease in the efficiency as the particle size increases.

- All three models predict a decrease in the efficiency as the flow rate increases.

- The Battelle model predicts the highest efficiencies. The Texas A&M model and the University of Duisburg model predict identical but lower efficiencies.

MASS MEDIUM AERODYNAMIC DIAMETER (MMAD)(μ)	INLET PROBE ORIENTATION (α)	FLOW RATE (l/min)	SAMPLING EFFICIENCY (% mass) FOR HORIZONTAL SECTION		
			TEXAS A & M	BATTELLE	UNIVERSITY OF DUISBURG
1. 5	0°	70	99.0	98.5	99.96
2. 15	0°	70	91.8	88.0	98.7
3. 5	0°	130	99.4	99.2	99.8
4. 15	0°	130	92.6	93.2	91.9
5. 5	90°	70	99.1	98.5	N/A
6. 15	90°	70	93.9	88.0	N/A
7. 5	90°	130	99.5	99.2	N/A
8. 15	90°	130	94.4	93.2	N/A

Table 10. Model Efficiency Calculations (Polydispersed Particle Sizes)
for Horizontal Region of Aerosol Sampling Train

59

Figure 15. Penetration Efficiency

Figure 16. Penetration Efficiency

Polydispersed – Horizontal Sec. – 90°

Legend:
- □ 70 L/min Texas A&M
- + 130 L/min Texas A&M
- ◊ 70 L/min Battelle
- △ 130 L/min Battelle

PARTICLE SIZE (μ)	FLOW RATE (l/min)	SAMPLING EFFICIENCY (% mass) FOR 90° ELBOW REGION		
		TEXAS A & M	BATTELLE	UNIVERSITY OF DUISBURG
1. 3	70	99.0	99.8	99.0
2. 5	70	97.3	99.8	97.3
3. 7	70	94.9	99.7	94.9
4. 10	70	89.9	99.6	89.9
5. 15	70	78.9	99.4	78.9
6. 20	70	65.7	98.8	65.7
7. 25	70	51.9	97.5	51.9
8. 3	130	98.2	99.4	98.2
9. 5	130	95.1	99.3	95.1
10. 7	130	90.8	99.1	90.7
11. 10	130	82.1	98.5	82.1
12. 15	130	64.4	94.2	64.4
13. 20	130	45.8	89.1	45.8
14. 25	130	29.6	84.1	29.6

Table 11. Numerical Model Calculations (Monodispersed Particle Sizes) for 90° Elbow Region of Aerosol Sampling Train

Figure 17. Penetration Efficiency

Monodispersed Results – 90° Elbow

Percent Penetration

Aerodynamic Particle Diameter (μm)

□	70 L/min Texas A&M	+	130 L/min Texas A&M
◊	70 L/min Battelle	△	130 L/min Battelle
X	70 L/min Duisburg	▽	130 L/min Duisburg

4.5.3.2 Polydispersed Particle Distribution - 90° Elbow Region

Table 12 presents the three model's numerical results for the 90° elbow region of the sampling train. Figures 18 and 19 provide a graphical presentation of the numerical results. It is important to note that only the Texas A&M model considers air stream orientations other than parallel to the inlet. The German model only considers a 0° inlet orientation. The Battelle model does not consider inlet orientation.

The 90° elbow sampling efficiency results for a polydispersed particle distribution indicate the following:

- All three models predict a decrease in the sampling efficiency as the particle MMAD increases.

- All three models predict a decrease in the sampling efficiency as the flow rate increases.

- The Texas A&M model predicts an increase in the sampling efficiency as the inlet orientation increases from 0° to 90°.

4.5.4 Numerical Efficiency Calculations for Vertical Region of Aerosol Sampling Train

4.5.4.1 Monodispersed Particle Distribution - Vertical Region

Table 13 presents the three model's numerical results for the vertical region of the sampling train. Figure 20 provides a graphical presentation of the numerical results. It is important to note that for these calculations, the vertical region is not affected by the inlet's orientation to the air stream.

The vertical region's sampling efficiency results indicate the following:

- The Texas A&M model and the German model predict a decrease in the efficiency as the particle size increases. The Battelle model predicts no change in the efficiency as the particle size increases.

- The Texas A&M model and the German model predict a decrease in the efficiency as the flow rate increases. The Battelle model predicts no change in the efficiency as the particle size increases.

4.5.4.2 Polydispersed Particle Distribution - Vertical Region

Table 14 presents the three model's numerical results for the vertical region of the sampling train. Figures 21 and 22 provide a graphical presentation of the numerical results. It

MASS MEDIUM AERODYNAMIC DIAMETER (MMAD)(μ)	INLET PROBE ORIENTATION (α)	FLOW RATE (l/min)	SAMPLING EFFICIENCY (% mass) FOR 90° ELBOW SECTION		
			TEXAS A & M	BATTELLE	UNIVERSITY OF DUISBURG
1. 5	0°	70	96.5	99.7	96.4
2. 15	0°	70	76.6	98.9	74.7
3. 5	0°	130	93.8	99.2	93.5
4. 15	0°	130	63.8	93.5	60.5
5. 5	90°	70	96.7	99.7	N/A
6. 15	90°	70	81.1	98.9	N/A
7. 5	90°	130	94.0	99.2	N/A
8. 15	90°	130	68.2	93.5	N/A

Table 12. Model Efficiency Calculations (Polydispersed Particle Sizes) for 90° Elbow Region of Aerosol Sampling Train

Figure 18. Penetration Efficiency

Polydispersed – 90° Elbow – 0° Inlet

Mass Median Aerodynamic Diameter (μm)

| □ | 70 L/min Texas A&M | + | 130 L/min Texas A&M | ◇ | 70 L/min Battelle |
| Δ | 130 L/min Battelle | X | 70 L/min Duisburg | ▽ | 130 L/min Duisburg |

Figure 19. Penetration Efficiency

Polydispersed – 90° Elbow – 90° Inlet

Legend:
□ 70 L/min Texas A&M + 130 L/min Texas A&M ◊ 70 L/min Battelle
△ 130 L/min Battelle

	PARTICLE SIZE (μ)	FLOW RATE (l/min)	SAMPLING EFFICIENCY (% mass) FOR VERTICAL REGION		
			TEXAS A & M	BATTELLE	UNIVERSITY OF DUISBURG
1.	3	70	100.0	100.0	100.0
2.	5	70	99.99	100.0	99.99
3.	7	70	99.98	100.0	99.98
4.	10	70	99.9	100.0	99.9
5.	15	70	99.6	100.0	99.6
6.	20	70	98.8	100.0	98.8
7.	25	70	96.9	100.0	97.2
8.	3	130	99.99	100.0	99.99
9.	5	130	99.96	100.0	99.96
10.	7	130	99.9	100.0	99.9
11.	10	130	99.4	100.0	99.4
12.	15	130	96.8	100.0	97.1
13.	20	130	84.4	100.0	91.0
14.	25	130	73.7	100.0	79.6

Table 13. Numerical Model Calculations (Monodispersed Particle Sizes) for Vertical Region of Aerosol Sampling Train

Figure 20. Penetration Efficiency

Monodispersed Results — Vertical Sec.

Percent Penetration

Aerodynamic Particle Diameter (μm)

☐ 70 L/min Texas A&M   + 130 L/min Texas A&M   ◊ 70 L/min Battelle

△ 130 L/min Battelle   ✕ 70 L/min Duisburg   ▽ 130 L/min Duisburg

MASS MEDIUM AERODYNAMIC DIAMETER (MMAD)(μ)	INLET PROBE ORIENTATION (α)	FLOW RATE (l/min)	SAMPLING EFFICIENCY (% mass) FOR VERTICAL SECTION		
			TEXAS A & M	BATTELLE	UNIVERSITY OF DUISBURG
1. 5	0°	70	99.98	100.0	99.96
2. 15	0°	70	99.3	100.0	98.7
3. 5	0°	130	99.9	100.0	99.8
4. 15	0°	130	95.7	100.0	91.9
5. 5	90°	70	99.98	100.0	N/A
6. 15	90°	70	99.6	100.0	N/A
7. 5	90°	130	99.9	100.0	N/A
8. 15	90°	130	96.7	100.0	N/A

Table 14. Model Efficiency Calculations (Polydispersed Particle Sizes) for Vertical Region of Aerosol Sampling Train
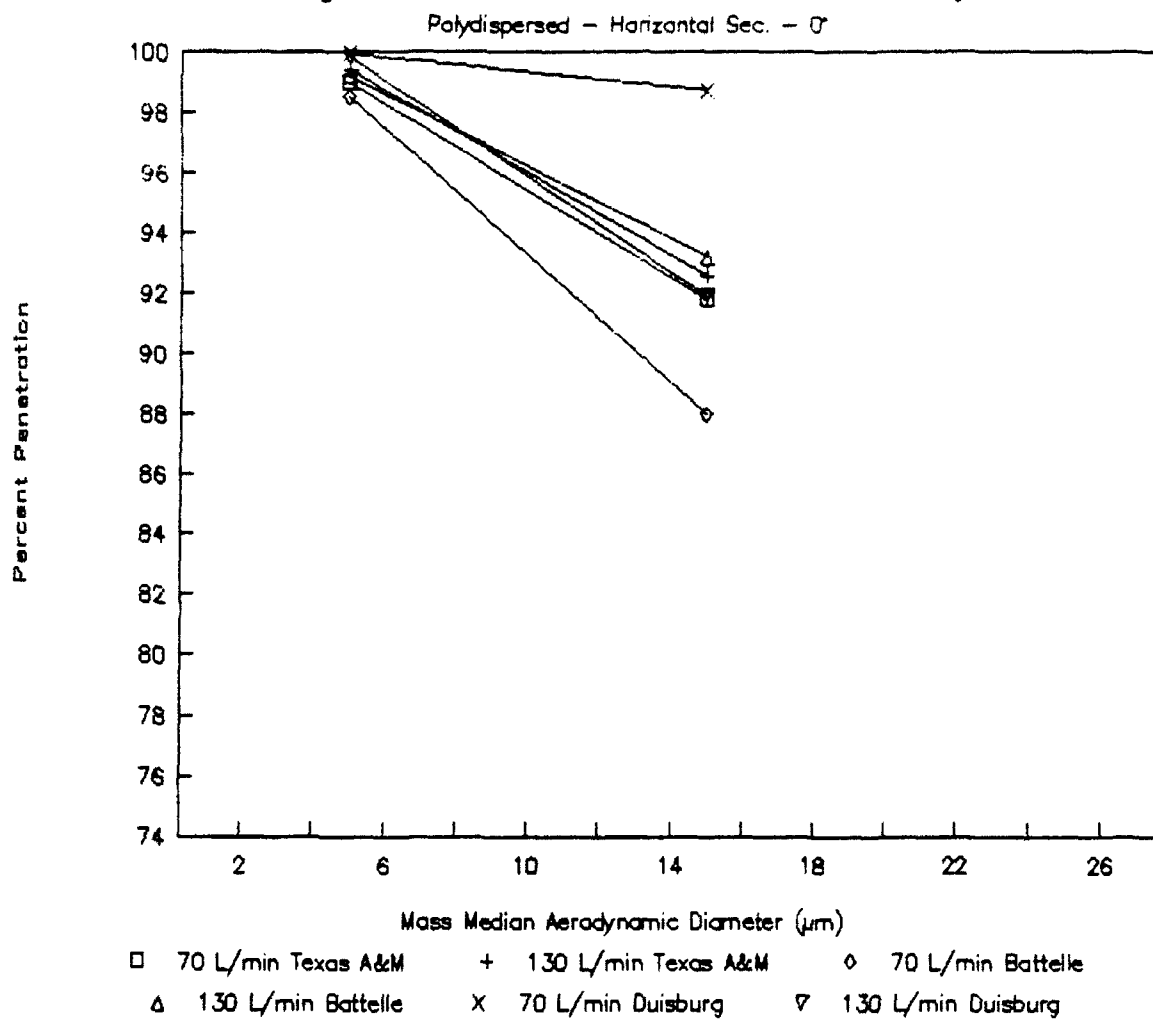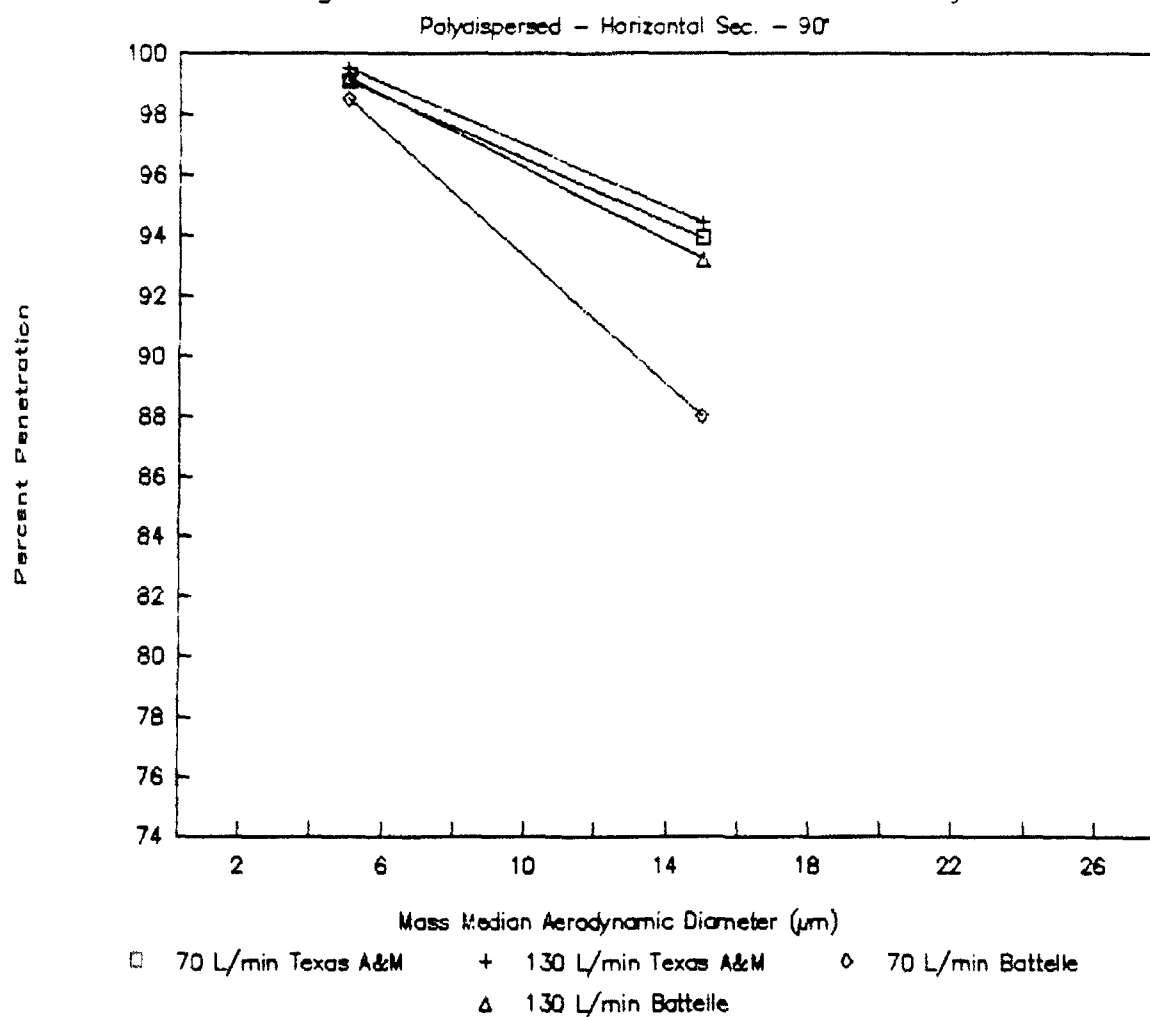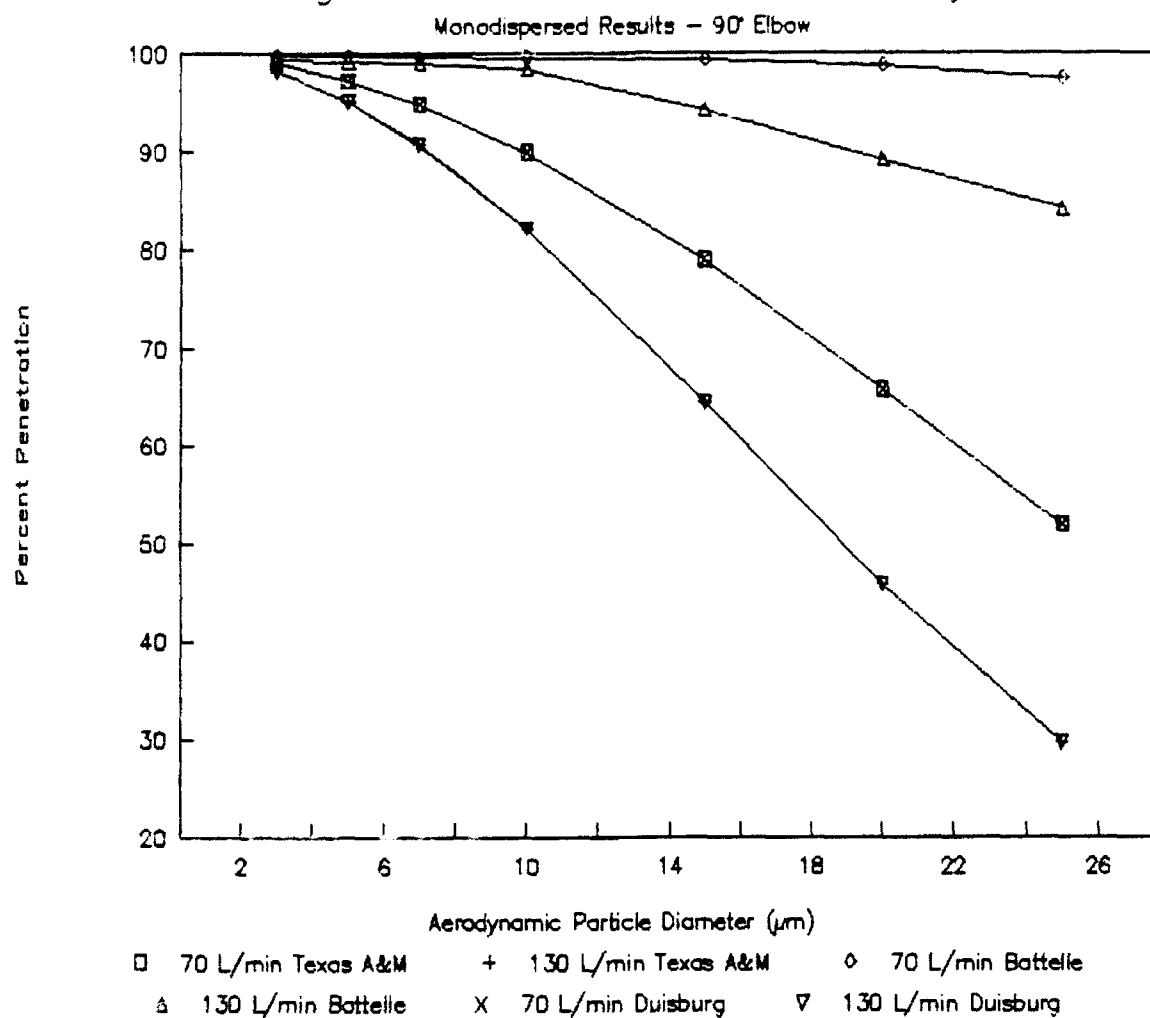
70

Figure 21. Penetration Efficiency

Polydispersed — Vertical — 0° Inlet

- □ 70 L/min Texas A&M
- + 130 L/min Texas A&M
- ◊ 70 L/min Battelle
- △ 130 L/min Battelle
- X 70 L/min Duisburg
- ▽ 130 L/min Duisburg
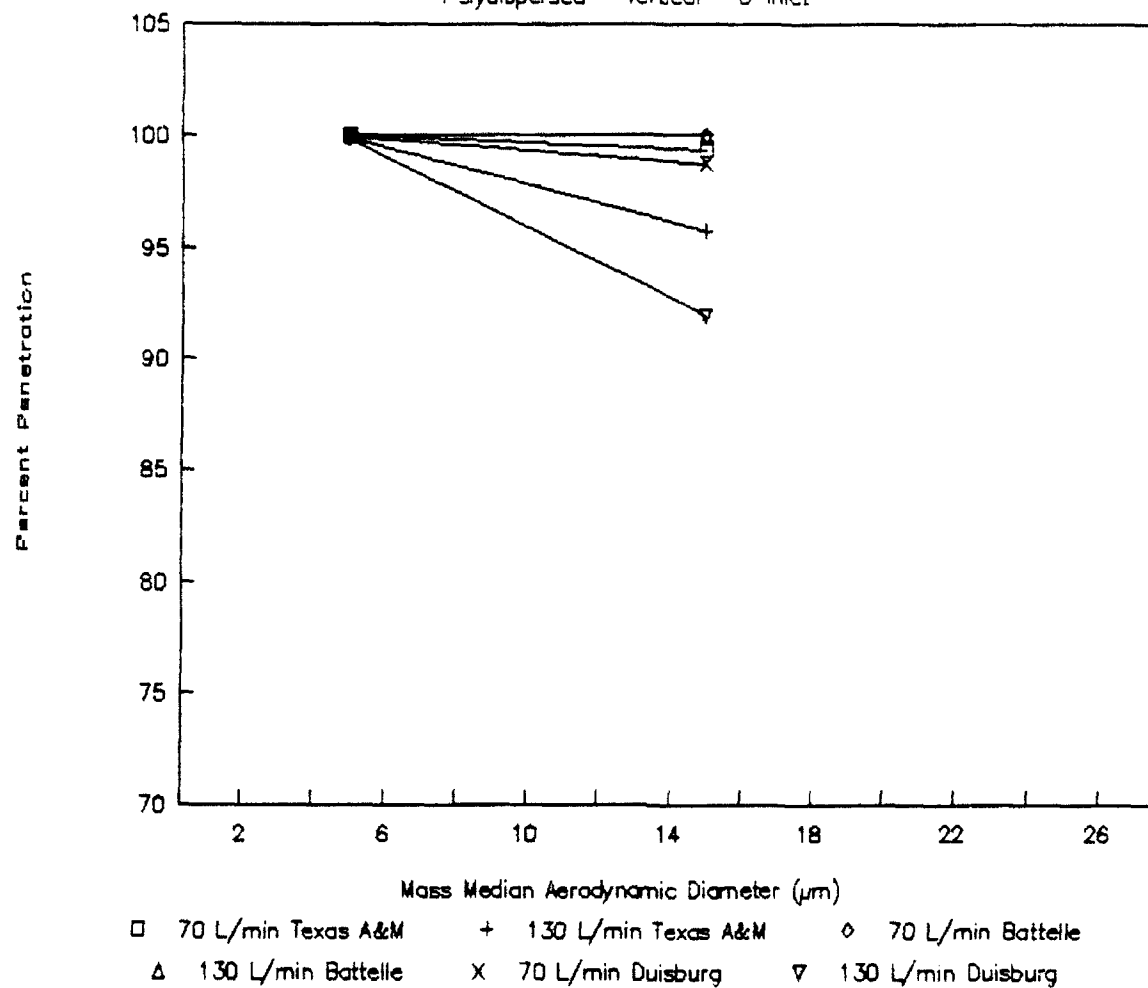
Figure 22. Penetration Efficiency

Polydispersed — Vertical — 90° Inlet
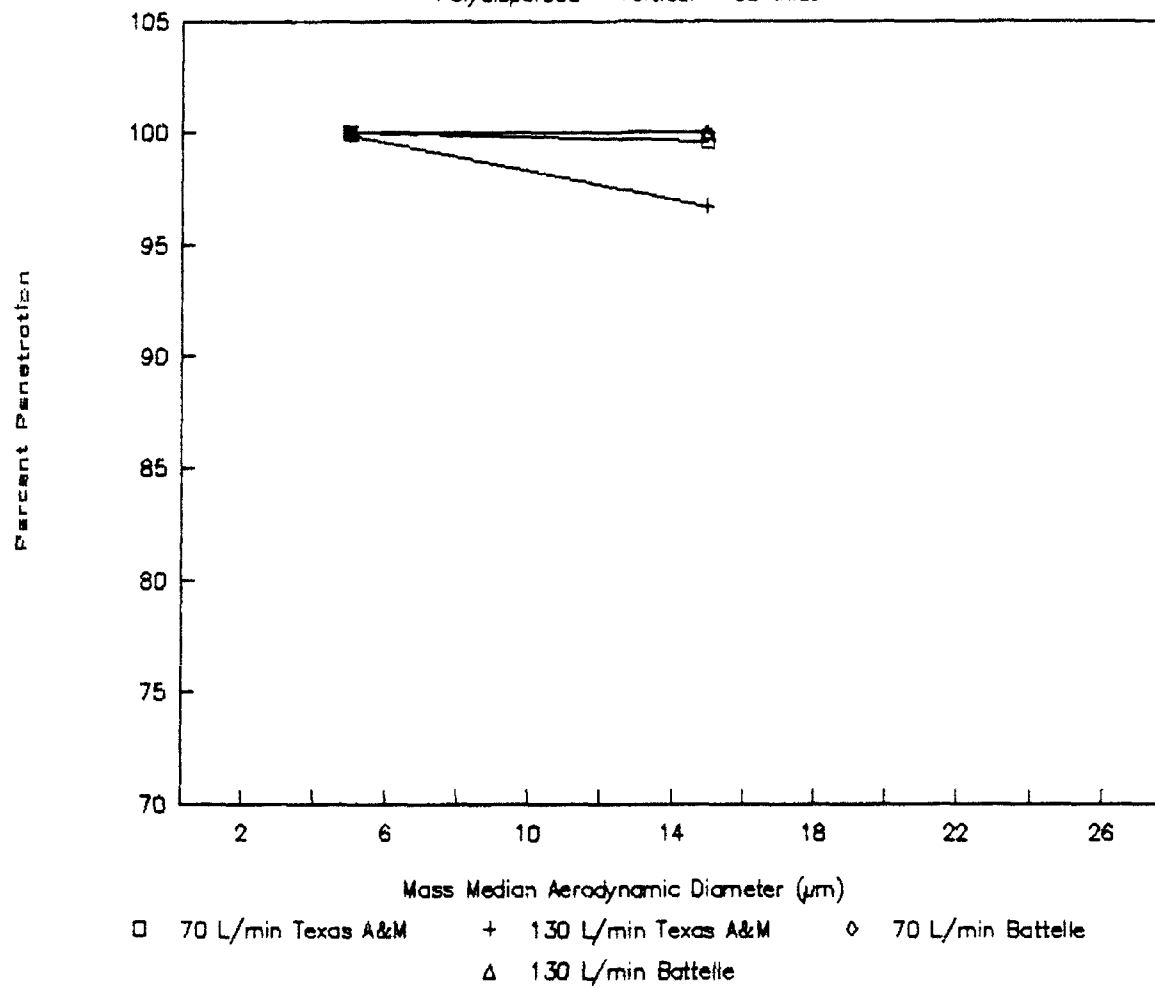
Legend:
- □ 70 L/min Texas A&M
- + 130 L/min Texas A&M
- ◊ 70 L/min Battelle
- △ 130 L/min Battelle

is important to note that only the Texas A&M model considers inlet orientations other than parallel to the air stream. The German model only considers a 0° inlet orientation. The Battelle model does not consider inlet orientation.

The vertical region sampling efficiency results for a polydispersed particle distribution indicate the following:

- The Texas A&M and German models predict a decrease in the sampling efficiency as the particle MMAD increases. The Battelle model predicts no change in efficiency.

- The Texas A&M and German models predict a decrease in the sampling efficiency as the flow rate increases. The Battelle model predicts no change in efficiency.

- The Texas A&M model predicts an increase in the sampling efficiency as the inlet orientation increases from 0° to 90°.

4.5.5 Numerical Efficiency Calculations for 45° Elbow Region of Aerosol Sampling Train

4.5.5.1 Monodispersed Particle Distribution - 45° Elbow Region

Table 15 presents the two model's numerical results for the 45° elbow region of the sampling train. Figure 23 provides a graphical presentation of the numerical results. It is important to note that for these calculations, the 45° elbow region is not affected by the inlet's orientation to the air stream. The 45° elbow region's sampling efficiency results indicate the following:

- Both models (Texas A&M and Battelle) predict a decrease in the efficiency as the particle size increases. The Texas A&M model predicts a greater decrease in efficiency than does the Battelle model at the larger particle sizes.

- Both models predict a decrease in the efficiency as the flow rate increases. The Texas A&M model predicts a greater decrease in efficiency than does the Battelle model at the larger particle sizes.
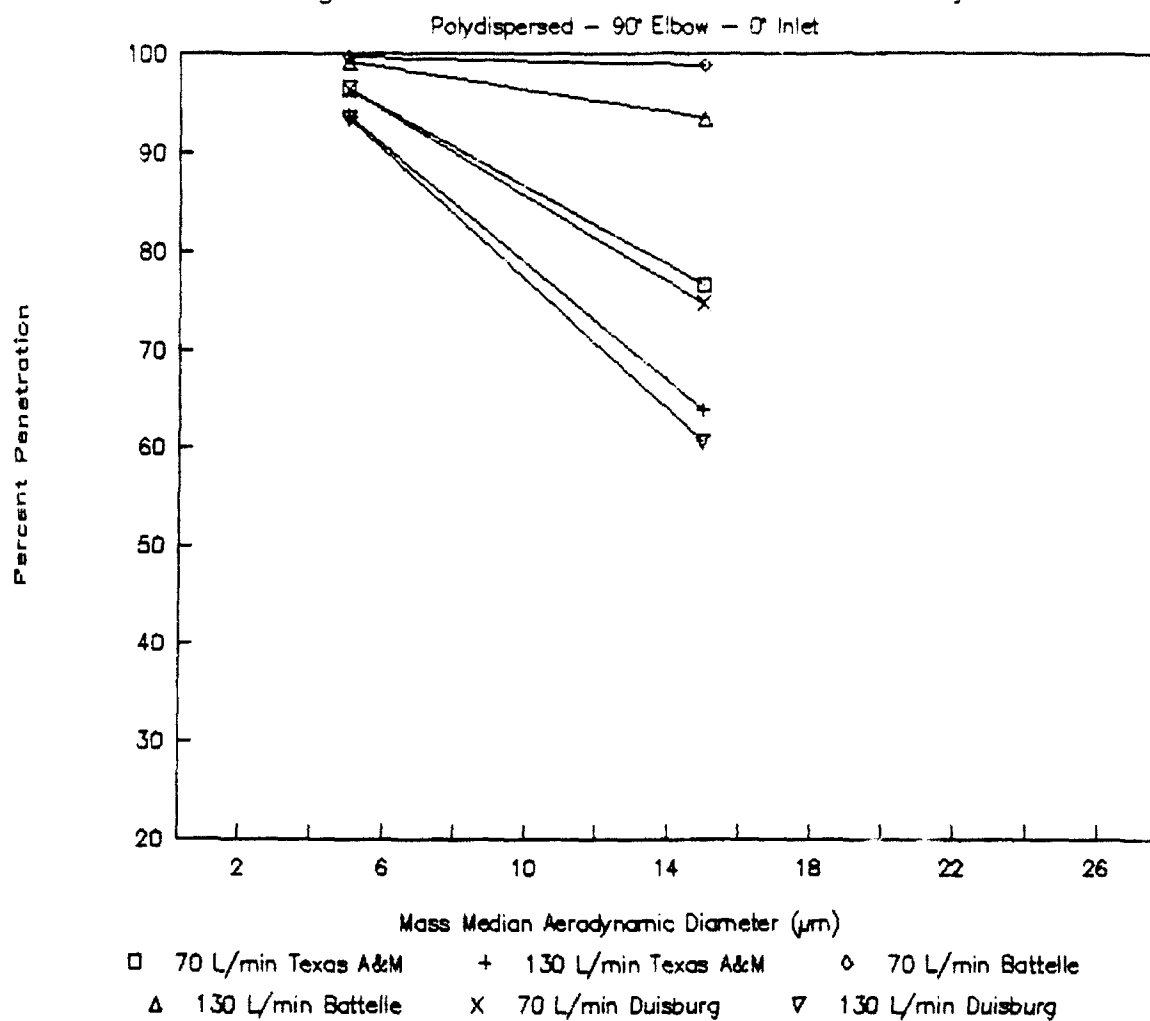
4.5.5.2 Polydispersed Particle Distribution - 45° Elbow Region

Table 16 presents the three model's numerical results for the 45° elbow region of the sampling train. Figures 24 and 25 provide a graphical presentation of the numerical results. It

73

	PARTICLE SIZE (μ)	FLOW RATE (l/min)	SAMPLING EFFICIENCY (% mass) FOR 45° ELBOW REGION	
			TEXAS A & M	BATTELLE
1.	3	70	99.5	99.9
2.	5	70	98.7	99.9
3.	7	70	97.4	99.9
4.	10	70	94.8	99.8
5.	15	70	88.8	99.7
6.	20	70	81.0	99.4
7.	25	70	72.0	98.8
8.	3	130	99.1	99.7
9.	5	130	97.5	99.7
10.	7	130	95.3	99.6
11.	10	130	90.6	99.2
12.	15	130	80.2	97.1
13.	20	130	67.7	94.4
14.	25	130	54.4	91.7

Table 15. Numerical Model Calculations (Monodispersed Particle Sizes) for 45° Elbow Region of Aerosol Sampling Train

Figure 23. Penetration Efficiency
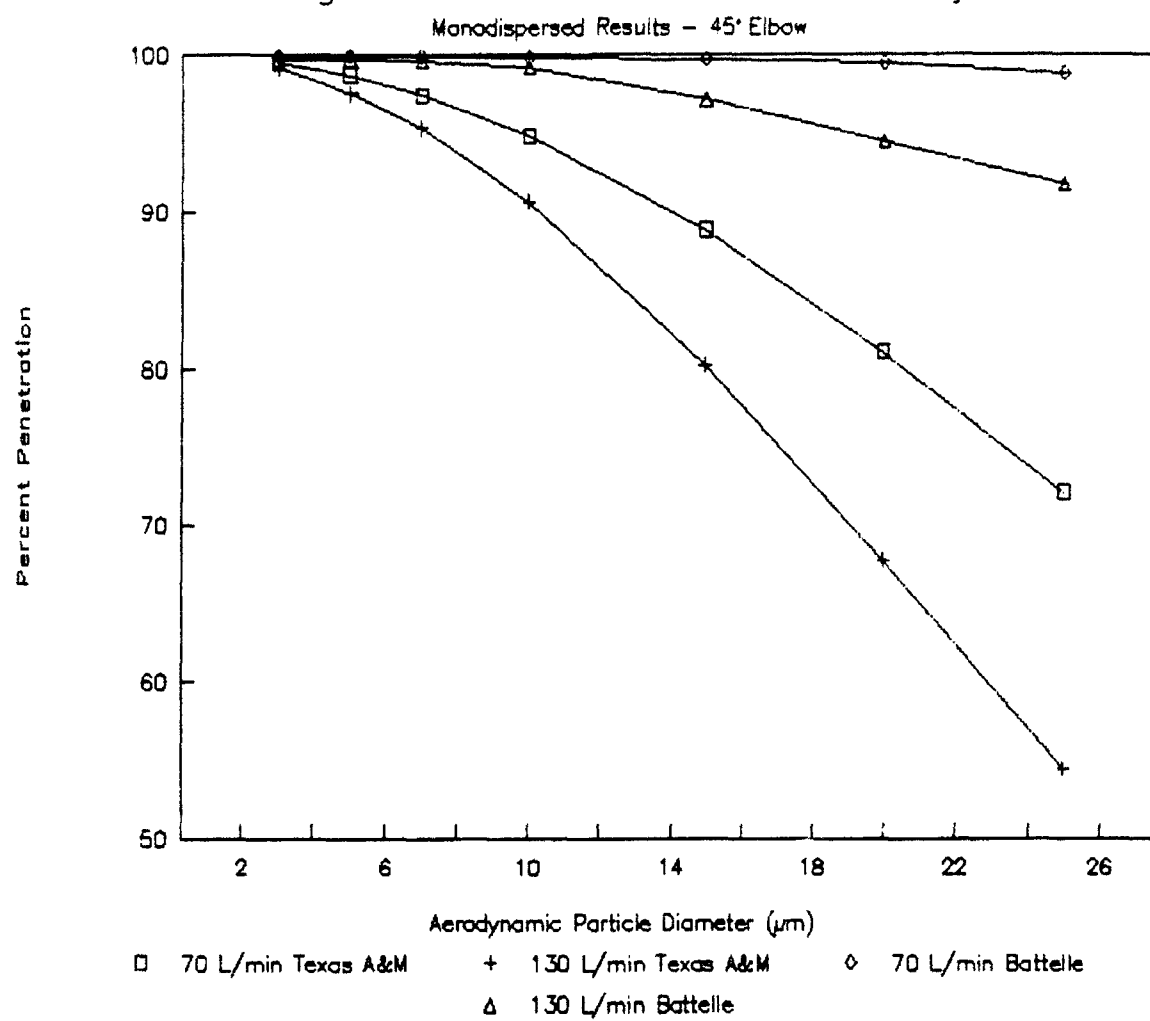
Monodispersed Results — 45° Elbow

Percent Penetration

Aerodynamic Particle Diameter (μm)

□　70 L/min Texas A&M　　　+　130 L/min Texas A&M　　　◊　70 L/min Battelle

△　130 L/min Battelle

MASS MEDIUM AERODYNAMIC DIAMETER (MMAD)(μ)	INLET PROBE ORIENTATION (α)	FLOW RATE (l/min)	SAMPLING EFFICIENCY (% mass) FOR 45° ELBOW SECTION		
			TEXAS A & M	BATTELLE	UNIVERSITY OF DUISBURG
1. 5	0°	70	98.3	99.9	96.4
2. 15	0°	70	88.9	99.5	74.7
3. 5	0°	130	96.9	99.6	93.5
4. 15	0°	130	83.6	96.8	60.5
5. 5	90°	70	98.4	99.9	N/A
6. 15	90°	70	90.9	99.5	N/A
7. 5	90°	130	97.0	99.6	N/A
8. 15	90°	130	85.2	96.8	N/A

Table 16. Model Efficiency Calculations (Polydispersed Particle Sizes) for 45° Elbow Region of Aerosol Sampling Train

76

Figure 24. Penetration Efficiency
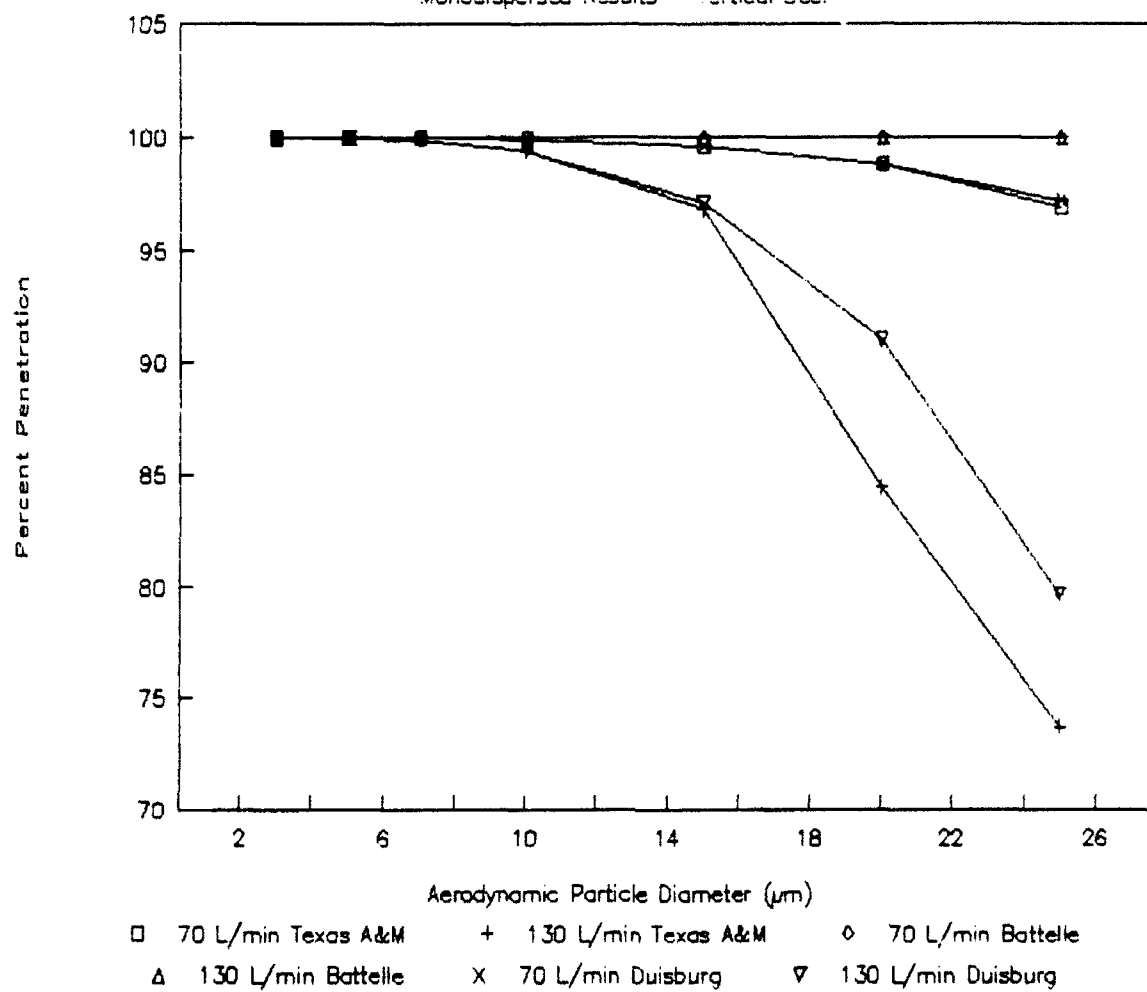
Polydispersed – 45° Elbow – 0° Inlet

70 L/min Texas A&M   + 130 L/min Texas A&M   ◇ 70 L/min Battelle
Δ 130 L/min Battelle   X 70 L/min Duisburg   ▽ 130 L/min Duisburg
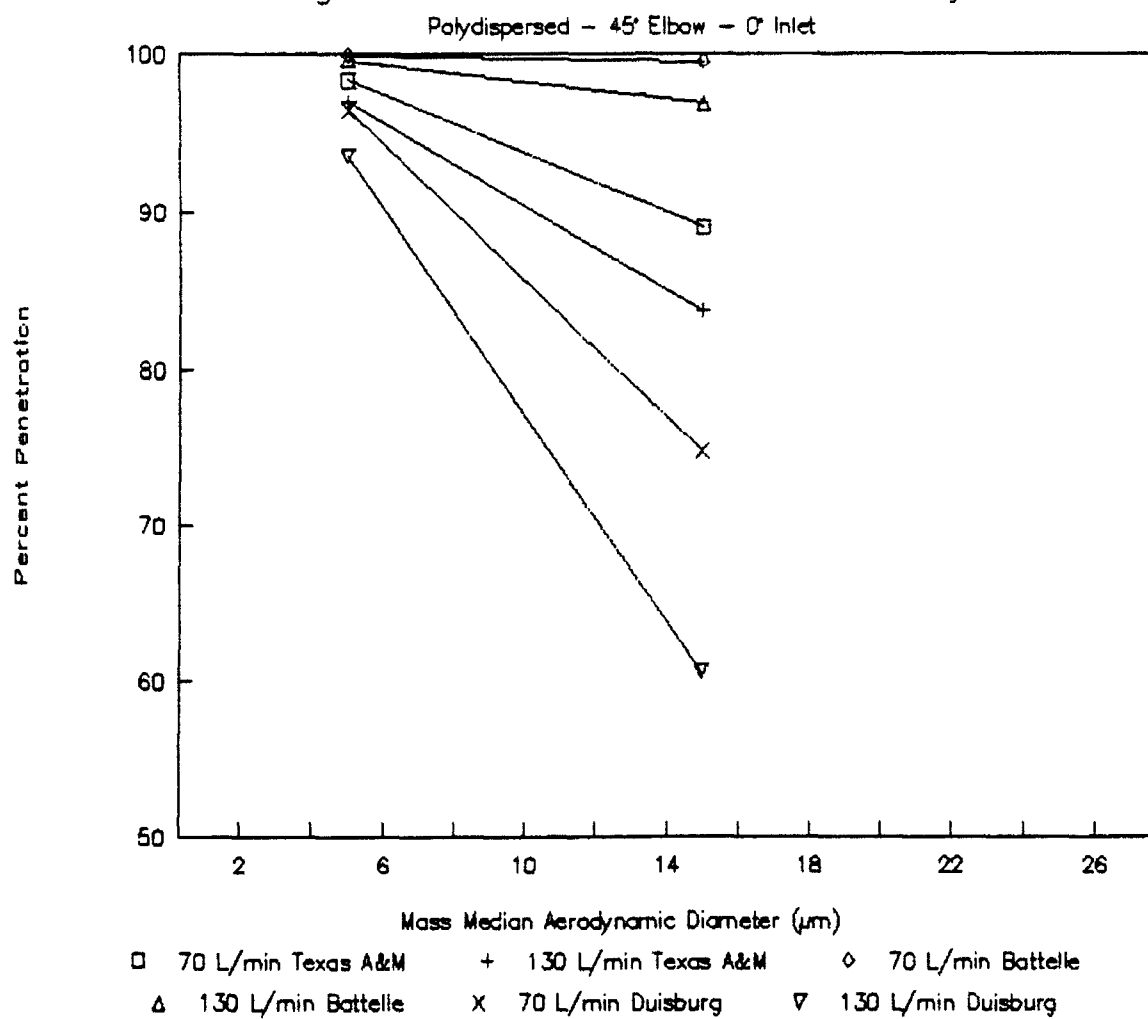
Figure 25. Penetration Efficiency
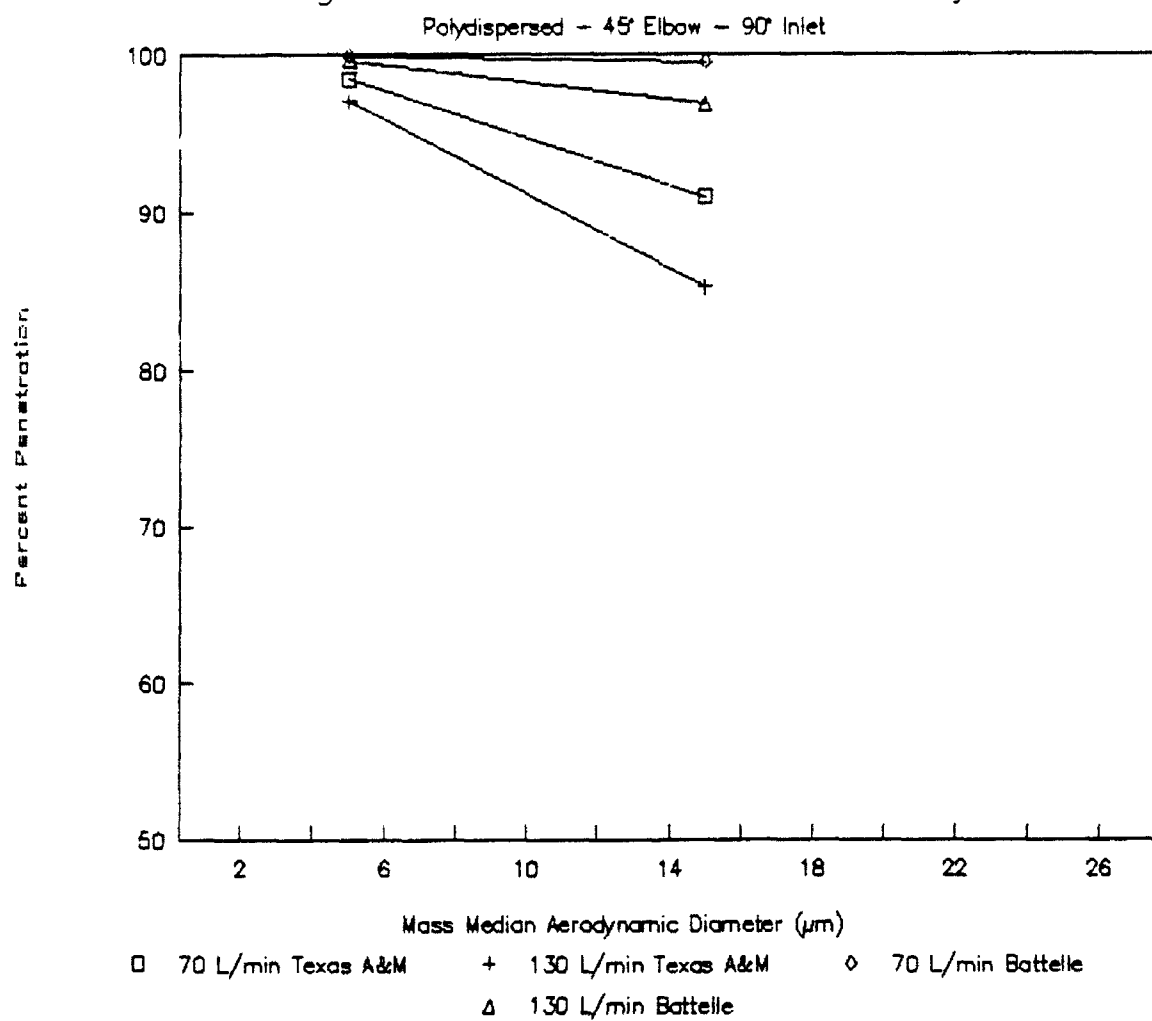
Polydispersed – 45° Elbow – 90° Inlet

Legend:
□ 70 L/min Texas A&M   + 130 L/min Texas A&M   ◊ 70 L/min Battelle
△ 130 L/min Battelle

is important to note that only the Texas A&M model considers air stream orientations other than parallel to the inlet. The German model only considers a $0°$ inlet orientation. The Battelle model does not consider inlet orientation.

The $45°$ elbow sampling efficiency results for a polydispersed particle distribution indicate the following:

- All three models predict a decrease in the sampling efficiency as the particle MMAD increases.

- All three models predict a decrease in the sampling efficiency as the flow rate increases.

- The Texas A&M model predicts an increase in the sampling efficiency as the inlet orientation increases from $0°$ to $90°$.

4.5.6   Numerical Efficiency Calculations for Inclined Region of Aerosol Sampling Train

4.5.6.1   Monodispersed Particle Distribution - Inclined Region

Table 17 presents the three model's numerical results for the inclined region of the sampling train. Figure 26 provides a graphical presentation of the numerical results. It is important to note that for these calculations, the vertical region is not affected by the inlet's orientation to the air stream.

The inclined region's sampling efficiency results indicate the following:

- All three models predict a decrease in the efficiency as the particle size increases.

- The Battelle and German models predict an increase in the efficiency as the flow rate increases. In addition the German model predicts a decrease in the sampling efficiency at the largest particle size (25μm). The Texas A&M model also predicts an increase in the efficiency as the flow rate increases except at the two largest particle sizes (20 and 25μm).

4.5.6.2   Polydispersed Particle Distribution - Inclined Region

Table 18 presents the three model's numerical results for the inclined region of the sampling train. Figures 27 and 28 provide a graphical presentation of the numerical results. It is

PARTICLE SIZE (μ)	FLOW RATE (l/min)	SAMPLING EFFICIENCY (% mass) FOR INCLINED REGION		
		TEXAS A & M	BATTELLE	UNIVERSITY OF DUISBURG*
1. 3	70	99.7	99.7	99.7
2. 5	70	99.3	99.2	99.2
3. 7	70	98.5	98.5	98.5
4. 10	70	97.1	9t.99	97.0
5. 15	70	93.4	93.3	93.4
6. 20	70	88.4	88.5	88.5
7. 25	70	82.0	82.6	82.2
8. 3	130	99.9	99.8	99.9
9. 5	130	99.6	99.6	99.6
10. 7	130	99.1	99.2	99.1
11. 10	130	98.1	98.4	98.1
12. 15	130	94.8	96.4	95.0
13. 20	130	84.1	93.6	90.7
14. 25	130	73.7	90.2	79.6

* Efficiency calculations based on model modifications provided by General Management Associates

Table 17. Numerical Model Calculations (Monodispersed Particle Sizes) for Inclined Region of Aerosol Sampling Train

Figure 26. Penetration Efficiency
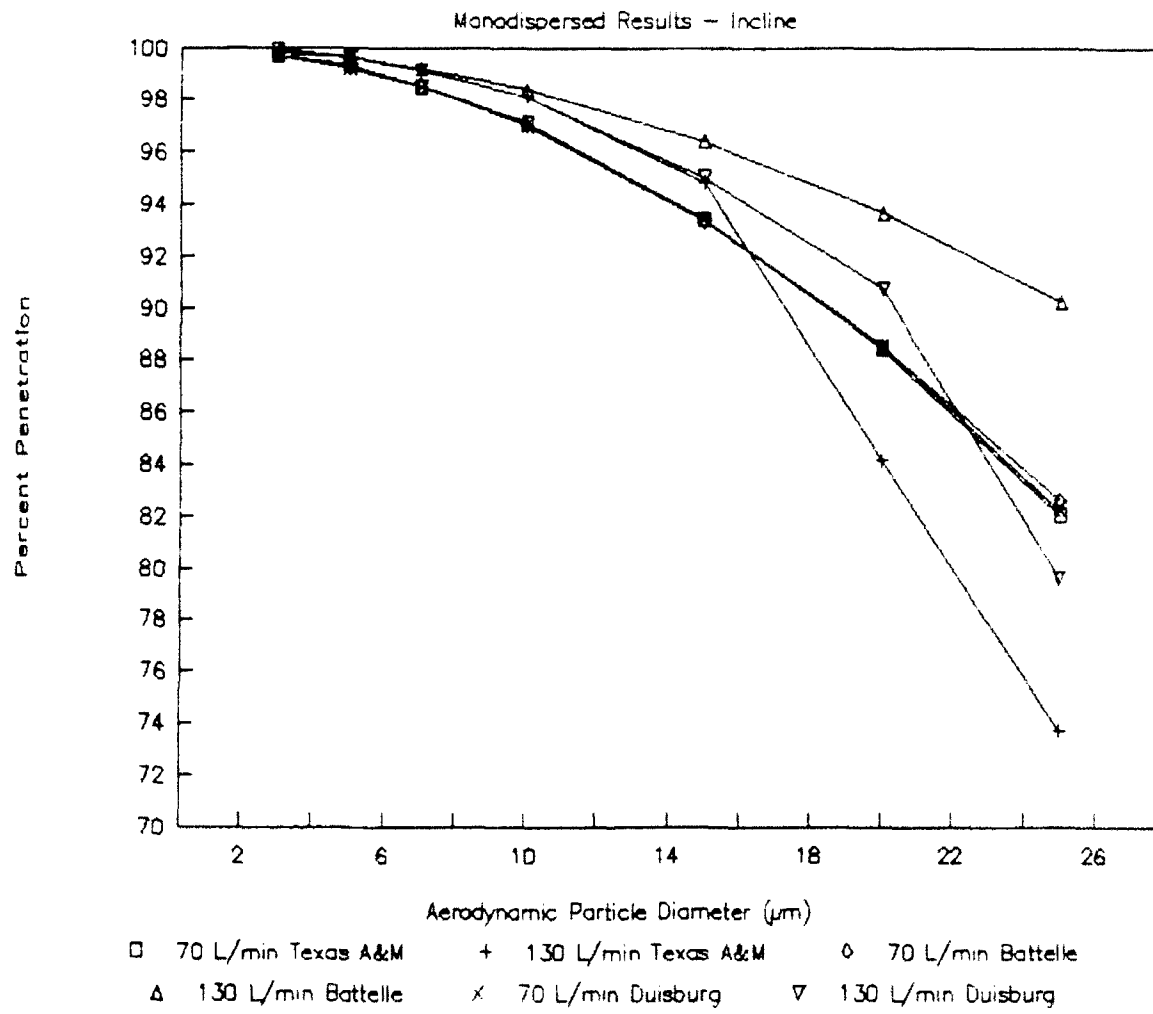
Monodispersed Results – Incline

Legend:
- □ 70 L/min Texas A&M
- + 130 L/min Texas A&M
- ◇ 70 L/min Battelle
- △ 130 L/min Battelle
- ✗ 70 L/min Duisburg
- ▽ 130 L/min Duisburg

	MASS MEDIUM AERODYNAMIC DIAMETER (MMAD)(μ)	INLET PROBE ORIENTATION (α)	FLOW RATE (l/min)	SAMPLING EFFICIENCY (% mass) FOR INCLINED SECTION		
				TEXAS A & M	BATTELLE	UNIVERSITY OF DUISBURG
1.	5	0°	70	99.0	98.96	98.9
2.	15	0°	70	93.7	92.2	91.0
3.	5	0°	130	99.4	99.4	99.4
4.	15	0°	130	95.4	95.6	90.8
5.	5	90°	70	99.1	98.96	N/A
6.	15	90°	70	94.9	92.2	N/A
7.	5	90°	130	99.5	99.4	N/A
8.	15	90°	130	96.1	95.6	N/A

Table 18. Model Efficiency Calculations (Polydispersed Particle Sizes)
for Inclined Region of Aerosol Sampling Train

Figure 27. Penetration Efficiency

Polydispersed — Incline — 0° Inlet

Mass Median Aerodynamic Diameter (μm)

| □ | 70 L/min Texas A&M | + | 130 L/min Texas A&M | ◊ | 70 L/min Battelle |
| Δ | 130 L/min Battelle | X | 70 L/min Duisburg | ▽ | 130 L/min Duisburg |

83
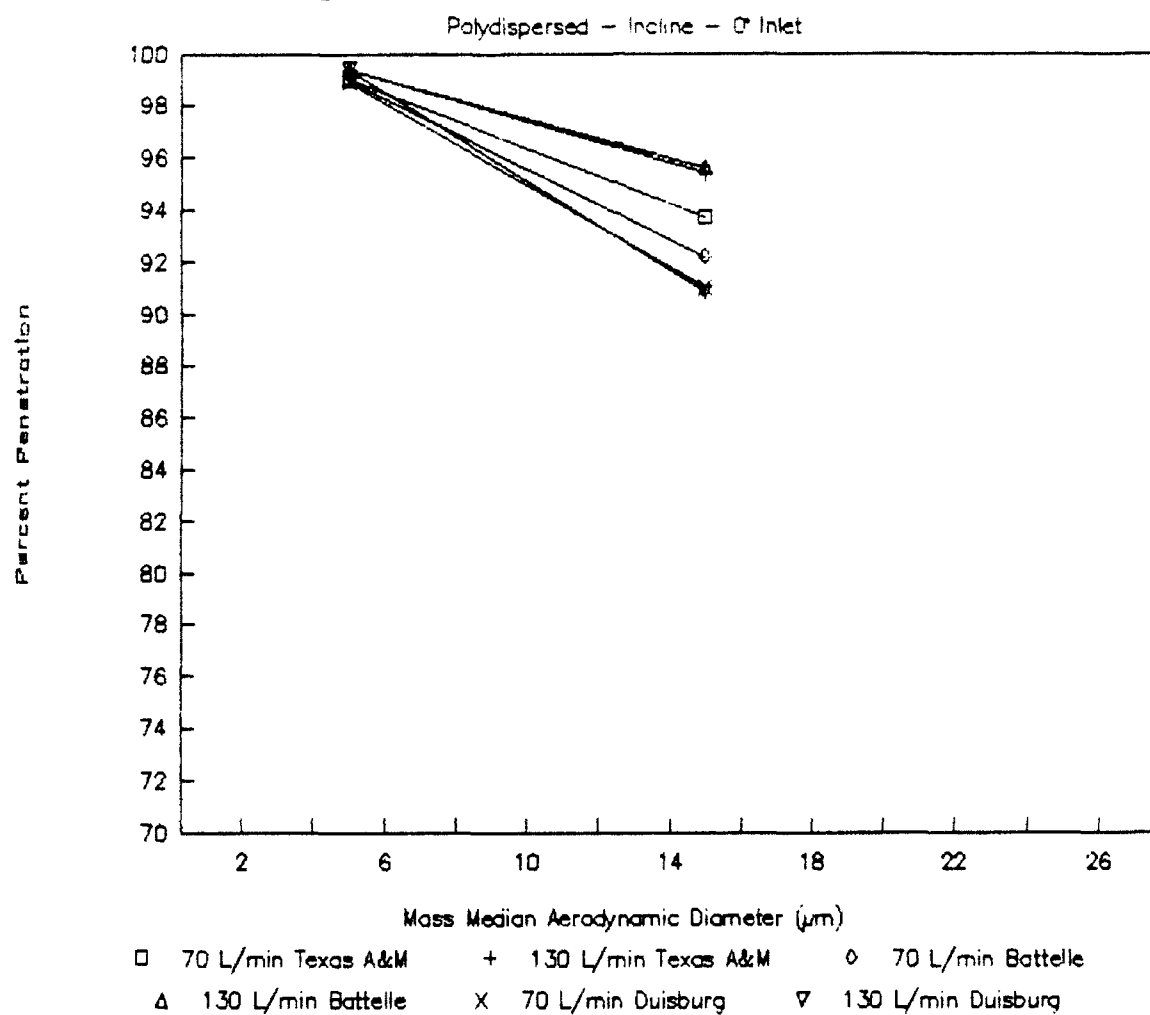
Figure 28. Penetration Efficiency
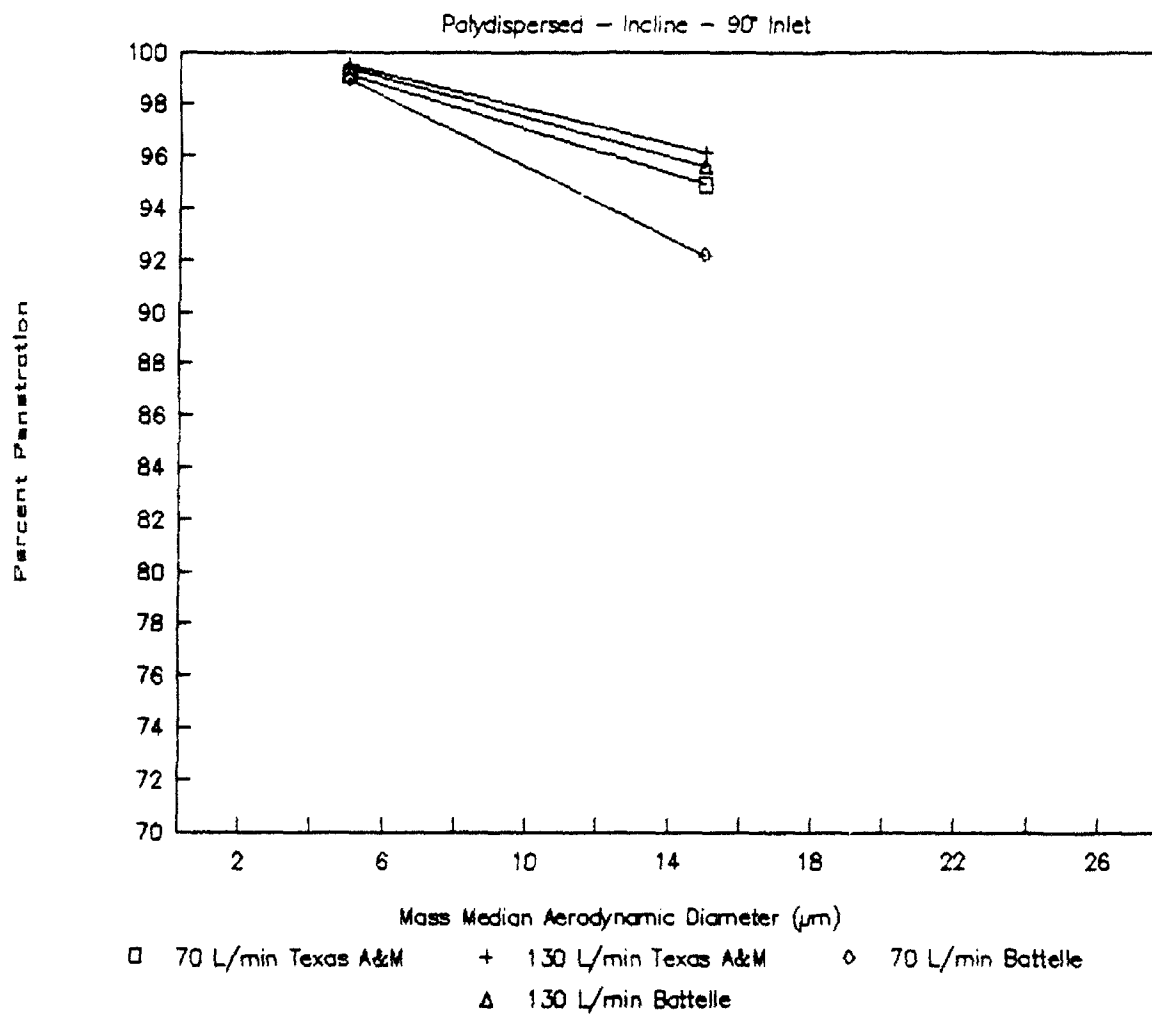
Polydispersed — Incline — 90° Inlet

Mass Median Aerodynamic Diameter (μm)

□ 70 L/min Texas A&M   + 130 L/min Texas A&M   ◊ 70 L/min Battelle

△ 130 L/min Battelle

important to note that only the Texas A&M model considers inlet orientations other than parallel to the air stream. The German model only considers a 0° inlet orientation. The Battelle model does not consider inlet orientation.

The inclined sampling efficiency results for a polydispersed particle distribution indicate the following:

- All three models predict a decrease in the sampling efficiency as the particle MMAD increases.

- All three models predict an increase in the sampling efficiency as the flow rate increases. However, the German model predicts a decrease in the efficiency as the flow rate increases for the 15μm MMAD.

- The Texas A&M model predicts an increase in the sampling efficiency as the inlet orientation increases from 0° to 90°.

4.5.7   Cumulative Efficiency Calculations for Overall Sampling Train

4.5.7.1   Monodispersed Particle Distribution - Overall Efficiencies

Table 19 presents the three model's numerical efficiency results for the overall sampling train. Figure 29 provides a graphical presentation of the numerical results for the monodispersed conditions. It is important to note that for these calculations, the Battelle model does not consider inlet orientation, the German model considers only a 0° inlet orientation and the Texas A&M model considers variable inlet orientations.

The cumulative efficiency results for monodispersed aerosol particles penetrating through the overall sampling train indicate the following:

- All three models predict a decrease in the cumulative efficiency as the particle size increases.

- Both the Texas A&M and University of Duisburg models predict a decrease in the cumulative sampling efficiency as the flow rate increases. The Battelle model overall predicts a decrease in the cumulative efficiency as the flow rate increases except at the 5 and 7μm particle sizes where an increase occurs in the efficiency.

85

TYPE OF PARTICLE DISTRIBUTION	PARTICLE SIZE (μ)	INLET PROBE ORIENTATION (α)	FLOW RATE (l/min)	AIR VELOCITY (m/sec)	CUMULATIVE SAMPLING EFFICIENCY (% mass)		
					TEXAS A & M	BATTELLE	UNIVERSITY OF DUISBURG
1. MONODISPERSED	3	0°	70	3	97.4	99.0	98.4
2. MONODISPERSED	5	0°	70	3	93.6	97.8	95.7
3. MONODISPERSED	7	0°	70	3	88.4	96.0	91.7
4. MONODISPERSED	10	0°	70	3	78.6	92.4	83.3
5. MONODISPERSED	15	0°	70	3	59.0	83.9	64.6
6. MONODISPERSED	20	0°	70	3	39.2	73.1	43.8
7. MONODISPERSED	25	0°	70	3	22.8	60.7	25.6
8. MONODISPERSED	3	0°	130	3	96.3	98.8	95.9
9. MONODISPERSED	5	0°	130	3	90.4	98.0	89.1
10. MONODISPERSED	7	0°	130	3	82.5	96.7	79.8
11. MONODISPERSED	10	0°	130	3	67.8	93.9	63.0
12. MONODISPERSED	15	0°	130	3	41.0	83.7	34.6
13. MONODISPERSED	20	0°	130	3	16.6	71.7	14.2
14. MONODISPERSED	25	0°	130	3	5.6	60.2	3.9
15. POLYDISPERSED	MMAD=5 (σ =1.5)	0°	70	3	91.9	97.1	94.1
16. POLYDISPERSED	MMAD=15 (σ =1.5)	0°	70	3	55.5	79.8	59.9
17. POLYDISPERSED	MMAD=5 (σ =1.5)	0°	130	3	87.8	97.4	86.0
18. POLYDISPERSED	MMAD=15 (σ =1.5)	0°	130	3	40.1	80.7	35.8

Table 19. Cumulative Sampling Efficiency Results Generated by the Three Aerosol Models

Figure 29. Penetration Efficiency

Monodispersed — Cumulative — 0° Inlet

Legend:
- □ 70 L/min Texas A&M
- + 130 L/min Texas A&M
- ◇ 70 L/min Battelle
- Δ 130 L/min Battelle
- X 70 L/min Duisburg
- ▽ 130 L/min Duisburg

Y-axis: Percent Penetration
X-axis: Aerodynamic Particle Diameter (μm)
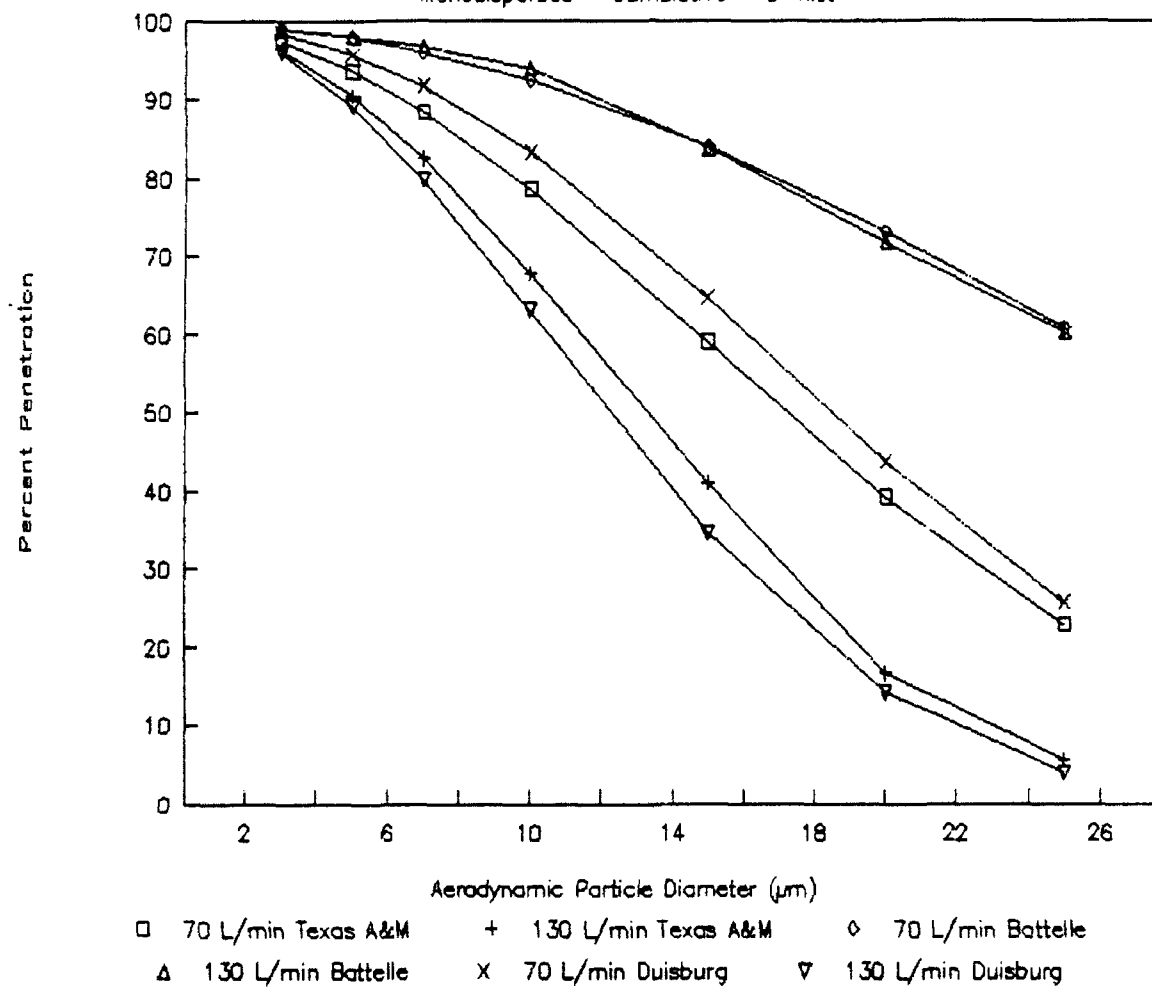
- Both the Texas A&M and German models produce very comparable predicted results across all seven particle sizes and for the two flow rates. The Battelle model as compared to the other two models produces very comparable predicted results at the 3 and 5μm particle sizes but produces significantly higher predicted efficiencies at the other five particle sizes.

4.5.7.2 Polydispersed Particle Distribution - Overall Efficiencies

Table 19 cited earlier also presents the three model's numerical efficiency results for the overall sampling train based on a polydispersed particle distribution. Figure 30 provides a graphical presentation of the numerical results for the polydispersed condition. It is important to note that for these calculations, the Battelle model does not consider inlet orientation, the University of Duisburg model considers only a 0° inlet orientation, and the Texas A&M model considers variable inlet orientations.

The cumulative efficiency results for polydispersed aerosol particles penetrating through the overall sampling train indicate the following:

- All three models predict a decrease in the cumulative efficiency as the particle MMAD increases.

- Both the Texas A&M and German models predict a decrease in the cumulative efficiency as the flow rate increases. The Battelle model predicts an increase in the cumulative efficiency as the flow rate increases.

- Both the Texas A&M and German models produce very comparable predicted results across the two particle MMADs and two flow rates. The Battelle model as compared to the other two models produces fairly comparable predicted results at the 5μm MMAD and 70 1/min flow rate. However, the model produces higher predicted efficiencies at the other three combinations of flow rates and particle MMAD.

Figure 30. Penetration Efficiency

Polydispersed – Cumulative – 0° Inlet

Legend:
- □ 70 L/min Texas A&M
- + 130 L/min Texas A&M
- ◊ 70 L/min Battelle
- △ 130 L/min Battelle
- X 70 L/min Duisburg
- ▽ 130 L/min Duisburg

Axis labels: Percent Penetration (vertical), Mass Median Aerodynamic Diameter (μm) (horizontal)
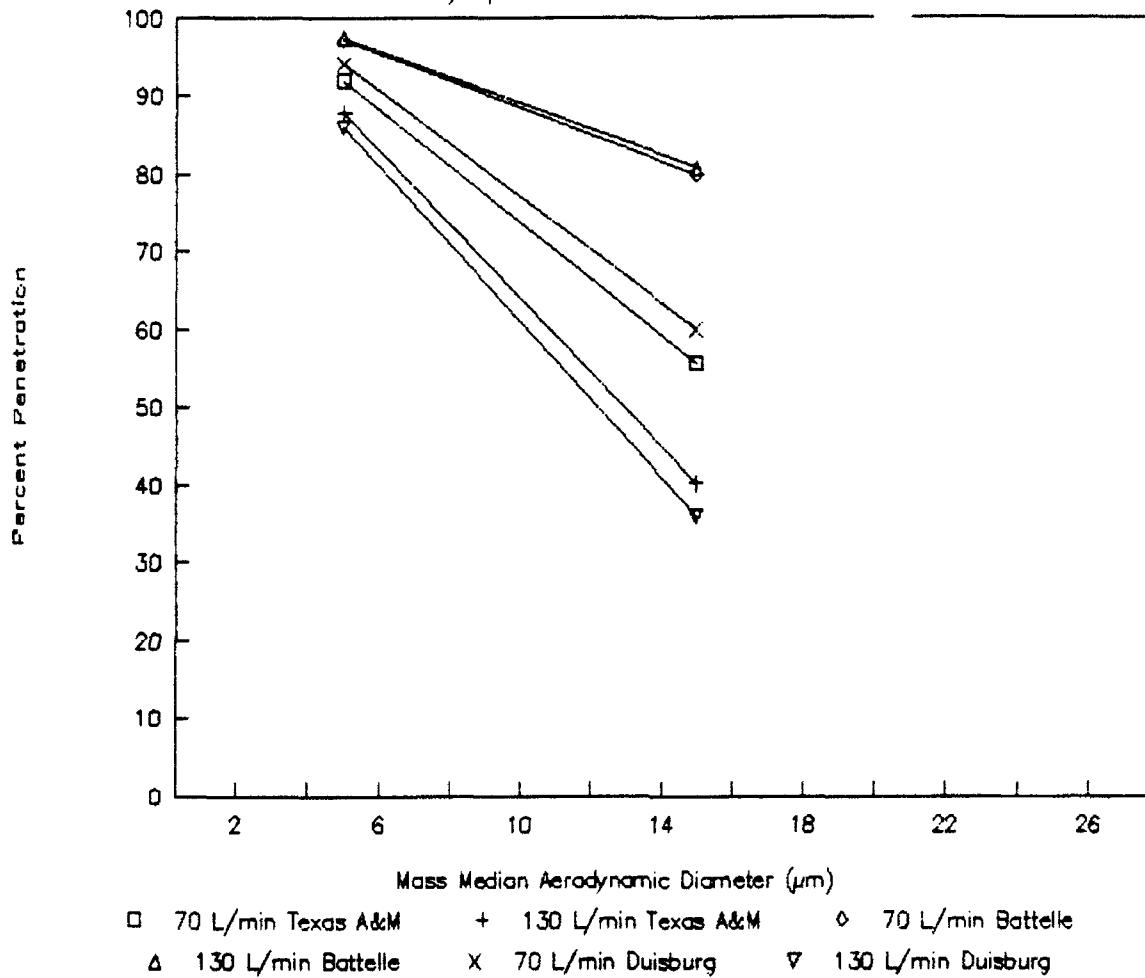
THIS PAGE INTENTIONALLY LEFT BLANK

SECTION 5.   RESULTS OF EXPERIMENTAL VERIFICATION

5.1   EXPERIMENTAL APPARATUS AND METHODOLOGY FOR AEROSOL
           PENETRATION MEASUREMENTS

The aerosol sampling setup as presented earlier in Figure 1 was the experimental configureation used to measure the penetration (losses) of monodispersed aerosol particles through the sampling train. Seven monodispersed particle sizes were generated in the experiment. They were 3, 5, 7, 10, 15, 20 and 25μm aerodynamic equivalent diameter (AED). Two inlet configurations were considered. They were 0° and 90° whereby the inlet of the transport system is parallel to the wind tunnel air stream and perpendicular to the air stream, respectively.

The aerosol transport system was constructed from a single piece of 1-inch Schedule 40 PVC pipe. The inlet was chamfered at 30° relative to the tube axis and was machined to a sharp edge. Elbows were formed by electrically heating the appropriate region of the tube, carefully bending it, and clamping the tube into a mold as it cooled. The mold prevented flattening of the tube at the elbow. The elbow curvature of the mold was patterned from electrical conduit bends.

An aerosol wind tunnel with a basic 600 mm x 600 mm cross section was used for the testing. Monodisperse aerosol droplets were created with a vibrating jet atomizer (Ref. 16) at the tunnel entrance. A Stairmand disc is used to create large scale mixing at the tunnel entrance and to help uniformize the aerosol concentration profiles across the center 2/3 of the wind tunnel. Downstream from the Stairmand disc is a fan which further stirs the aerosol to help obtain uniform concentration profiles. A perforated plate is placed downstream from the fan to reduce the scale of turbulence and to uniformize the velocity profile. At the test section, the wind tunnel body is expanded to a cross section of 1.2 m x 1.2 m and the air stream is reduced in cross section to 360 mm x 360 mm. This arrangement reduces blockage effects that could arise from the presence of artifacts in the test section.

Aerosol was generated from a mixture of oleic acid and an analytical tracer (sodium fluorescein) dissolved in alcohol. Immediately after generation, the alcohol evaporates, leaving a residual droplet that consists of 12.4% (m/m) analytical tracer and oleic acid. Particle size of the aerosol was determined microscopically with the droplets collected on glass slides which had been treated with an oil phobic agent. Size observed under the microscope was converted to an equivalent sperical diameter through use of the flattening factor of Olan-Figuroa et al. (Ref. 17). This factor takes into account the phenomenon that gravity flattens droplets on the slide and causes them to appear larger

91

than they were in the aerosol state. The equivalent spherical
diameter was converted to aerodynamic equivalent diameter (AED)
through use of the expression:

$$C_a \ D_a^2 \ P_w = C_p \ P_p \ D_p^2 \qquad (41)$$

Where: C_a = Cunningham's slip correction for the aerodynamic
equivalent diameter size, D_a = AED, P_w = density of water (1000
kg/m^3), C_p = Cunningham's slip correction for the equivalent
spherical diameter, D_p = equivalent spherical diameter, and P_p =
particle density. Cunningham's correction C_1 for the two sizes
was calculated from:

$$C_1 = 1 + \frac{2.52 \ L}{D_i} \qquad (42)$$

Where: L = mean free path of the air molecules (taken as 0.068
μm). The aerosol density is kg/m^3 as calculated from the mass
fractions of oleic acid and sodium fluorescein.

In conducting a test, the aerosol would be sampled in
the wind tunnel with an isokinetic probe which consists of a
sharp edged inlet, a conical diffuser and a filter collector.
Either in parallel with operation of the isokinetic probe or
subsequent to use of the isokinetic probe, we would draw an
aerosol sample through the model transport system. Aerosol which
was transmitted through the system was collected with a filter.

In an analysis laboratory, sodium fluorescein was
extracted from the filter of the isokinetic probe, from the
internal walls of the isokinetic probe, and from the filter of
the aerosol transport system. The concentration of fluorescein
in the extracts was determined with a Sequoia-Turner Model 450
Fluorometer (Sequoia-Turner Corp., Mountain View, CA).

Penetration of aerosol through the transport system was
calculated from:

$$P = \frac{C_{ts}}{C_{iso}} \qquad (43)$$

Where: C_{iso} = concentration of aerosol in the wind tunnel based
on the fluorescein collected by the isokinetic filter and the
fluorescein deposited on the internal walls of the isokinetic
probe, C_{ts} = concentration of aerosol calculated from the
fluorescein collected by the filter at the downstream end of the
transport system.

5.2 EXPERIMENTAL RESULTS

Tests were conducted with a range of monodispersed aerosol particle sizes of approximately 3-25μm AED, with the inlet of the transport system parallel to the wind tunnel air stream (0°) and with the inlet perpendicular to the air stream (90°). Tests were conducted with two flow rates through the system (70 and 130 l/min). The cumulative sampling efficiency results from these tests are presented in Table 20 and Figures 31 and 32. The complete set of experimental data are provided at Appendix F. The cumulative sampling efficiency results for a monodispersed particle distribution indicate the following:

- As the particle size increases, the sampling efficiency decreases.

- As the flow rate (70 l/min to 130 l/min) increases, the sampling efficiency decreases.

- The larger the particle size, the greater the decrease in sampling efficiency.

- As the inlet orientation increases, the sampling efficiency appears to decrease based on a comparison of similar sized particles across the two inlet orientaticns.

- Increase in the inlet orientation appears to produce a more dramatic decrease in the sampling efficiency than does an increase in the flow rate based on a comparison of similiar sized particles across the two inlet orientations.

At the completion of the regular test program, the sampling train was to be segmentized in straight sections, elbows, and the inlet. The system was then to be reassembled using couplings in order to run two tests, one at a flow rate of 130 l/min and one at a flow rate of 70 l/min, in which the wall deposits would be extracted for the individual components and determine the regional losses. The particle size to be cnosen for these tests were those which give penetration values on the order of 50% for the overall system. This phase of testing was never performed due to time and money constraints. Therefore, no experimental data was gathered to determine the penetration of aerosols through each of the tubing sections of the sampling train. In addition, no experiments were conducted which utilized polydispersed particle distributions.

SIZE OF MONODISPERSED PARTICLE (μ)	INLET ORIENTATION [A] (α)	FLOW RATE (l/min)	CUMULATIVE SAMPLING PENETRATION EFFICIENCY (% mass)
3.0	0°	70	105.3
5.1	0°	70	96.3
7.0	0°	70	89.9
9.8	0°	70	83.0
12.0	0°	70	73.7
15.2	0°	70	55.8
19.4	0°	70	32.8
26.7	0°	70	6.5
3.0	0°	130	93.1
5.1	0°	130	90.4
7.0	0°	130	86.4
9.8	0°	130	69.6
12.0	0°	130	57.6
15.2	0°	130	31.5
19.4	0°	130	11.1
26.7	0°	130	1.1
3.5	90°	70	93.1
4.9	90°	70	92.5
7.2	90°	70	76.0
7.4	90°	70	75.4
10.1	90°	70	61.9
11.5	90°	70	44.7
14.9	90°	70	20.4
19.6	90°	70	4.3
25.4	90°	70	1.9
3.5	90°	130	92.4
4.9	90°	130	87.6
7.2	90°	130	82.9
7.4	90°	130	81.8
10.1	90°	130	62.5
11.5	90°	130	56.0
14.9	90°	130	27.1
19.6	90°	130	4.0
25.4	90°	130	0.5

[A]   Relative to the Wind Tunnel Air Flow Direction

Table 20. Cumulative Penetration Efficiency Results Derived Experimentally by Texas A & M

Figure 31. Experimental Results

Cumulative Penetration Efficiency

70 L/min 0° Inlet   +   130 L/min 0° Inlet
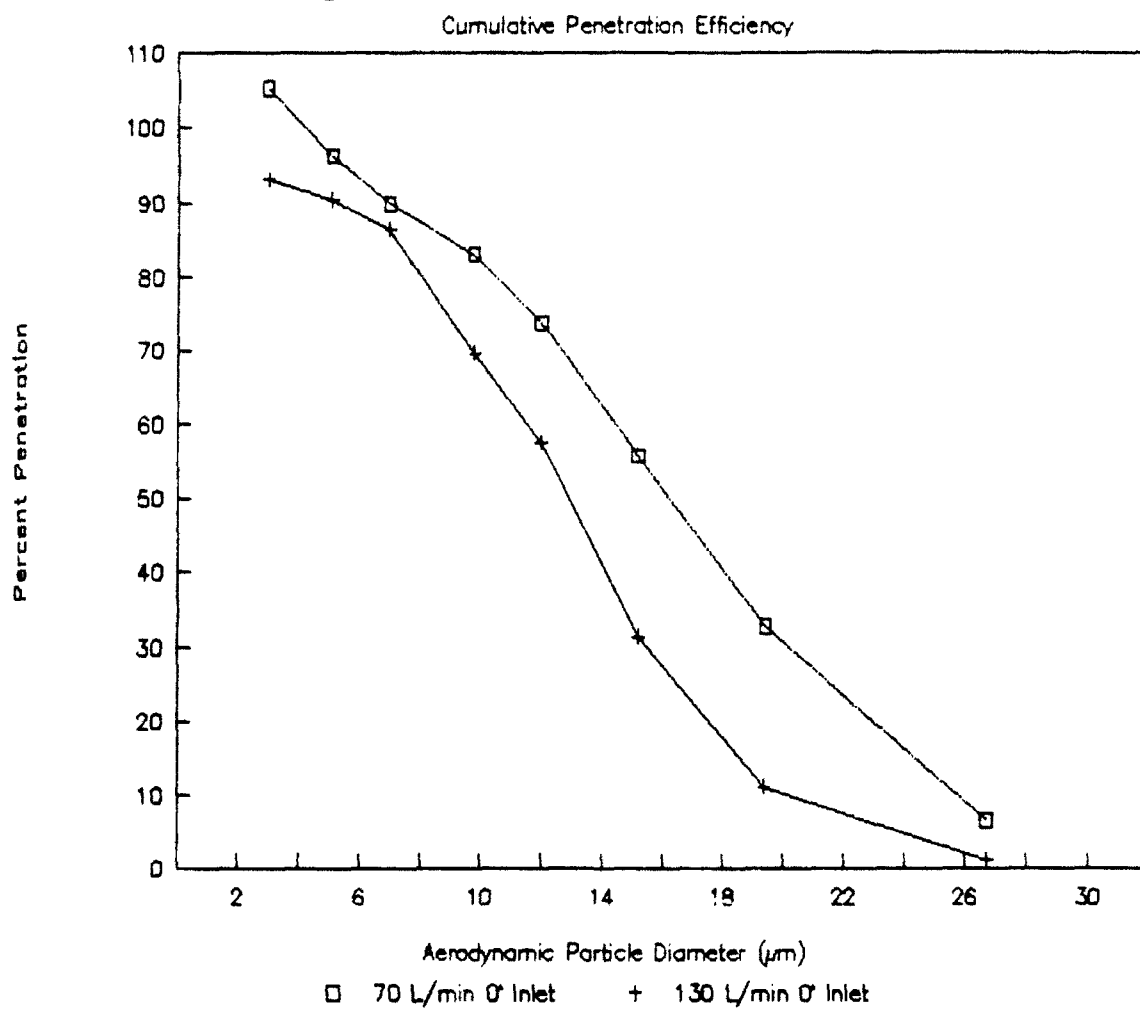
Figure 32. Experimental Results

Cumulative Penetration Efficiency

Aerodynamic Particle Diameter (μm)

□   70 L/min 90° Inlet   +   130 L/min 90° Inlet
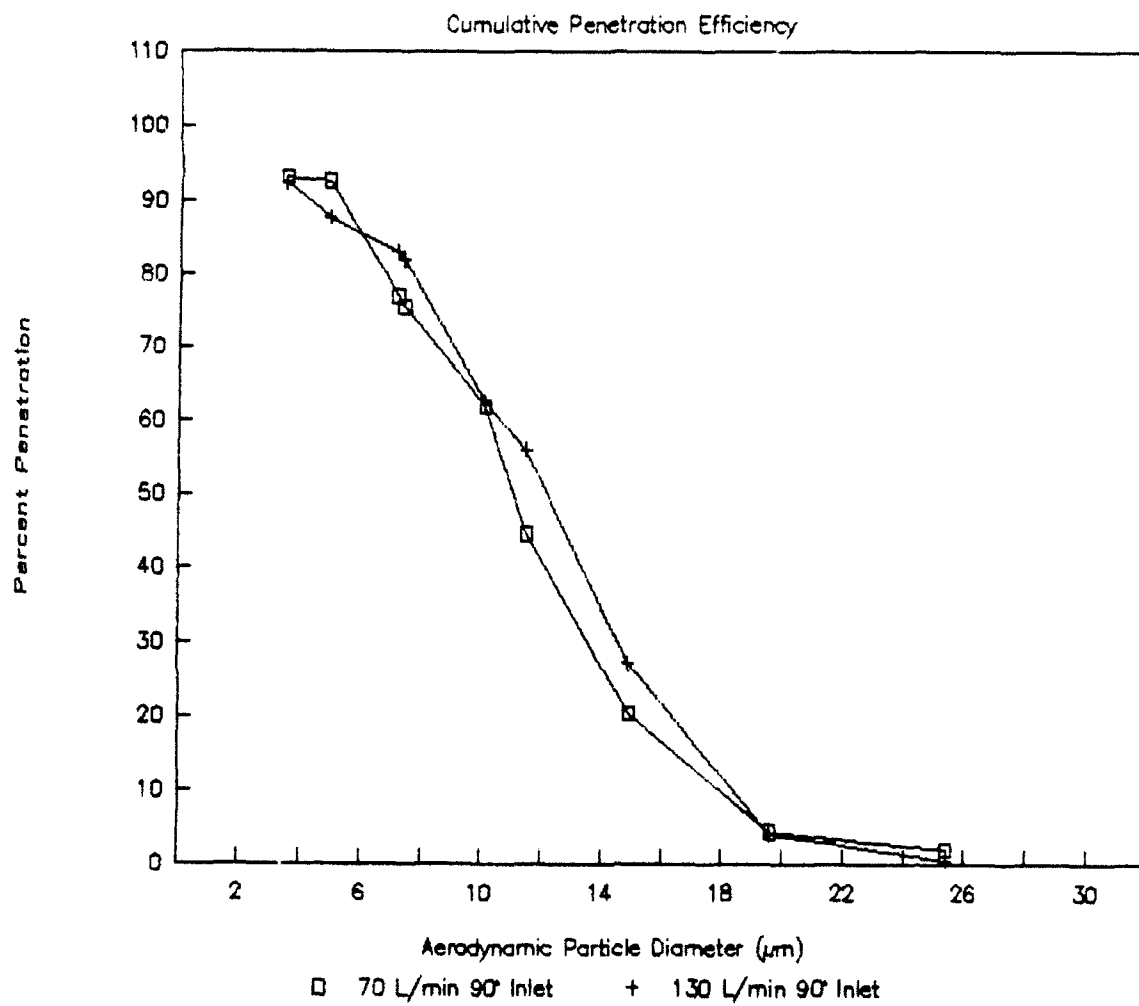
SECTION 6. COMPARISON OF EXPERIMENTAL AND NUMERICAL RESULTS

6.1 LIMITATIONS IN COMPARISON OF EXPERIMENTAL AND NUMERICAL RESULTS

As discussed earlier in Section 5.2, only the cumulative penetration efficiency of monodispersed aerosol particles through the sampling train was measured in the experiments. Therefore, no comparison could be made to determine how realistic the model's predicted penetration efficiency through each section of the sampling train was to experimental data. Furthermore, only the Texas A&M and German models predicted cumulative penetration efficiencies through all six regions of the sampling train. The Battelle model predicted cumulative penetration efficiencies through five sections (inlet region was not included) of the sampling train and the IITRI model predicted cumulative penetration efficiencies through one region (inlet only) of the sampling train. Consequently, comparison of the experimental results will be made to only numerical results for the Texas A&M, Battelle, and German models. It is important to note that the experimental apparatus was not able to achieve, for each experimental run, the specified particle size to be disseminated at the inlet section of the train. However, the model results are based on a specified particle size being disseminated at the inlet section. Therefore, the model predictions are compared to experimental data which may be for similar and not necessarily identical particle size disseminated in the wind tunnel. Comparison of the model results to the experimental measurements are presented in Table 21 and Figures 33 and 34.

6.2 DISCUSSION OF EXPERIMENTAL VS NUMERICAL RESULTS

6.2.1 Comparison of Results for 0° Inlet Orientation and 70 l/min Flow Rate Conditions

The Texas A&M model and the University of Duisburg model simulate a 0° inlet orientation and 70 l/min flow rate. However, the Battelle model does not consider different inlet orientations but instead assumes 100% inlet efficiency. The Battelle model does consider different flow rates.

Both the Texas A&M and German models provide predictions of cumulative penetration efficiencies for the seven monodispersed particle distributions which are reasonably close to those measured in the wind tunnel. The Battelle model predicts cumulative efficiency values which are in close agreement with the measured values at the 3.0 and 5.0 μm particle sizes. However, at the 15, 20 and 25 μm particle sizes, the Battelle model predictions differ significantly from the measured

SIZE OF MONODISPERSED PARTICLE (μ)	INLET ORIENTATION (α)	FLOW RATE (l/min)	CUMULATIVE SAMPLING PENETRATION EFFICIENCY (% mass)			
			EXPERIMENTALLY MEASURED	MODEL PREDICTIONS		
				TEXAS A & M	GERMAN [B]	BATTELLE [A]
3.0	0°	70	105.3	97.4	98.4	99.0
5.1	0°	70	96.3	93.6	95.7	97.8
7.0	0°	70	89.9	88.4	91.7	96.0
9.8	0°	70	83.0	78.6	83.3	92.4
12.0	0°	70	73.7	—	—	—
15.2	0°	70	55.8	59.0	64.6	83.9
19.4	0°	70	32.8	39.2	43.8	73.1
26.7	0°	70	6.5	22.8	25.6	60.7
3.0	0°	130	93.1	96.3	95.9	98.8
5.1	0°	130	90.4	90.4	89.1	98.0
7.0	0°	130	86.4	82.5	79.8	96.7
9.8	0°	130	69.6	67.8	63.0	93.9
12.0	0°	130	57.6	—	—	—
15.2	0°	130	31.5	41.0	34.6	83.7
19.4	0°	130	11.1	16.6	14.2	7?.7
26.7	0°	130	1.1	5.6	3.9	60.2
3.5	90°	70	93.1	94.3	—	—
4.9	90°	70	92.5	85.6	—	—
7.2	90°	70	76.9	74.7	—	—
7.4	90°	70	75.4	—	—	—
10.1	90°	70	61.9	57.0	—	—
11.5	90°	70	44.7	—	—	—
14.9	90°	70	20.4	31.5	—	—
19.6	90°	70	4.3	15.2	—	—
25.4	90°	70	1.9	6.4	—	—
3.5	90°	130	92.4	94.3	—	—
4.9	90°	130	87.6	85.5	—	—
7.2	90°	130	82.9	74.0	—	—
7.4	90°	130	81.8	—	—	—
10.1	90°	130	62.5	55.1	—	—
11.5	90°	130	56.0	—	—	—
14.9	90°	130	27.1	27.1	—	—
19.6	90°	130	4.0	8.7	—	—
25.4	90°	130	0.5	2.4	—	—

A The Battelle Model does not consider Inlet Orientation. Therefore, the predictions most closely correspond to a 0° Inlet Orientation

B These predictions reflect the extension made by General Management Associates to include a 45° bend and inclined section predictions

Table 21. Cumulative Penetration Efficiency Results: Model Predictions vs. Experimental Data

Figure 33. Penetration Efficiency

70 L/min, 0° Inlet

Legend: □ Experimental + Texas A&M Model ◇ Duisburg Model △ Battelle Model

X-axis: Aerodynamic Particle Diameter (μm)

Y-axis: Percent Penetration
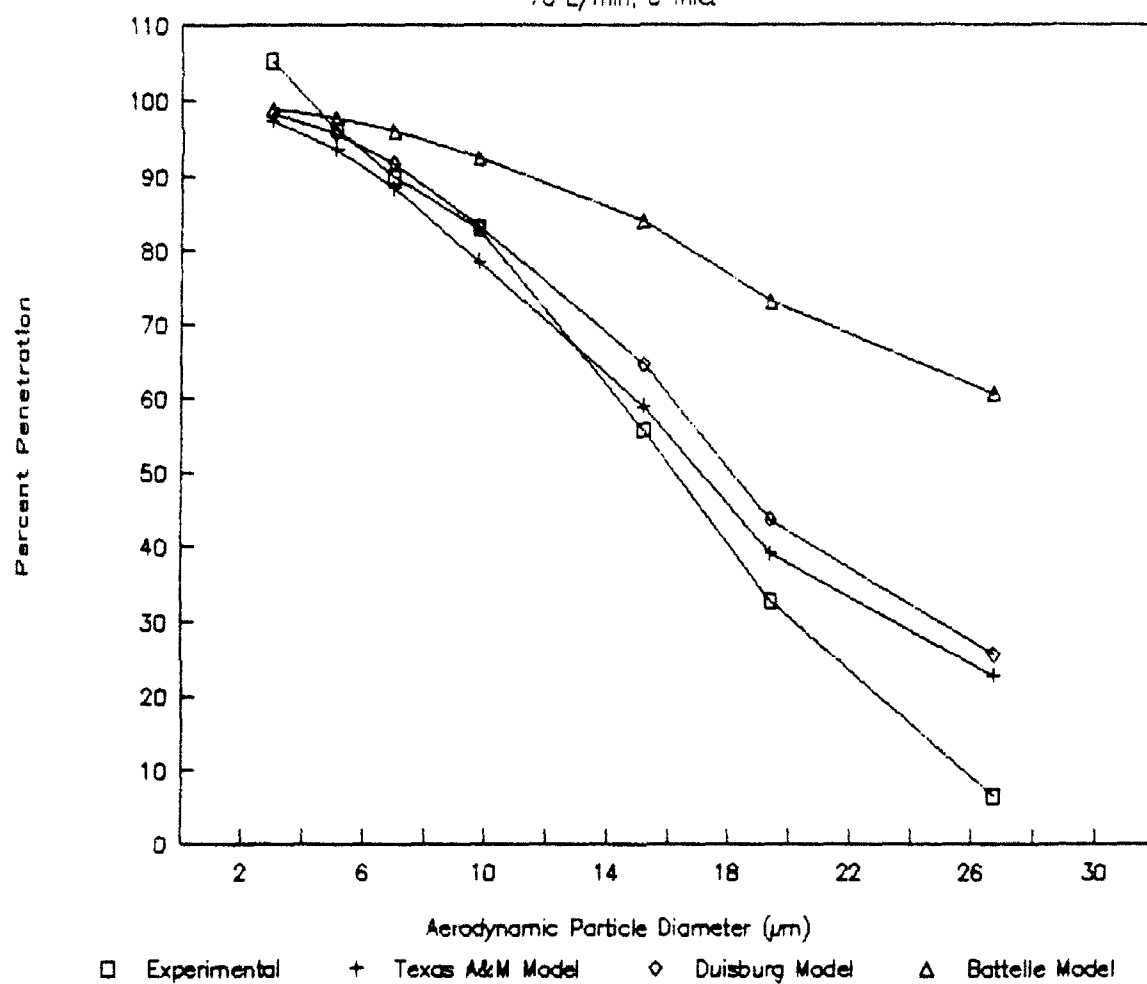
Figure 34. Penetration Efficiency

130 L/min, 0° Inlet

Percent Penetration

Aerodynamic Particle Diameter (μm)

□ Experimental   + Texas A&M Model   ◇ Duisburg Model   △ Battelle Model
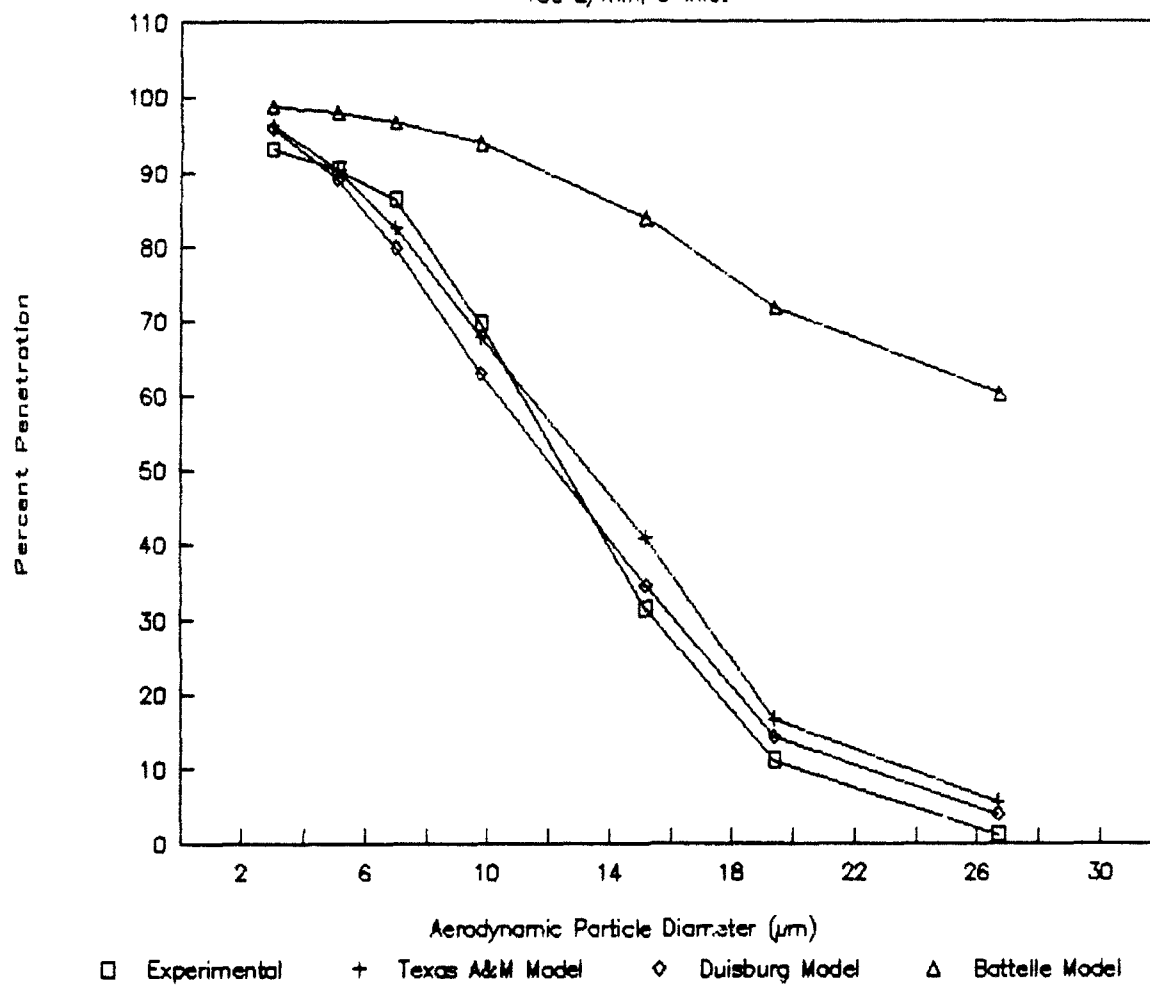
values, the model overpredicts, and as the particle size increases the discrepancy (percentage difference) between the predicted and measured values becomes larger.

6.2.2   Comparison of Results for 0° Inlet Orientation and 130 l/min Flow Rate Conditions

The Texas A&M model and the University of Duisburg model simulate a 0° inlet orientation and 130 l/min flow rate. The Battelle model only simulates the 130 l/min flow rate and assumes 100% inlet efficiency.

The Texas A&M model provides predictions of cumulative penetration efficiencies for the 3, 5, 7 and 10 μm particle sizes which are reasonably close to penetration efficiencies measured in the wind tunnel. The model's cumulative efficiency predictions for the 15, 20 and 25 μm particle sizes differ significantly from the measured values, are over predictions, and as the particle size increases, the discrepancy (percent difference) between the predicted and measured values becomes larger.

The University of Duisburg model provides predictions of cumulative penetration efficiencies for the 3, 5, 7, 10 and 15 μm particle sizes which are reasonably close to penetration efficiencies measured in the wind tunnel. The model's cumulative efficiency predictions for the 20 and 25 μm particle sizes differs significantly for the measured values, are over predictions, and as the particle size increases, the discrepancy (percent difference) between the predicted and measured values become larger. However, it is interesting to note that for these two particle sizes, the German model's predicted values are in closer agreement to the measured values than are the Texas A&M model's predictions.

The Battelle model's predictions for the cumulative penetration efficiencies at the 3 and 5 μm particle sizes are in agreement to penetration efficiencies measured in the wind tunnel. However, the model's cumulative efficiency predictions for the 7, 10, 15, 20 and 25 μm particle sizes which differ significantly from the measured values are overpredictions and as the particle size increases, the discrepancy (percent difference) between the predicted and measured values becomes larger.

6.2.3   Comparison of Results for 90° Inlet Orientation and 70 l/min Flow Rate Conditions

The Texas A&M model is the only model of the three which provides predictions of cumulative penetration efficiencies based on a 90° inlet orientation and 70 l/min flow rate. These predicted results are in close agreement to the efficiencies measured in the wind tunnel at the 3, 5, 7 and 10 μm particle

101

sizes. The model predictions which differ significantly from the measured values at the 15, 20 and 25 μm particle sizes are over predictions and as the particle size increases, the discrepancy (percent difference) between the predicted and measured values becomes larger.

6.2.4   Comparison of Results for 90° Inlet Orientation and 130 l/min Flow Rate Conditions

The Texas A&M model is the only model of the three which provides predictions of cumulative penetration efficiencies based on a 90° inlet orientation and 130 l/min flow rate. These predicted results are in close agreement to the efficiencies measured in the wind tunnel at the 3, 5, 7, 10 and 15 μm particle sizes. The model predictions which differ significantly from the measured values at the 20 and 25 μm particle sizes are over-predictions and as the particle size increases, the discrepancy (percent difference) between the predicted and measured values becomes larger.

SECTION 7.   CONCLUSIONS AND RECOMMENDATIONS

7.1   CONCLUSIONS

In general, aerosol sampling models are available which can be used to design aerosol sampling and transport systems. Four candidate models/algorithms were reviewed which showed the greatest potential for this application. They were the following:

- Texas A&M model

- Battelle model

- IITRI model

- Equations compiled/developed by the University of Duisburg

Each candidate model/algorithms was evaluated relative to an aerosol sampling train configuration upon which the model calculations would be generated and compared and the experimental data would be compared. The sampling train consisted of six regions. They were the following: (1) inlet, (2) horizontal section, (3) vertical section, (4) inclined section, (5) 90° elbow, and (6) 45° elbow.

7.1.1   Capabilities of Numerical Models/Algorithms

Of the four models evaluated, the Texas A&M model was the only one which simulated the six regions of the sampling train. The Battelle model simulated all regions of the sampling train except for the inlet area. For this model, the inlet efficiency was assumed to be 100% for all inlet orientations. The University of Duisburg equations addressed four sections of the sampling train. However, the 45° elbow and inclined sections were incorporated in GMA's version of the University of Duisburg computer program. The IITRI model only simulated the inlet region. Each model predicts penetration efficiency through each region simulated as well as cumulative penetration efficiency through all regions simulated. Penetration efficiency predictions for each of the models revealed self-consistency.

7.1.2   Numerical Calculations Generated by Four Models

The Texas A&M model, the Battelle model and the University of Duisburg model generated penetration efficiencies for both monodispersed and polydispersed (log-normal) particle distributions. The IITRI model generated numerical calculations for only monodispersed particles.

The penetration efficiency calculations produced by both the Texas A&M model and the University of Duisbuurg model are very comparable across the monodispersed particle distributions and the polydispersed distributions. The Battelle model predicts penetration efficiency values comparable to those generated by the Texas A&M and University of Duisburg models, however, only at the smaller monodispersed particle size distributions. For the larger particle sizes, the Battelle model produces significantly higher penetration efficiency values than those predicted by the Texas A&M and the University of Duisburg models.

The IITRI model only predicts efficiency values at the inlet regions of the sampling train. Results from the IITRI model compared to the inlet efficiency results produced by the Texas A&M model and the University of Duisburg model indicate comparability with the University of Duisburg model results but noncomparability with the Texas A&M model results.

7.1.3 Comparison of Experimental Measurements and Numerical Calculations

Only the cumulative penetration efficiency of monodispersed aerosol particles through the sampling train was measured in the experiments. Consequently, no comparison could be made to determine how realistic the model's predicted penetration efficiency through each section of the sampling train was to experimental data. Instead, only a comparison could be made between predicted and measured cumulative penetration efficiency.

Overall, the Texas A&M model and the University of Duisburg model predictions produce the closest agreement to the cumulative penetration efficiencies measured in the wind tunnel. The Battelle model predictions on the other hand, produce the greatest difference to the measured values. At the larger particle sizes, the Battelle model significantly overpredicts the penetration efficiency.

7.2 RECOMMENDATIONS

The primary focus of this study was not only to compare numerical calculations among the four candidate models but also to compare these model results to the experimental data. Although both aspects were addressed, a comparison of model calculations to experimental data on the penetration efficiency for each individual section of the aerosol sampling train was never gathered due to time and money constraints. Without this experimental data, a determination of the model's realism in predicting penetration efficiency for individual sections of the sampling train could not be made. Therefore, it is recommended

that the following be accomplished in order to identify a comprehensive model that already exists and could be used to design aerosol sampling and transport systems:

A. Texas A&M conduct wind tunnel experiments to measure monodispersed particle penetration efficiencies through individual components of the sampling train. Experimental conditions identical to the ones used in this study should be used as well as a limited set of additional conditions.

B. The Texas A&M model as the preferred model, should be used to compare its predicted results to this new set of experimental data.

C. Further investigation should be given to extending the University of Duisburg equations to incorporate theoretically/empirically based equations which will predict penetration efficiencies through a 45° elbow section and an inclined section. Calculations of monodispersed penetration efficiencies produced by these "new" equations for single sections of a sampling train should be compared to the new experimental data.

D. Inlet efficiency predictions for the IITRI model should be compared against the new experimental data.

E. Further investigation should be made into understanding why the Battelle model, when compared to experimental data, significantly overpredicts penetration efficiency for monodispersed particle sizes in the 10 to 25 μm region.

THIS PAGE INTENTIONALLY LEFT BLANK

REFERENCES

1. Kogan, Vladimir, <u>Analytic Evaluation of Aerosol Sampling Efficiency</u>, final report prepared by Battelle, Columbus, OH under subcontract to General Management Associates, Abingdon, MD, October 1, 1990.

2. Fissan, H. and Schwientek G., "Sampling and Transport of Aerosols", <u>TSI Journal of Particle Instrumentation</u>, 2(2): 3-9, July - December 1987.

3. Anand, N.K. and McFarland, A.R., "Particle Deposition in Aerosol Sampling Lines Caused by Turbulent Diffusion and Gravitational Settling, "<u>Journal of American Industrial Hygiene Association</u>, 50: 307-312, 1989.

4. Vincent, J.H., Stevens, D.C., Mark, D., Marshall, M., and Smith, T.A., "On the Aspiration Characteristics of Large-Diameter, Thin-Walled Aerosol Sampling Probes at Yaw Orientations with Respect to the Wind", <u>Journal of Aerosol Science</u>, 17:211-224, 1986.

5. Fuchs, N.A., <u>The Mechanics of Aerosols</u>, The Macmillan Company, New York, NY, 1964.

6. Okazaki, K. and Willeke, K., "Transmission and Depositional Behavior of Aerosols in Sampling Inlets", <u>Aerosol Science and Technology</u>, 7:275-283, 1987.

7. Liu, B.Y.H. and Agarwal, J.K. "Experimental Observation of Aerosol Deposition in Turbulent Flow", <u>Journal of Aerosol Science</u>, 5:145-155, 1974.

8. Beal, S.K., "Deposition of Particles in Turbulent Flow on Channel or Pipe Walls", <u>Nuclear Science and Engineering</u>, 40:1-11, 1970.

9. Cheng, Y.S. and Wang, C.S., "Motion of Particles in Bends of Circular Pipes", <u>Atmospheric Environment</u>, 15(3): 301-306, 1981.

10. Pui, D.Y.H., Romay-Novas, F., and Liu, B.Y.H., "Experimental Study of Particle Deposition in Bends of Circular Cross Section", <u>Aerosol Science and Technology</u>, 7:301-315, 1987.

11 McFarland, Andrew R., Wong, Fermin S., Anand, N.K., and Ortiz, Carlos A., <u>Particle Deposition in a Model Aerosol Transport System: Numerical Predictions</u>, prepared by Texas A&M University, College Station, TX under subcontract to General Management Associates, Abingdon, MD, December 1990.

12. Rajendran, Naragana, Discussion Paper on IITRI Computer Program System, prepared by IITRI, Chicago, IL under subcontract to General Management Associates, Abingdon, MD, December 4, 1990.

13. Kuhlman, M.R., Kogan, V., and Schumacher, P.M., Trap-Melt2 Code: Development and Improvement of Transport Modeling, NUREG/CR-4677, BMI-2141, Battelle, Columbus, OH, 1986.

14. Wood, N.B., Journal of Aerosol Science, 12(3):275-290, 1981.

15. Perry's Chemical Engineers' Handbook, Sixth Edition, McGraw-Hill, Inc., pg 5-24, 1984.

16. Berglund, R. N. and Liu, B.Y.H., "Generation of Monodisperse Aerosol Standards," Environmental Science and Technology, 7:147-153, 1973.

17. Olan-Figuesoa, E.O., McFarland, A.R., and Ortiz, C.A., "Flattening Coefficients for DOP and Oleic Acid Deposited on Treated Glass Slides," American Industrial Hygiene Association, 43:395-399, 1982.

APPENDIX A
LISTING OF COMPUTER PROGRAM DEVELOPED
BY GENERAL MANAGEMENT ASSOCIATES

```
10 REM **This program calculates the "vertice diameters" of a **
20 REM **log-normal distribution of diameter sizes, using     **
30 REM **equal logarithmic intervals.  This program reads in   **
40 REM **the mass median diameter, standard deviation, number **
50 REM **of intervals, and the name of the output file.  There**
60 REM **can be as many intervals as possible, but if this     **
70 REM **program is to be used in conjunction with the program**
80 REM **"average.bas", the number of intervals must be 20.   **
90 INPUT"Mass Median Diameter -->", MMD
100 INPUT"Standard Deviation ---->", SIGMA
110 INPUT"Number of Intervals --->", N
120 INPUT"Diameter Filename ----->", LOGFILE$
130 OPEN "a:"+LOGFILE$ FOR OUTPUT AS #1
140 PRINT#1,"MMD =";MMD;"fm";"  Standard Deviation =";SIGMA;"fm";"  Size [=] fm"
150 DMIN = MMD * (SIGMA ^ -3.62)
160 DMAX = MMD * (SIGMA ^ 3.62)
170 INTLIN = (DMAX - DMIN) / N
180 INTLOG = (LOG(DMAX) - LOG(DMIN)) / (N * LOG(10))
190 REM **DIAMETERS USING EQUAL LOGARITHMIC INTERVALS**
200 FOR J = 0 TO N
210 LD = (LOG(DMIN) / LOG(10)) + (J * INTLOG)
220 D1 = EXP(LD * LOG(10))
230 PRINT#1,D1
240 NEXT J
250 CLOSE#1
260 END
```

```
10 REM **This program calculates the geometric average particle**
20 REM **diameter between two adjacent vertice diameters.  The **
30 REM **input to this program is the output from the program  **
40 REM **"diameter.bas".  This program prompts for the names of**
50 REM **input and output files.                                **
60 DIM D(21)
70 DIM GEOMEAN(20)
80 INPUT"Input Filename ----->",IFILE$
90 INPUT"Output Filename ---->",OFILE$
100 OPEN "a:"+IFILE$ FOR INPUT AS #1
110 INPUT#1,A$
120 FOR I = 0 TO 20
130 INPUT#1, D(I)
140 NEXT I
150 CLOSE #1
160 OPEN "a:"+OFILE$ FOR OUTPUT AS #1
170 PRINT#1,A$
180 FOR I = 1 TO 20
190 GEOMEAN(I) = SQR(D(I-1) * D(I))
200 PRINT#1, GEOMEAN(I)
210 NEXT I
220 CLOSE #1
```

```basic
10    REM **This program calculates the sampling and transport efficiency**
20    REM **of an aerosol.  The program prompts for the input filename,  **
30    REM **output filename and sampling rate.  The input filename is the**
40    REM **name of the data file that contains the particle sizes.  The **
50    REM **output filename is the name of the file that the efficiencies**
60    REM **are output to.                                               **
70    CLS
80    REM **VALUE OF PROCESS CONSTANTS**
90   REM **AMBIENT TEMPERATURE, KELVINS**
100   TEMP = 298
110   REM **AMBIENT PRESSURE, CM HG**
120   PRESS = 76
130   REM **AEROSOL DENSITY, GM/CM3**
140   RHO = 1
150   REM **PROBE DIAMETER, INCHES**
160   DS = 1.05
170   REM **AIR VISCOSITY, KG/M/S**
180   NU = .0000185
190   REM **AIR DENSITY, KG/M3**
200   RHOAIR = 1.1769
210   REM **HORIZONTAL TUBE LENGTH, FT**
220   HLENGTH = 2
230   REM **VERTICAL TUBE LENGTH, FT**
240   VLENGTH = 2
250   REM **ACCELERATION OF GRAVITY, m/s2**
260   G = 9.810001
270   REM **INPUT OF PROCESS VARIABLES**
280   ·WS = 3
290   INPUT "Input Filename ";IFILES
300   INPUT "Output Filename ";OFILES
310   INPUT "Flow Rate (1/min) ";VDOT
320   OPEN "a:"+IFILE$ FOR INPUT AS #1
330 INPUT#1, A$
340   OPEN "a:"+OFILE$ FOR OUTPUT AS #2
350 PRINT#2, A$
360 PRINT#2,"Volumetric Flow Rate =";VDOT;"1/min"
370 PRINT#2,"                              FRACTIONAL PENETRATION OF AEROSOL"
380 PRINT#2," SIZE    INLET       HORIZ.  90x BEND  VERTICAL  45x BEND  INCLINED  O
VERALL"
390   FOR I = 1 TO 20
400   INPUT#1, DP
410   IF DP <= 0 THEN GOTO 1120
420   REM **CALCULATION OF CUNNINGHAM SLIP CORRECTION**
430   A = -.1095 * PRESS * DP
440   B = 6.32 + 2.01 * EXP(A)
450   C = 2 * B / PRESS / DP
460   CC = 1 + C
470   REM **CALCULATION OF GRAVITATIONAL SETTLING VELOCITY**
480   VS = .003 * RHO * DP * DP
490   REM **CALCULATION OF BROWNIAN DIFFUSION COEFFICIENT, MKS**
500 DIFF = 1.46529E-18 * TEMP * CC / NU / DP
510 REM **CALCULATION OF SAMPLING EFFICIENCY**
520 STKW = 4.37445E-09 * CC * RHO * DP * DP * WS / NU / DS
530 OMEGA = 30.40245 * WS * DS * DS / VDOT
540 A = (OMEGA / STKW) + (2 * OMEGA) + .62
550 B = (2 * OMEGA) + .62
560 C = OMEGA - 1
570 SAMPEFF = 1 + (C * B / A)
580 REM **CALCULATION OF REYNOLD'S NUMBER**
590 NRE = 8.35459E-04 * VDOT * RHOAIR / DS / NU
600 REM **CALCULATION OF STOKES NUMBER FOR BENDS**
610 STK = 1.438849E-10 * CC * RHO * DP * DP * VDOT / NU / DS / DS / DS
```

```
620 IF NRE =< 2300 THEN 640
630 IF NRE > 2300 THEN 740
640 REM **TRANSPORT EFFICIENCY LOSS BY BROWNIAN DIFFUSION, LAMINAR FLOW**
650 XSI = 57453.446# * DIFF * HLENGTH / VDOT
660 IF XSI =< .02 THEN GOTO 1150
670 IF XSI > .02 THEN GOTO 1210
680 REM **GRAVITATIONAL SEDIMENTATION LOSSES, LAMINAR FLOW**
690 LENGTH = HLENGTH
700 GOSUB 1270
710 REM **LAMINAR, 90x BEND**
720 GOSUB 1380
730 GOTO 800
740 REM **LOSSES IN TURBULENT FLOW**
750 REM **TURBULENT, HORIZONTAL TUBE**
760 LENGTH = HLENGTH
770 GOSUB 1410
780 REM **TURBULENT, 90x BEND**
790 GOSUB 1600
800 IF NRE =< 2300 THEN 930
810 IF NRE > 2300 THEN 820
820 INLET = SAMPEFF
830 HORIZ = TBREFF * TINEFF
840 BEND90 = TBENDEFF
850 VERT = TBREFF * TINEFF
860 BEND45 = TBENDEFF
870 REM**CALCULATION OF INCLINED PIPE SCALING FACTOR**
880 IF VDOT = 130 THEN GOSUB 1650
890 IF VDOT = 70 THEN GOSUB 1720
900 INCLINE = TBREFF * TINEFF * FACTOR
910 TOTAL = INLET * HORIZ * BEND90 * VERT * BEND45 * INCLINE
920 GOTO 1020
930 INLET = SAMPEFF
940 HORIZ = BREFF * LGREFF
950 BEND90 = LBNDEFF
960 VERT = BREFF
970 BEND45 = LBNDEFF
980 GOSUB 1720
990 INCLINE = BREFF * LGREFF * FACTOR
1000 TOTAL = INLET * HORIZ * BEND90 * VERT * BEND45 * INCLINE
1010 GOTO 1020
1020 PRINT#2, USING"##.##";DP;
1030 PRINT#2, USING"##.###^^^^";INLET;
1040 PRINT#2, USING"##.###^^^^";HORIZ;
1050 PRINT#2, USING"##.###^^^^";BEND90;
1060 PRINT#2, USING"##.###^^^^";VERT;
1070 PRINT#2, USING"##.###^^^^";BEND45;
1080 PRINT#2, USING"##.###^^^^";INCLINE;
1090 PRINT#2, USING"##.###^^^^";TOTAL
1100 GOTO 1110
1110 NEXT I
1120 CLOSE #1
1130 CLOSE #2
1140 END
1150 REM **CALCULATION OF BROWNIAN LOSSES, XSI =< .02**
1160 A = .177 * (XSI ^ 1.3333333333333#)
1170 B = 1.2 * XSI
1180 C = 2.56 * (XSI ^ .66666667#)
1190 BREFF = 1 - C + B + A
1200 GOTO 680
1210 REM **CALCULATION OF BROWNIAN LOSSES, XSI >.02**
1220 A = .032 * EXP(-57 * XSI)
1230 B = .097 * EXP(-22.3 * XSI)
```

```
1240 C = .819 * EXP(-3.657 * XSI)
1250 BREFF = A + B + C
1260 GOTO 680
1270 REM **LAMINAR, GRAVITATIONAL SEDIMENTATION LOSSES**
1280 PHI = 4.56036 * LENGTH * VS * DS / VDOT
1290 IF PHI > 1! THEN GOTO 1630
1300 REM**For explanation of line 1010 see fig. 6 in Fissan paper**
1310 PHIONE = PHI^(1/3)
1320 PHITWO = PHI^(2/3)
1330 A = PHIONE * SQR(1 - PHITWO)
1340 B = ATN(PHIONE / SQR(-PHIONE * PHIONE + 1))
1350 C = 2 * PHI * SQR(1 - PHITWO)
1360 LGREFF = 1 - .6366198 * (C + B - A)
1370 RETURN
1380 REM **LAMINAR, 90x BEND CALCULATIONS**
1390 LBNDEFF = 1 - STK
1400 RETURN
1410 REM **TURBULENT FLOW MODELS**
1420 REM **CALCULATION OF SCHMIDT NUMBER**
1430 SC = NU / RHOAIR / DIFF
1440 REM **CALCULATION OF FANNING FRICTION FACTOR**
1450 FF = .316 / 4 / (NRE^.25)
1460 REM **CALCULATION OF PARTICLE DEPOSITION VELOCITY, BROWNIAN DIFFUSION**
1470 UBR = .0013814677# * VDOT * (FF^.5) * (SC^-.6666666667#) / DS / DS
1480 REM **CALCULATION OF LOSSES DUE TO BROWNIAN MOTION**
1490 ARGTBR = 1459.318 * DS * LENGTH * UBR / VDOT
1500 TBREFF = EXP(-ARGTBR)
1510 REM **TURBULENT LOSSES INERTIAL EFFECTS**
1520 TAU = 5.555556E-11 * RHO * DP * DP * CC / NU
1530 USTAR = 2.325822E-02 * (FF^.5) * VDOT / DS / DS
1540 TAUPLUS = TAU * USTAR * USTAR * RHOAIR / NU
1550 UPLUS = 6.000001E-04 * TAUPLUS * TAUPLUS
1560 UIN = UPLUS * USTAR
1570 ARGTIN = 1459.318 * DS * LENGTH * UIN / VDOT
1580 TINEFF = EXP(-ARGTIN)
1590 RETURN
1600 REM **TURBULENT FLOW BEND EFFICIENCY**
1610 TBENDEFF = 10^(-.963 * STK)
1620 RETURN
1630 LGREFF = 0!
1640 GOTO 1370
1650 REM**INCLINED PIPE FACTOR FOR 130 1/min**
1660 IF DP < 15 GOTO 1680
1670 IF DP => 15 GOTO 1700
1680 FACTOR = 1.000899 - (1.234803E-04 * DP) - (1.994214E-04 * DP * DP) + (7.352
604E-06 * DP * DP * DP)
1690 RETURN
1700 FACTOR = .8500409 + (1.249575E-02 * DP) - (2.598943E-04 * DP * DP)
1710 RETURN
1720 REM **INCLINED PIPE FACTOR FOR 70 1/min**
1730 FACTOR = .9994884 + (2.10849E-04 * DP) - (3.401449E-04 * DP * DP) + (3.4422-
3E-06 * DP * DP * DP)
1740 RETURN
```

```
10 REM **This program calculates the mass-weighted average efficiency**
20 REM **of a log-normal distribution of particles with equal       **
30 REM **logarithmic intervals.  This program only works for twenty  **
40 REM **intervals.  The input to this program is the output from the**
50 REM **"fissan.bas" program.  This program prompts for the input   **
60 REM **and output filenames.                                       **
70 DIM FRACMASS(20)
80 DIM BINEFF(20,8)
90 DIM AVGEFF(8)
100 INPUT"Input Filename ----->",IFILES
110 INPUT"Output Filename ---->",OFILES
120 OPEN "a:"+IFILES FOR INPUT AS #1
130 INPUT#1, AS
140 INPUT#1,BS
150 INPUT#1,CS
160 INPUT#1,DS
170 REM **LOAD ARRAY WITH EFFICIENCIES FOR EACH BIN**
180 FOR I = 1 TO 20
190 FOR J = 1 TO 8
200 INPUT#1, BINEFF(I,J)
210 NEXT J
220 NEXT I
230 CLOSE #1
240 REM **LOADING MASS FRACTION ARRAY**
250 FOR I = 1 TO 20
250 READ MASSFRAC
270 FRACMASS(I) = MASSFRAC
280 NEXT I
290 REM **WEIGHTED AVERAGE OF EFFICIENCIES TO OUTPUT FILE**
300 FOR J = 2 TO 8
310 AVGEFFO = 0!
320 FOR I = 1 TO 20
330 AVGEFF(J) = AVGEFFO + (BINEFF(I,J) * FRACMASS(I))
340 AVGEFFO = AVGEFF(J)
350 NEXT I
360 NEXT J
370 REM **OUTPUT AVERAGE EFFICIENCIES TO OUTPUT FILE**
380 OPEN "a:"+OFILES FOR OUTPUT AS #1
390 PRINT#1,AS
400 PRINT#1,BS
410 PRINT#1," "
420 PRINT#1,"MASS-WEIGHTED FRACTIONAL PENETRATION OF LOG-NORMAL DISTRIBUTION OF
AEROSOLS"
430 PRINT#1,"   INLET     HORIZ.  90x BEND  VERTICAL  45x BEND  INCLINED  OVERAL
L"
440 FOR I = 2 TO 8
450 PRINT#1,USING "##.###^^^^"; AVGEFF(I);
460 NEXT I
470 CLOSE #1
480 DATA .0005, .0013, .0038, .0093, .0201, .0384, .0644, .0979, .1236, .1406, .
1406, .1236, .0979, .0644, .0384, .0201, .0093, .0038, .0013, .0005
```

THIS PAGE INTENTIONALLY LEFT BLANK

APPENDIX B
COMPLETE SET OF NUMERICAL CALCULATIONS GENERATED
BY TEXAS A&M MODEL

Table B-1   Transmission of Monodisperse Aerosol Particles through Individual Components of the Aerosol Transport System. Case 1: Flow rate = 70 L/min, Inlet Orientation = 90°. The column entitled "inlet" includes the aspiration efficiency (Vincent et al.; 1986) and losses in the developing boundary layer (Okazaki and Willeke, 1987). Identification of components is given in Figure 1.

Aero-dynamic Particle Diameter	Component					
	Inlet	P1	P2	P3	E1	E2
3 μm	96.21%	99.74%	100.00%	99.72%	99.02%	99.51%
5	90.49	99.29	99.99	99.25	97.34	98.66
7	83.16	98.62	99.98	98.54	94.91	97.42
10	70.86	97.21	99.92	97.05	89.94	94.89
15	51.52	93.80	99.62	93.43	78.88	88.82
20	36.60	89.11	98.80	88.41	65.67	81.04
25	26.08	83.18	96.91	81.99	51.89	72.04

Table B-2   Transmission of   Monodisperse   Aerosol
Particles through Individual Components of the Aerosol
Transport System. Case 2: Flow rate = 130 L/min, Inlet
Orientation = 90°. The column entitled "inlet" includes
the aspiration efficiency (Vincent et al.; 1986) and
losses in the developing boundary layer (Okazaki and
Willeke, 1987). Identification of components is given
in Figure 1.

Aero-dynamic Particle Diameter	Component					
	Inlet	P1	P2	P3	E1	E2
3 μm	97.22	99.86	99.99	99.85	98.18	99.09
5	92.92	99.60	99.96	99.57	95.12	97.53
7	87.22	99.21	99.85	99.14	90.75	95.26
10	77.16	98.30	99.39	98.11	82.13	90.63
15	59.89	95.55	96.79	94.80	64.37	80.23
20	45.13	87.97	84.41	84.13	45.79	67.67
25	33.82	80.24	73.65	73.65	29.57	54.38

Table B-3   Transmission of a Polydisperse Aerosol through Individual Components of the Transport System. Case 3: Flow rate = 70 L/min, Inlet Orientation = 90°. The column entitled "inlet" includes the aspiration efficiency (Vincent et al.; 1986) and losses in the developing boundary layer (Okazaki and Willeke, 1987).

Mass Median Aero- dynamic Diameter	Component					
	Inlet	P1	P2	P3	E1	E2
5 μm	88.36%	99.11%	99.98%	99.10%	96.74%	98.39%
15	51.00	93.92	99.56	94.87	81.14	90.93

Table B-4   Transmission of a Polydisperse Aerosol through Individual Components of the Transport System. Case 4: Flowrate = 130 L/min, Inlet Orientation = 90°. The column entitled "inlet" includes the aspiration efficiency (Vincent et al.; 1986) and losses in the developing boundary layer (Okazaki and Willeke), 1987.

Mass Median Aero- dynamic Diameter	Component					
	Inlet	P1	P2	P3	E1	E2
5 μm	91.15%	99.47%	99.90%	99.47%	93.97%	97.04%
15	58.40	94.35	96.70	96.12	68.17	85.22

Table B-5 Transmission of Monodisperse Aerosol Particles through Individual Components of the Aerosol Transport System. Case 5: Flow rate = 70 L/min, Inlet Orientation = 0°. The column entitled "inlet" includes the aspiration efficiency (Vincent et al.; 1986) and losses in the developing boundary layer (Okazaki and Willeke, 1987). Identification of components is given in Figure 1.

Aero-dynamic Particle Diameter	Component					
	Inlet	P1	P2	P3	E1	E2
3 μm	99.43%	99.74%	100.00%	99.72%	99.02%	99.51%
5	98.94	99.29	99.99	99.25	97.34	98.66
7	98.44	98.62	99.98	98.54	94.91	97.42
10	97.71	97.21	99.92	97.05	89.94	94.84
15	96.40	93.80	99.62	93.43	78.88	88.82
20	94.73	89.11	98.80	88.41	65.67	81.04
25	92.44	83.18	96.91	81.99	51.89	72.04

Table B-6 Transmission of Monodisperse Aerosol Particles through Individual Components of the Aerosol Transport System. Case 6: Flow rate = 130 L/min, Inlet Orientation = 0°. The column entitled "inlet" includes the aspiration efficiency (Vincent et al.; 1986) and losses in the developing boundary layer (Okazaki and Willeke, 1987). Identification of components is given in Figure 1.

Aero-dynamic Particle Diameter	Component					
	Inlet	P1	P2	P3	E1	E2
3 μm	99.26%	99.89%	99.99%	99.85%	98.18%	99.09%
5	98.33	99.60	99.96	99.57	95.12	97.53
7	97.14	99.21	99.85	99.14	90.75	95.26
10	94.97	98.30	99.39	98.11	82.13	90.63
15	90.60	95.55	96.79	94.80	64.37	80.23
20	85.67	87.97	84.41	84.13	45.79	67.67
25	80.54	80.24	73.65	73.65	29.57	54.38

Table B-7   Penetration of Monodisperse Aerosols through the Overall Tubing System.

Aerodynamic Particle Diameter	Case 1	Case 2	Case 5	Case 6
	90°	Inlet Orientation		0°
	Flow Rate, L/min			
	70	130	70	130
3 μm	94.28%	94.29%	97.43%	96.27%
5	85.64	85.46	93.63	90.43
7	74.70	74.04	88.43	82.46
10	56.98	55.05	78.57	67.76
15	31.51	27.12	58.96	41.02
20	15.16	8.74	39.24	16.59
25	6.44	2.37	22.84	5.64

Table B-8   Transmission of a Polydisperse Aerosol through Individual Components of the Transport System. Case 7: Flowrate = 70 L/min, Inlet Orientation = 0°. The column entitled "inlet" includes the aspiration efficiency (Vincent et al.; 1986) and losses in the developing boundary layer (Okazaki and Willeke, 1987).

Mass Median Aero- dynamic Diameter	Component					
	Inlet	P1	P2	P3	E1	E2
5 μm	98.83%	99.03%	99.98%	99.03%	96.49%	98.26%
15	95.58	91.82	99.26	93.71	76.47	88.91

Table B-9   Transmission of a Polydisperse Aerosol through Individual Components of the Transport System. Case 8: Flowrate = 130 L/min, Inlet Orientation = 0°. The column entitled "inlet" includes the aspiration efficiency (Vincent et al.; 1986) and losses in the developing boundary layer (Okazaki and Willeke), 1987).

Mass Median Aero- dynamic Diameter	Component					
	Inlet	P1	P2	P3	E1	E2
5 μm	97.96%	99.44%	99.88%	99.44% -	93.67%	96.90%
15	89.10	92.58	95.65	95.42	63.78	83.57

Table B-10 Penetration of Polydisperse Aerosols through the Overall Tubing System. The aerosol in the free stream is assumed to be log-normally distributed with a geometric standard deviation of 1.5.

Mass Median Aerodynamic Particle Diameter	Case 3	Case 4	Case 7	Case 8
	Inlet Orientation			
	90°		0°	
	Flow Rate, L/min			
	70	130	70	130
5 μm	82.58%	82.15%	91.88%	87.82%
15	33.38	29.75	55.51	40.13

THIS PAGE INTENTIONALLY LEFT BLANK

APPENDIX C
COMPLETE SET OF NUMERICAL CALCULATIONS GENERATED
BY IITRI MODEL

Table C-1 Sampling Efficiency as a Function of Particle Size
(Alpha = 0 degrees;Velocity Ratio = 1.3)

0	1 DIAMETER, micron	2 STOKES #	3 CONC. RATIO
1	3	0.0058	0.940611
2	5	0.0162	0.940611
3	7	0.0318	0.940611
4	10	0.0649	0.930008
5	15	0.1459	0.919466
6	20	0.2595	0.919466
7	25	0.4054	0.908984

Table C-2 Sampling Efficiency as a Function of Particle Size
(Alpha = 0; Velocity Ratio = 0.7)

0	1 DIAMETER micron	2 STOKES #	3 CONC RATIO
1	3	0.0058	1.007484
2	5	0.0162	1.007484
3	7	0.0318	1.007484
4	10	0.0649	1.007484
5	15	0.1459	1.083860
6	20	0.2595	1.146970
7	25	0.4054	1.211865

Table C-3 Sampling Efficiency as a Function of Particle Size
(Alpha = 90 degrees; Velocity Ratio = 1.3)

0	1 DIAMETER micron	2 STOKES #	3 CONC RATIO
1	3	0.0058	0.854107
2	5	0.0162	0.852980
3	7	0.0318	0.847058
4	10	0.0649	0.848458
5	15	0.1459	0.811773
6	20	0.2595	0.760660
7	25	0.4054	0.701941

Table C-4 Sampling Efficiency as a Function of Particle Size
(Alpha = 90 degrees; Velocity Ratio = 0.7)

0	1 DIAMETER micron	2 STOKES #	3 CONC RATIO
1	3	0.0058	0.892986
2	5	0.0162	0.893216
3	7	0.0318	0.883381
4	10	0.0649	0.871970
5	15	0.1459	0.799119
6	20	0.2595	0.759128
7	25	0.4054	0.713426

THIS PAGE INTENTIONALLY LEFT BLANK

APPENDIX D
COMPLETE SET OF NUMERICAL CALCULATIONS
GENERATED BY UNIVERSITY OF DUISBURG MODEL

Table D-1. Penetration Efficiency Calculations For Monodispersed Particle
Distributions - 0° Inlet Orientation & 70 L/min Flow Rate

Monodispersed Aerosol   Size [=] µm
Volumetric Flow Rate = 70 L/min, Wind Speed = 3 m/sec

FRACTIONAL PENETRATION OF AEROSOL

SIZE	INLET	HORIZ.	90° BEND	VERTICAL	45° BEND	INCLINED	CUM.
3.00	1.007E+00	1.000E+00	9.901E-01	1.000E+00	9.901E-01	9.971E-01	9.841E-01
5.00	1.018E+00	9.999E-01	9.734E-01	9.999E-01	9.734E-01	9.924E-01	9.569E-01
7.00	1.033E+00	9.998E-01	9.490E-01	9.998E-01	9.490E-01	9.853E-01	9.165E-01
10.00	1.062E+00	9.993E-01	8.994E-01	9.993E-01	8.994E-01	9.703E-01	8.327E-01
15.00	1.119E+00	9.963E-01	7.888E-01	9.963E-01	7.888E-01	9.343E-01	6.455E-01
20.00	1.174E+00	9.884E-01	6.567E-01	9.884E-01	6.567E-01	8.848E-01	4.376E-01
25.00	1.222E+00	9.721E-01	5.189E-01	9.721E-01	5.189E-01	8.224E-01	2.556E-01

Table D-2. Penetration Efficiency Calculations For Monodispersed Particle
Distributions - 0° Inlet Orientation & 130 L/min Flow Rate

Monodispersed Aerosol   Size [=] µm
Volumetric Flow Rate = 130 L/min, Wind Speed = 3 m/sec

FRACTIONAL PENETRATION OF AEROSOL

SIZE	INLET	HORIZ.	90° BEND	VERTICAL	45° BEND	INCLINED	CUM.
3.00	9.960E-01	9.999E-01	9.818E-01	9.999E-01	9.818E-01	9.989E-01	9.588E-01
5.00	9.894E-01	9.996E-01	9.512E-01	9.996E-01	9.512E-01	9.958E-01	8.908E-01
7.00	9.804E-01	9.985E-01	9.074E-01	9.985E-01	9.074E-01	9.913E-01	7.979E-01
10.00	9.635E-01	9.940E-01	8.213E-01	9.940E-01	8.213E-01	9.812E-01	6.301E-01
15.00	9.318E-01	9.706E-01	6.437E-01	9.706E-01	6.437E-01	9.502E-01	3.456E-01
20.00	9.020E-01	9.104E-01	4.579E-01	9.104E-01	4.579E-01	9.068E-01	1.421E-01
25.00	8.769E-01	7.958E-01	2.957E-01	7.958E-01	2.957E-01	7.958E-01	3.864E-02

Table D-3. Penetration Efficiency Calculations for Polydispersed Particle
Distributions - MMD = 15µm, Inlet Orientation = 0°,
Flow Rate = 70 L/min

MMD = 15 µm σ = 1.5 µm Size [=] µm
Volumetric Flow Rate = 70 l/min, Wind Speed = 3 m/sec

FRACTIONAL PENETRATION OF AEROSOL

SIZE	INLET	HORIZ.	90° BEND	VERTICAL	45° BEND	INCLINED	CUM.
3.72	1.010E+00	1.000E+00	9.850E-01	1.000E+00	9.850E-01	9.957E-01	9.758E-01
4.31	1.013E+00	1.000E+00	9.801E-01	1.000E+00	9.801E-01	9.943E-01	9.678E-01
4.99	1.018E+00	9.999E-01	9.735E-01	9.999E-01	9.735E-01	9.924E-01	9.571E-01
5.78	1.023E+00	9.999E-01	9.648E-01	9.999E-01	9.648E-01	9.899E-01	9.428E-01
6.69	1.031E+00	9.998E-01	9.533E-01	9.998E-01	9.533E-01	9.865E-01	9.236E-01
7.75	1.040E+00	9.997E-01	9.380E-01	9.997E-01	9.380E-01	9.820E-01	8.981E-01
8.97	1.052E+00	9.995E-01	9.180E-01	9.995E-01	9.180E-01	9.760E-01	8.643E-01
10.39	1.067E+00	9.991E-01	8.919E-01	9.991E-01	8.919E-01	9.680E-01	8.198E-01
12.04	1.085E+00	9.985E-01	8.580E-01	9.985E-01	8.580E-01	9.573E-01	7.621E-01
13.94	1.107E+00	9.972E-01	8.146E-01	9.972E-01	8.146E-01	9.430E-01	6.887E-01
16.14	1.132E+00	9.951E-01	7.599E-01	9.951E-01	7.599E-01	9.241E-01	5.981E-01
18.69	1.160E+00	9.912E-01	6.923E-01	9.912E-01	6.923E-01	8.990E-01	4.911E-01
21.65	1.191E+00	9.842E-01	6.111E-01	9.842E-01	6.111E-01	8.656E-01	3.728E-01
25.07	1.222E+00	9.718E-01	5.169E-01	9.718E-01	5.169E-01	8.214E-01	2.534E-01
29.04	1.254E+00	9.499E-01	4.130E-01	9.499E-01	4.130E-01	7.629E-01	1.473E-01
33.63	1.284E+00	9.119E-01	3.057E-01	9.119E-01	3.057E-01	6.865E-01	6.853E-02
38.94	1.312E+00	8.473E-01	2.043E-01	8.473E-01	2.043E-01	5.890E-01	2.315E-02
45.10	1.336E+00	7.425E-01	1.190E-01	7.425E-01	1.190E-01	4.700E-01	4.900E-03
52.23	1.357E+00	5.857E-01	5.762E-02	5.857E-01	5.762E-02	3.356E-01	5.187E-04
60.49	1.374E+00	3.824E-01	2.180E-02	3.824E-01	2.180E-02	2.025E-01	1.933E-05

MMD = 15 µm σ = 1.5 µm Size [=] µm
Volumetric Flow Rate = 70 l/min, Wind Speed = 3 m/sec

MASS-WEIGHTED FRACTIONAL PENETRATION OF LOG-NORMAL DISTRIBUTION OF AEROSOLS

INLET	HORIZ.	90° BEND	VERTICAL	45° BEND	INCLINED	CUM.
1.129E+00	9.870E-01	7.466E-01	9.870E-01	7.466E-01	9.104E-01	5.990E-01

Table D-4. Penetration Efficiency Calculations For Polydispersed Particle
Distributions - MMD = 15 μm, Inlet Orientation = 0˚,
Flow Rate = 130 L/min

MMD = 15 μm σ = 1.5 μm Size [=] μm
Volumetric Flow Rate = 130 1/min, Wind Speed = 3 m/sec

FRACTIONAL PENETRATION OF AEROSOL

SIZE	INLET	HORIZ.	90˚ BEND	VERTICAL	45˚ BEND	INCLINED	CUM.
3.72	9.940E-01	9.999E-01	9.724E-01	9.999E-01	9.724E-01	9.979E-01	9.376E-01
4.31	9.920E-01	9.998E-01	9.634E-01	9.998E-01	9.634E-01	9.970E-01	9.175E-01
4.99	9.895E-01	9.996E-01	9.514E-01	9.996E-01	9.514E-01	9.958E-01	8.912E-01
5.78	9.862E-01	9.993E-01	9.357E-01	9 993E-01	9.357E-01	9.943E-01	8.572E-01
6.69	9.819E-01	9.988E-01	9.150E-01	9.988E-01	9.150E-01	9.921E-01	8.136E-01
7.75	9.764E-01	9.978E-01	8.880E-01	9.978E-01	8.880E-01	9.892E-01	7.584E-01
8.97	9.696E-01	9.961E-01	8.531E-01	9.961E-01	8.531E-01	9.852E-01	6.898E-01
10.39	9.610E-01	9.931E-01	8.085E-01	9.931E-01	8.085E-01	9.795E-01	6.069E-01
12.04	9.507E-01	9.876E-01	7.524E-01	9.876E-01	7.524E-01	9.712E-01	5.099E-01
13.94	9.386E-01	9.779E-01	6.833E-01	9.779E-01	6.833E-01	9.587E-01	4.018E-01
16.14	9.247E-01	9.608E-01	6.006E-01	9.608E-01	6.006E-01	9.454E-01	2.911E-01
18.69	9.093E-01	9.308E-01	5.052E-01	9.308E-01	5.052E-01	9.241E-01	1.858E-01
21.65	8.931E-01	8.792E-01	4.006E-01	8.792E-01	4.006E-01	8.781E-01	9.730E-02
25.07	8.766E-01	7.937E-01	2.936E-01	7.937E-01	2.936E-01	7.937E-01	3.778E-02
29.04	8.605E-01	6.604E-01	1.936E-01	6.604E-01	1.936E-01	6.563E-01	9.227E-03
33.63	8.454E-01	4.747E-01	1.107E-01	4.747E-01	1.107E-01	4.634E-01	1.082E-03
38.94	8.318E-01	2.622E-01	5.235E-02	2.622E-01	5.235E-02	2.472E-01	3.875E-05
45.10	8.201E-01	9.027E-02	1.918E-02	9.027E-02	1.918E-02	7.989E-02	1.964E-07
52.23	8.102E-01	1.328E-02	4.991E-03	1.328E-02	4.991E-03	1.054E-02	3.749E-11
60.49	8.020E-01	4.235E-04	8.206E-04	4.235E-04	8.206E-04	2.774E-04	2.686E-17

MMD = 15 μm σ = 1.5 μm Size [=] μm
Volumetric Flow Rate = 130 1/min, Wind Speed = 3 m/sec

MASS-WEIGHTED FRACTIONAL PENETRATION OF LOG-NORMAL DISTRIBUTION OF AEROSOLS

INLET	HORIZ.	90˚ BEND	VERTICAL	45˚ BEND	INCLINED	CUM.
9.266E-01	9.192E-01	6.049E-01	9.192E-01	6.049E-01	9.083E-01	3.581E-01

Table D-5. Penetration Efficiency Calculations For Polydispersed Particle
Distributions - MMD = 5 μm, Inlet Orientation = 0°,
Flow Rate = 70 L/min

MMD = 5 μm σ = 1.5 μm Size [=] μm
Volumetric Flow Rate = 70 l/min, Wind Speed = 3 m/sec

FRACTIONAL PENETRATION OF AEROSOL

SIZE	INLET	HORIZ.	90° BEND	VERTICAL	45° BEND	INCLINED	CUM.
1.24	1.001E+00	1.000E+00	9.982E-01	1.000E+00	9.982E-01	9.992E-01	9.967E-01
1.44	1.002E+00	1.000E+00	9.976E-01	1.000E+00	9.976E-01	9.991E-01	9.958E-01
1.66	1.002E+00	1.000E+00	9.968E-01	1.000E+00	9.968E-01	9.989E-01	9.946E-01
1.93	1.003E+00	1.000E+00	9.958E-01	1.000E+00	9.958E-01	9.986E-01	9.930E-01
2.23	1.004E+00	1.000E+00	9.944E-01	1.000E+00	9.944E-01	9.983E-01	9.909E-01
2.58	1.005E+00	1.000E+00	9.926E-01	1.000E+00	9.926E-01	9.978E-01	9.880E-01
2.99	1.007E+00	1.000E+00	9.902E-01	1.000E+00	9.902E-01	9.971E-01	9.841E-01
3.46	1.009E+00	1.000E+00	9.870E-01	1.000E+00	9.870E-01	9.962E-01	9.790E-01
4.01	1.012E+00	1.000E+00	9.827E-01	1.000E+00	9.827E-01	9.950E-01	9.720E-01
4.65	1.015E+00	9.999E-01	9.770E-01	9.999E-01	9.770E-01	9.934E-01	9.627E-01
5.38	1.020E+00	9.999E-01	9.694E-01	9.999E-01	9.694E-01	9.912E-01	9.503E-01
6.23	1.027E+00	9.999E-01	9.593E-01	9.999E-01	9.593E-01	9.883E-01	9.336E-01
7.22	1.035E+00	9.998E-01	9.460E-01	9.998E-01	9.460E-01	9.844E-01	9.114E-01
8.36	1.046E+00	9.996E-01	9.284E-01	9.996E-01	9.284E-01	9.791E-01	8.819E-01
9.68	1.059E+00	9.993E-01	9.054E-01	9.993E-01	9.054E-01	9.721E-01	8.429E-01
11.21	1.076E+00	9.988E-01	8.755E-01	9.988E-01	8.755E-01	9.628E-01	7.919E-01
12.98	1.096E+00	9.979E-01	8.370E-01	9.979E-01	8.370E-01	9.504E-01	7.264E-01
15.03	1.119E+00	9.963E-01	7.880E-01	9.963E-01	7.880E-01	9.340E-01	6.442E-01
17.41	1.146E+00	9.933E-01	7.268E-01	9.933E-01	7.268E-01	9.121E-01	5.448E-01
20.16	1.176E+00	9.881E-01	6.522E-01	9.881E-01	6.522E-01	8.830E-01	4.311E-01

MMD = 5 μm σ = 1.5 μm Size [=] μm
Volumetric Flow Rate = 70 l/min, Wind Speed = 3 m/sec

MASS-WEIGHTED FRACTIONAL PENETRATION OF LOG-NORMAL DISTRIBUTION OF AEROSOLS

INLET	HORIZ.	90° BEND	VERTICAL	45° BEND	INCLINED	CUM.
1.023E+00	9.996E-01	9.639E-01	9.996E-01	9.639E-01	9.893E-01	9.408E-01

Table D-6. Penetration Efficiency Calculations For Polydispersed Particle
Distributions - MMD = 5 μm, Inlet Orientation = 0°,
Flow Rate = 130 L/min

MMD = 5 μm   σ = 1.5 μm   Size [=] μm
Volumetric Flow Rate = 130 l/min, Wind Speed = 3 m/sec

FRACTIONAL PENETRATION OF AEROSOL

SIZE	INLET	HORIZ.	90° BEND	VERTICAL	45° BEND	INCLINED	CUM.
1.24	9.993E-01	1.000E+00	9.966E-01	1.000E+00	9.966E-01	1.000E+00	9.928E-01
1.44	9.990E-01	1.000E+00	9.956E-01	1.000E+00	9.956E-01	1.000E+00	9.904E-01
1.66	9.987E-01	1.000E+00	9.941E-01	1.000E+00	9.941E-01	1.000E+00	9.871E-01
1.93	9.983E-01	1.000E+00	9.922E-01	1.000E+00	9.922E-01	9.999E-01	9.827E-01
2.23	9.977E-01	1.000E+00	9.897E-01	1.000E+00	9.897E-01	9.997E-01	9.769E-01
2.58	9.970E-01	9.999E-01	9.863E-01	9.999E-01	9.863E-01	9.993E-01	9.692E-01
2.99	9.960E-01	9.999E-01	9.819E-01	9.999E-01	9.819E-01	9.989E-01	9.590E-01
3.46	9.947E-01	9.999E-01	9.759E-01	9.999E-01	9.759E-01	9.983E-01	9.456E-01
4.01	9.930E-01	9.998E-01	9.681E-01	9.998E-01	9.681E-01	9.975E-01	9.279E-01
4.65	9.908E-01	9.997E-01	9.576E-01	9.997E-01	9.576E-01	9.965E-01	9.048E-01
5.38	9.879E-01	9.995E-01	9.438E-01	9.995E-01	9.438E-01	9.951E-01	8.748E-01
6.23	9.841E-01	9.991E-01	9.257E-01	9.991E-01	9.257E-01	9.932E-01	8.360E-01
7.22	9.793E-01	9.984E-01	9.020E-01	9.984E-01	9.020E-01	9.907E-01	7.867E-01
8.36	9.731E-01	9.971E-01	8.711E-01	9.971E-01	8.711E-01	9.873E-01	7.248E-01
9.68	9.654E-01	9.948E-01	8.315E-01	9.948E-01	8.315E-01	9.825E-01	6.489E-01
11.21	9.560E-01	9.907E-01	7.812E-01	9.907E-01	7.812E-01	9.756E-01	5.586E-01
12.98	9.447E-01	9.833E-01	7.185E-01	9.833E-01	7.185E-01	9.654E-01	4.553E-01
15.03	9.316E-01	9.703E-01	6.424E-01	9.703E-01	6.424E-01	9.501E-01	3.439E-01
17.41	9.169E-01	9.474E-01	5.529E-01	9.474E-01	5.529E-01	9.368E-01	2.357E-01
20.16	9.011E-01	9.076E-01	4.521E-01	9.076E-01	4.521E-01	9.043E-01	1.372E-01

MMD = 5 μm σ = 1.5 μm Size [=] μm
Volumetric Flow Rate = 130 l/min, Wind Speed = 130 L/min

MASS-WEIGHTED FRACTIONAL PENETRATION OF LOG-NORMAL DISTRIBUTION OF AEROSOLS

INLET	HORIZ.	90° BEND	VERTICAL	45° BEND	INCLINED	CUM.
9.861E-01	9.984E-01	9.349E-01	9.984E-01	9.349E-01	9.937E-01	8.598E-01

APPENDIX E
COMPLETE SET OF NUMERICAL CALCULATIONS GENERATED
BY BATTELLE MODEL

Table E-1 RESULTS OF SAMPLF CALCULATIONS USING MMD = 5 μm AND Q = 70 L/min

Inlet Train Section	Local Deposition Rate, mg/min	Exit Concentration, mg/m^3	Cumulative Sampling Efficiency, % (mass)
Horizontal pipe	0.208E-5	0.197E-2	98.52
90° bend	0.362E-6	0.197E-2	98.26
Vertical pipe	0.272E-8	0.197E-2	98.26
45° bend	0.181E-6	0.196E-2	98.13
Inclined pipe	0.143E-5	0.194E-2	97.11

Table E-2 RESULTS OF SAMPLF CALCULATIONS USING MMD = 15 μm AND Q = 70 L/min

Inlet Train Section	Local Deposition Rate, mg/min	Exit Concentration, mg/m^3	Cumulative Sampling Efficiency, % (mass)
Horizontal pipe	0.168E-4	0.176E-2	87.99
90° bend	0.136E-5	0.174E-2	87.02
Vertical pipe	0.122E-8	0.174E-2	87.02
45° bend	0.659E-6	0.173E-2	86.55
Inclined pipe	0.950E-5	0.160E-2	79.76

Table E-3 RESULTS OF SAMPLF CALCULATIONS USING MMD = 5 μm AND Q = 130 L/min

Inlet Train Section	Local Deposition Rate, mg/min	Exit Concentration, mg/m^3	Cumulative Sampling Efficiency, % mass
Horizontal pipe	0.209E-5	0.198E-2	99.19
90° bend	0.212E-5	0.197E-2	98.38
Vertical pipe	0.482E-8	0.197E-2	98.38
45° bend	0.105E-5	0.196E-2	97.97
Inclined pipe	0.143E-5	0.195E-2	97.42

Table E-4 RESULTS OF SAMPLF CALCULATIONS USING MMD = 15 μm AND Q = 130 L/min

Inlet Train Section	Local Deposition Rate, mg/min	Exit Concentration, mg/m^3	Cumulative Sampling Efficiency, % (mass)
Horizontal pipe	0.177E-4	0.186E-2	93.18
90° bend	0.158E-4	0.174E-2	87.11
Vertical pipe	0.220E-8	0.174E-2	87.11
45° bend	0.725E-5	0.169E-2	84.32
Inclined pipe	0.956E-5	0.161E-2	80.65

Table E-5   RESULTS OF SAMPLF CALCULATIONS USING D = 3 μm
AND Q = 70 L/min

Inlet Train Section	Local Deposition Rate, mg/min	Exit Concentration, mg/m^3	Cumulative Sampling Efficiency, % mass
Horizontal pipe	0.548E-6	0.199E-2	99.61
90° bend	0.315E-6	0.199E-2	99.38
Vertical pipe	0.369E-8	0.199E-2	99.38
45° bend	0.157E-6	0.199E-2	99.27
Inclined pipe	0.386E-6	0.198E-2	98.99

Table E-6   RESULTS OF SAMPLF CALCULATIONS USING D = 5 μm
AND Q = 70 L/min

Inlet Train Section	Local Deposition Rate, mg/min	Exit Concentration, mg/m^3	Cumulative Sampling Efficiency, % (mass)
Horizontal pipe	0.151E-5	0.198E-2	98.92
90° bend	0.342E-6	0.197E-2	98.68
Vertical pipe	0.263E-8	0.197E-2	98.68
45° bend	0.171E-6	0.197E-2	98.55
Inclined pipe	0.106E-5	0.196E-2	97.80

Table E-7   RESULTS OF SAMPLF CALCULATIONS USING D = 7 μm
AND Q = 70 L/min

Inlet Train Section	Local Deposition Rate, mg/min	Exit Concentration, mg/m^3	Cumulative Sampling Efficiency, % mass
Horizontal pipe	0.294E-5	0.196E-2	97.90
90° bend	0.385E-6	0.195E-2	97.62
Vertical pipe	0.209E-8	0.195E-2	97.62
45° bend	0.192E-6	0.195E-2	97.48
Inclined pipe	0.204E-5	0.192E-2	96.03

Table E-8   RESULTS OF SAMPLF CALCULATIONS USING D = 10 μm
AND Q = 70 L/min

Inlet Train Section	Local Deposition Rate, mg/min	Exit Concentration, mg/m^3	Cumulative Sampling Efficiency, % (mass)
Horizontal pipe	0.594E-5	0.192E-2	95.76
90° bend	0.486E-6	0.191E-2	95.41
Vertical pipe	0.163E-8	0.191E-2	95.41
45° bend	0.242E-6	0.191E-2	95.24
Inclined pipe	0.402E-5	0.185E-2	92.37

Table E-9   RESULTS OF SAMPLF CALCULATIONS USING D = 15 μm
AND Q = 70 L/min

Inlet Train Section	Local Deposition Rate, mg/min	Exit Concentration, mg/m^3	Cumulative Sampling Efficiency, % (mass)
Horizontal pipe	0.130E-4	0.181E-2	90.71
90° bend	0.789E-6	0.180E-2	90.15
Vertical pipe	0.119E-8	0.180E-2	90.15
45° bend	0.393E-6	0.180E-2	89.87
Inclined pipe	0.838E-5	0.168E-2	83.89

Table E-10   RESULTS OF SAMPLF CALCULATIONS USING D = 20 μm
AND Q = 70 L/min

Inlet Train Section	Local Deposition Rate, mg/min	Exit Concentration, mg/m^3	Cumulative Sampling Efficiency, % mass
Horizontal pipe	0.223E-4	0.168E-2	84.09
90° bend	0.139E-5	0.166E-2	83.10
Vertical pipe	0.912E-9	0.166E-2	83.10
45° bend	0.687E-6	0.165E-2	82.61
Inclined pipe	0.133E-4	0.146E-2	73.09

Table E-11 RESULTS OF SAMPLF CALCULATIONS USING D = 25 μm
AND Q = 70 L/min

Inlet Train Section	Local Deposition Rate, mg/min	Exit Concentration, mg/m^3	Cumulative Sampling Efficiency, % (mass)
Horizontal pipe	0.332E-4	0.153E-2	76.29
90° bend	0.265E-5	0.149E-2	74.40
Vertical pipe	0.709E-9	0.149E-2	74.40
45° bend	0.130E-5	0.147E-2	73.47
Inclined pipe	0.179E-4	0.121E-2	60.67

Table E-12 RESULTS OF SAMPLF CALCULATIONS USING D = 3 μm
AND Q = 130 L/min

Inlet Train Section	Local Deposition Rate, mg/min	Exit Concentration, mg/m^3	Cumulative Sampling Efficiency, % mass
Horizontal pipe	0.552E-6	0.200E-2	99.79
90° bend	0.148E-5	0.198E-2	99.22
Vertical pipe	0.648E-8	0.198E-2	99.22
45° bend	0.736E-6	0.198E-2	98.93
Inclined pipe	0.388E-6	0.198E-2	98.78

Table E-13 RESULTS OF SAMPLF CALCULATIONS USING D = 5 μm
AND Q = 130 L/min

Inlet Train Section	Local Deposition Rate, mg/min	Exit Concentration, mg/m^3	Cumulative Sampling Efficiency, % (mass)
Horizontal pipe	0.152E-5	0.199E-2	99.42
90° bend	0.178E-5	0.198E-2	98.73
Vertical pipe	0.466E-8	0.198E-2	98.73
45° bend	0.886E-6	0.197E-2	98.39
Inclined pipe	0.106E-5	0.196E-2	97.98

Table E-14 RESULTS OF SAMPLF CALCULATIONS USING D = 7 μm
AND Q = 130 L/min

Inlet Train Section	Local Deposition Rate, mg/min	Exit Concentration, mg/m^3	Cumulative Sampling Efficiency, % (mass)
Horizontal pipe	0.296E-5	0.198E-2	98.86
90° bend	0.231E-5	0.196E-2	97.97
Vertical pipe	0.375E-8	0.196E-2	97.97
45° bend	0.115E-5	0.195E-2	97.53
Inclined pipe	0.204E-5	0.193E-2	96.74

144

Table E-15   RESULTS OF SAMPLF CALCULATIONS USING D = 10 μm
                  AND Q = 130 L/min

Inlet Train Section	Local Deposition Rate, mg/min	Exit Concentration, mg/m³	Cumulative Sampling Efficiency, % mass
Horizontal pipe	0.600E-5	0.195E-2	97.69
90° bend	0.388E-5	0.192E-2	96.20
Vertical pipe	0.294E-8	0.192E-2	96.20
45° bend	0.192E-5	0.191E-2	95.46
Inclined pipe	0.406E-5	0.188E-2	93.90

Table E-16   RESULTS OF SAMPLF CALCULATIONS USING D = 15 μm
                  AND Q = 130 L/min

Inlet Train Section	Local Deposition Rate, mg/min	Exit Concentration, mg/m³	Cumulative Sampling Efficiency, % (mass)
Horizontal pipe	0.133E-4	0.190E-2	94.89
90° bend	0.142E-4	0.179E-2	89.43
Vertical pipe	0.213E-8	0.179E-2	89.43
45° bend	0.678E-5	0.174E-2	86.82
Inclined pipe	0.822E-5	0.167E-2	83.66

Table E-17   RESULTS OF SAMPLF CALCULATIONS USING D = 20 μm
              AND Q = 130 L/min

Inlet Train Section	Local Deposition Rate, mg/min	Exit Concentration, mg/m^3	Cumulative Sampling Efficiency, % mass
Horizontal pipe	0.232E-4	0.182E-2	91.09
90° bend	0.258E-4	0.162E-2	81.17
Vertical pipe	0.162E-8	0.162E-2	81.17
45° bend	0.118E-4	0.153E-2	76.62
Inclined pipe	0.127E-4	0.143E-2	71.73

Table E-18   RESULTS OF SAMPLF CALCULATIONS USING D = 25 μm
              AND Q = 130 L/min

Inlet Train Section	Local Deposition Rate, mg/min	Exit Concentration, mg/m^3	Cumulative Sampling Efficiency, % (mass)
Horizontal pipe	0.353E-4	0.173E-2	86.44
90° bend	0.357E-4	0.145E-2	72.70
Vertical pipe	0.127E-8	0.145E-2	72.70
45° bend	0.157E-4	0.133E-2	66.68
Inclined pipe	0.170E-4	0.120E-2	60.15

APPENDIX F
COMPLETE SET OF EXPERIMENTAL DATA GENERATED BY
WIND TUNNEL TESTS

Table F-1 Experimental Values of Aerosol Penetration. Test Case 1. Wind Speed = 3 m/s, Inlet Oriented Perpendicular to Air Stream (90°), Sampled Flow Rate = 70 L/min.

AED Particle Size, μm	Penetration Values, Percent	Mean Penetration ± 1 Standard Deviation, Percent
3.5	94.6, 92.4, 92.2	93.1 ± 1.3
4.9	93.5, 95.9, 91.7, 89.0	92.5 ± 2.9
7.2	76.4, 75.7, 78.6	76.9 ± 1.5
7.4	78.3, 73.3, 73.7, 76.4	75.4 ± 2.4
10.1	62.9, 63.1, 60.0	61.9 ± 1.8
11.5	44.3, 42.3, 45.9, 46.1	44.7 ± 1.8
14.9	21.0, 19.9, 19.9, 21.1	20.4 ± 0.7
19.6	4.1, 4.0, 4.6, 4.2	4.3 ± 0.3
25.4	4.9, 0.8, 0.0	1.9 ± 2.6

Table F-2 Experimental Values of Aerosol Penetration. Test Case 2. Wind Speed = 3 m/s, Inlet Oriented Perpendicular to Air Stream (90°), Sampled Flow Rate = 130 L/min.

AED Particle Size, μm	Penetration Values, Percent	Mean Penetration ± 1 Standard Deviation, Percent
3.5	92.5, 92.8, 91.7	92.4 ± 0.6
4.9	92.4, 91.3, 91.4	91.7 ± 0.6
7.2	80.2, 84.5, 84.0	82.9 ± 2.4
7.4	80.6, 82.7, 83.4, 80.2	81.8 ± 1.6
10.1	64.7, 65.9, 61.4, 61.2	63.3 ± 2.4
11.5	53.1, 58.5, 56.4	56.0 ± 2.7
14.9	24.5, 25.8, 29.8, 26.8	26.8 ± 2.3
19.6	3.8, 4.3, 4.2, 3.9	4.0 ± 0.3
25.4	0.5, 0.0, 0.7, 0.9	0.5 ± 0.4

Table F-3   Experimental Values of Aerosol Penetration.
Test Case 5.   Wind Speed = 3 m/s, Inlet Oriented
Parallel to the Air Stream (0°), Sampled Flow Rate =
70 L/min.

AED Particle Size, μm	Penetration Values, Percent	Mean Penetration ± 1 Standard Deviation, Percent
3.0	100.3, 113.6, 97.4, 110.1	105.3 ± 7.7
5.1	95.3, 99.5, 95.9, 94.7	96.3 ± 2.2
7.0	90.8, 89.6, 90.5, 88.8	89.9 ± 0.9
9.8	83.3, 87.5, 80.3, 81.0	83.0 ± 3.2
12.0	73.7, 74.1, 72.4, 74.4	73.7 ± 0.9
15.2	55.6, 56.8, 51.8, 58.8	55.8 ± 2.9
19.4	29.3, 34.1, 35.2, 32.6	32.8 ± 2.6
25.7	7.1, 7.3, 5.4, 6.1	6.5 ± 0.9

Table F-4   Experimental Values of Aerosol Penetration.
Test Case 6.   Wind Speed = 3 m/s, Inlet Oriented
Parallel to the Air Stream (0°), Sampled Flow Rate =
130 L/min.

AED Particle Size, μm	Penetration Values, Percent	Mean Penetration ± 1 Standard Deviation, Percent
3.0	94.8, 91.5, 96.4, 89.8	93.1 ± 3.0
5.1	92.9, 89.9, 91.2, 87.9	90.4 ± 2.1
7.0	92.4, 83.5, 86.3, 81.7	86.4 ± 5.5
9.8	69.4, 70.7, 69.4, 69.1	69.6 ± 0.7
12.0	56.8, 59.8, 55.3, 58.1	57.6 ± 1.9
15.2	31.1, 32.7, 30.7	31.5 ± 1.0
19.4	11.9, 11.5, 9.8	11.1 ± 1.1
25.7	0.8, 1.4, 1.2	1.1 ± 0.3